# Characterizing ExOPlanet Satellite (CHEOPS)

***CHEOPS-INAF-INST-RP-001***

*Issue 3 Revision 7*

## CIS-TEL Straylight Analysis

**Mandatory Cover Page Attributes:**

| | |
|---|---|
| Document Title: | CIS-TEL Straylight Analysis |
| Origin Name: | INAF, Matteo Munari |
| Date of Issue: | 3. Jul. 2017 |
| WBS code: | N/A |
| Package code: | N/A |

**CHEOPS Cover Page Attributes:**

| | |
|---|---|
| Old document reference: | |
| Restrictions: | None |
| (additional attributes) | |

**Distribution List**

| | |
|---|---|
| Public | [ ] |
| CHEOPS<br>(Through Project Manager) | [ X ] |
| Industry:<br>specify in detail (Company Name, point of contact) | [ ] |

**Approval Sheet**

| | Name | Signature | Date |
|---|---|---|---|
| Prepared by: | M.Munari |  | 16.05.2014 |
| Verified by: | I. Pagano | 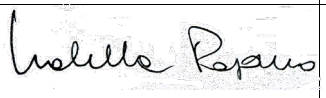 | 22.10.2015 |
| Approved by: | R: Ragazzoni |  | 22.10.2015 |
| Approved by: | | | |

**Document Change Record**

| Issue | Rev. | Date | Pages affected | Modification | DCR | Initials |
|---|---|---|---|---|---|---|
| 1 | 0 | 05.05.2013 | all | (new document) | N/A | MMU |
| 2 | 0 | 15.09.2013 | All | Modifications based on the new CIS Baseline | | MMU |
| 2 | 1 | 1.10.2013 | All | Minor changes on headers, added signatures | | IPA |
| 3 | 0 | 30.11.2013 | ALL | Changes after ISRR | | MMU |
| 3 | 1 | 16.03.2014 | ALL | Changed of Zemax Reference model<br>Changes in Model | | |

| | | | | | | |
|---|---|---|---|---|---|---|
| | | | | Changes in Materials<br>Changes in results of simulations | | |
| 3 | 2 | 24.04.2014 | All | Figure 1 Updated<br>Changes on the abbreviations<br>Modification of section 6 and 7 | | MMU |
| 3 | 3 | 15.05.2014 | Section 4<br>AD<br>Section 7 | Section 4.1 updated after IRS rev 11<br>Section 4.3 added ref to OICD<br>AD references updated<br>Section 4.2 Table 1 PM SM typo corrected<br>All: added labels to plots<br>Section 7 updated | CBR-6<br>CBR-7<br>CBR-8<br>AFO-1<br>AFO-3<br>AFO-6 | MMU |
| 3 | 4 | 25.05.2014 | | Sections added: 6.5.2 , 6.6.2.3 ,0, 6.6.2.4<br>Section 7 updated | | MMU |
| 3 | 5 | 16.10.2015 | All | Changed Model (added borders of mirrors)<br>Section 5.2: modified black coatings models<br>Section 5.2.3: modified Dust coverage BRDF models<br>Section 5.2.4: modified coating.<br>Section 6: modified analyses<br>Section 7: modified conclusions | | MMU |
| 3 | 6 | 31.01.16 | §6.5.1.1§ 6.5.1.2 | Removed (content updated and moved in 6.7 ) | | MMU |
| 3 | 7 | 1.07.17 | §8 | New | CBR-01 | MMU |

DCR = document change request number

## Table of Contents

## List of documents

| **Applicable documents:** | |
|---|---|
| **AD1.** | CHEOPS-UBE-INST-RS-001-i1.10_Instrument_Requirements_Specification |
| **AD2.** | CHEOPS-EST-SCI-RS-001_i2.3_SciRD, Scientific Requirements Document |
| **AD3.** | CHEOPS-EST-INST-EID-001_i2.5 |
| **AD4.** | CHEOPS-UBE-INST-EIDB-001-i3.5_EIDB |
| **AD5.** | CHEOPS-EST-INST-RS-001-ECSS-Engineering_Tailoring Issue 1, rev 0<br>CHEOPS tailoring for ECSS Engineering standards |

| **Reference documents:** | |
|---|---|
| **RD1.** | CHEOPS_RSSZ_TN_006_I1R1 |
| **RD2.** | Handbook of Optics, Michael Bass |
| **RD3.** | www.acktar.com |
| **RD4.** | The Design and Construction of Large Optical Telescopes, Pierre Bely |
| **RD5.** | http://www.zygo.com/?/opt/components/mirrors/ |
| **RD6.** | http://www.edmundoptics.com/optics/optical-mirrors/flat-mirrors/super-polished- |

| | |
|---|---|
| | mirror-substrates/3431 |
| **RD7.** | http://www.radiantzemax.com/zemax/ |
| **RD8.** | BCA - ISE-01_CHEOPS-CSL-INST-DD-001-i4.0_Baffle_Design_Description.pdf |
| **RD9.** | http://www.photonengr.com/files/2011/10/ApproximatedScatter.pdf |
| **RD10** | http://www.breault.com/sites/default/files/knowledge_base/brotg0922_scatter_1.pdf |
| **RD11** | CHEOPS TEL Optical Model by SES (in prep.) |
| **RD12** | http://www.breault.com/software/asap-pro.php |
| **RD13** | Robert P. Breault "Vane Structure Design Trade-Off And Performance Analysis", *Proc. SPIE* 0967, Stray Light and Contamination in Optical Systems, 90 ,April 5, 1989 |
| **RD14** | CHEOPS-INAF-INST-FI-001-i1.2.rar |
| **RD15** | CHEOPS-INAF-INST-ADD-007.ZMX |
| **RD16** | CHEOPS-INAF-INST-ICD-001 CHEOPS OICD, Optical ICD i1.7 |
| **RD17** | BCA - ISE-01_CHEOPS-CSL-INST-RP-007-i1.2_Black_coating_sample_measurement_report |
| **RD18** | CHEOPS-INAF-INST-FI-001-i1.1.rar |
| **RD19** | Gary L. Peterson in "Analytic expression for in-field scattered light distribution", Proc. SPIE 5178, Optical Modelling and Performance Predictions, 184 (January 26, 2004) |
| **RD20** | CHEOPS-SES-INST-NC-012 NCR CHEOPS roughness |

# 1 Introduction

## 1.1 Scope of the Document

Scope of this document is to present the results of the Straylight Analysis conducted on the CHEOPS Instrument System.

## 1.2 Abbreviations and Acronyms

BEO Back End Optics

PST Point Source Transmittance

BRDF Bidirectional reflectance distribution function

BSDF Bidirectional scattering distribution function

M1 Primary Mirror

M2 Secondary Mirror

M3 Tertiary Mirror

FP Focal Plane

D Detector

D1 First doublet of the BEO

D2 Second doublet of the BEO

FS Field Stop

LS Lyot Stop

BL Baseline

SL Straylight

TEL Telescope

TIS Total Integrated Scatter

CIS Cheops Instruments System

IB Internal baffle

EB External Baffle

EPB External Primary baffle

ESB External Secondary Baffle

# 2 Concept

The CHEOPS Instrument is, from the optical point of view, a Ritchey-Chretien telescope (TEL), coupled with an optical refractive relay (the Back End Optics, BEO). The detailed Optical Design is reported in [RD11].

The main concepts for the reduction of straylight for the CHEOPS instrument essentially are:

- The presence of an External Baffle (EB), split in two parts, the External Primary Baffle (EPB) and the External Secondary Baffle (ESB). The scope of the External

Baffle is to reduce, via absorption, the off-axis, out of field-of-view radiation that may reach the internal parts of the Optical system. In particular its presence aims:

- To avoid direct illumination of the Primary Mirror(M1) for off-axis angles greater than ~20°
- To avoid direct illumination of the support tube between Primary (M1) and Secondary Mirror (M2) for angles greater than ~35°

- The presence in the optical design of an intermediate focus and a pupil, where is possible to place
  - A Field Stop (FS)
  - A Lyot Stop (LS)

These types of straylight countermeasures are extensively described in literature (e.g. RD2, RD4 and references therein).

Moreover, the external tube of the telescope between M1 and M2, denominated Internal Baffle (IB), is, as the EB, designed with vanes to reduce the straylight.

The elements described are indicated in the schema reported in Figure 1.

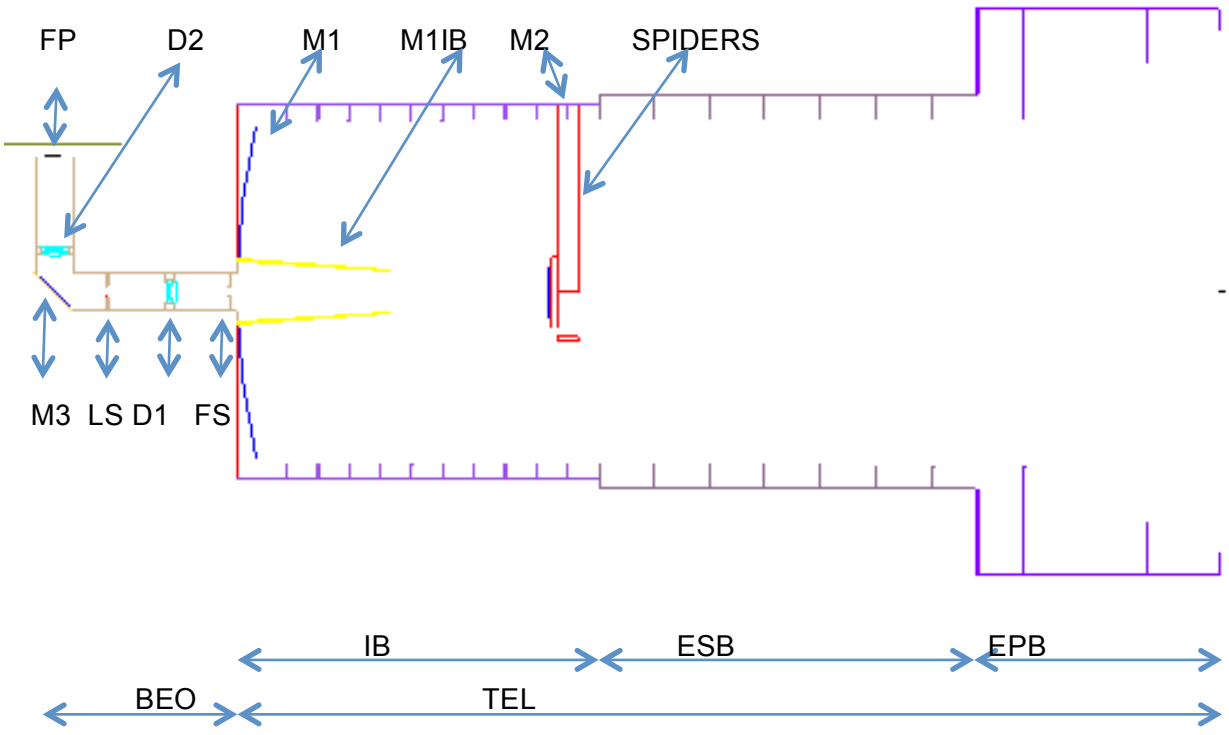


*Figure 1 Elements of the CIS*

# 3 Aim of the analysis

The aim of the analysis here presented is essentially to validate (from the point of view of straylight analysis) the Baseline design of the CHEOPS instrument. The Baseline Design has been recently assessed, taking into account evolution in requirements and design, from the point of view of optics, mechanics, interfaces, etc.

# 4 Inputs

## 4.1 Optical Design

The optical design of the Cheops instrument assumed as Baseline is described in [RD11] and in the ZEMAX [RD7] file (RD15). Some of its characteristics are shown in Table 1.

The design is not the last one but differences are minimal and we are confident will have no effects on this analysis.

As previously noted, the system is composed by two subsystem , the TEL and the BEO, the first one being a RC telescope and the second a reimaging system, that relays the image formed on the telescope focal plane F1 on the Cheops detector.

In the Design, the BEO is composed by two spaced doublets (D1 and D2), the first one forming a pupil of~10mm diameter, the second one refocusing on the detector (D). Between the two doublets, a mirror folds the path toward the detector.

*Table 1:Optical Design data and performances*

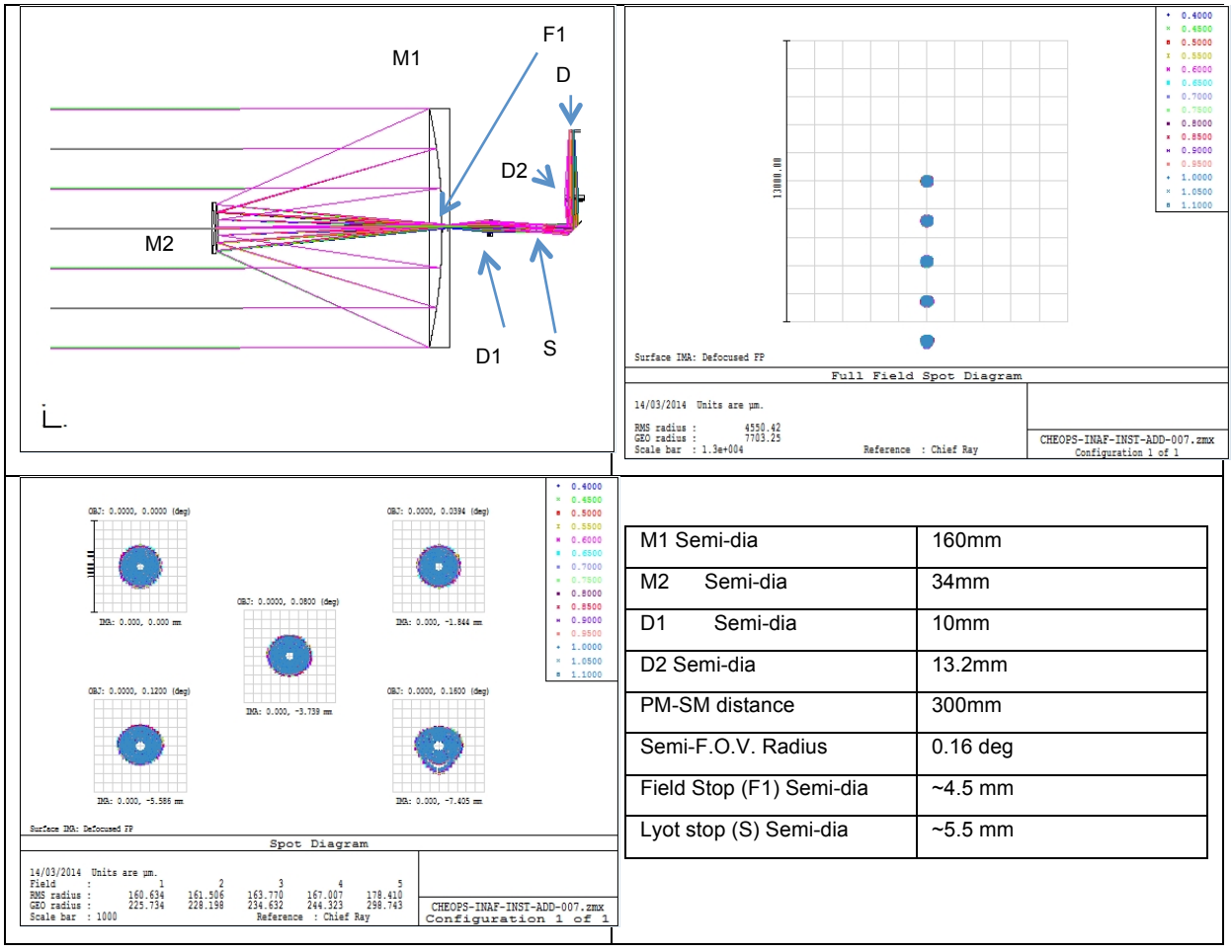


| | |
|---|---|
| M1 Semi-dia | 160mm |
| M2 Semi-dia | 34mm |
| D1 Semi-dia | 10mm |
| D2 Semi-dia | 13.2mm |
| PM-SM distance | 300mm |
| Semi-F.O.V. Radius | 0.16 deg |
| Field Stop (F1) Semi-dia | ~4.5 mm |
| Lyot stop (S) Semi-dia | ~5.5 mm |

## 4.2 Baffle Design

The design drivers for the baffle are described in RD8.

This design is purely geometrical: no thickness for vanes walls or precise shape of the vane edges is explicitly indicated.

In Figure 2 the dimensions of the baffle parts are reported. More details on the baffle geometry may be found in RD16

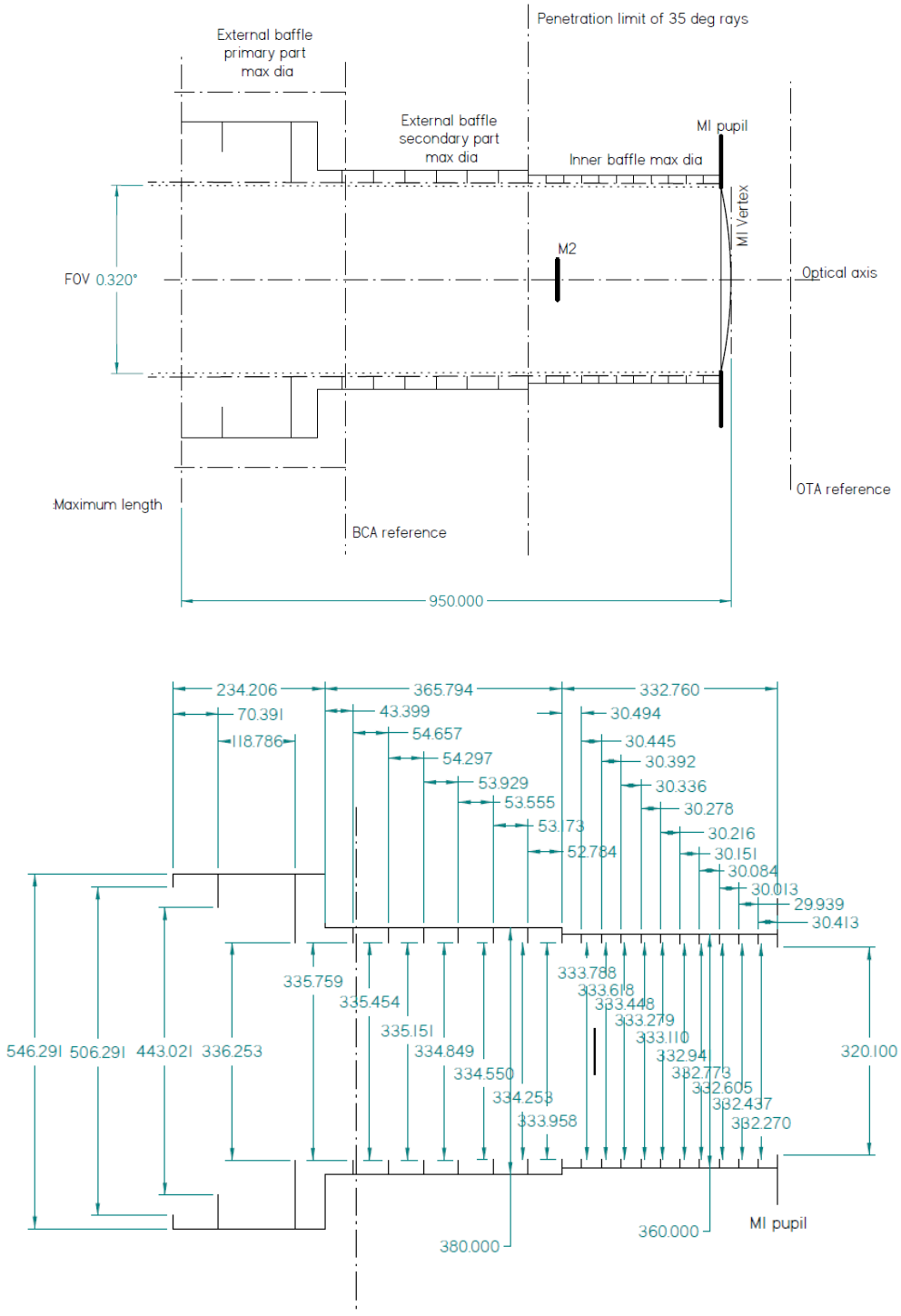


*Figure 2 Baffle Geometrical scheme*

# 5 ASAP Model

To perform the analysis an ASAP [RD15] model has been realized. The script used for the creation of the model, as for the material and coatings definition and the data analysis is in the file RD14. Please Note that model and scripts are modified wrt previous Issue of this report (3.4). Previous scripts are in RD18

## 5.1 Model geometry

The model geometry has been realized using internally defined object of ASAP.

It is composed by several elements, namely: primary secondary and tertiary mirrors, primary mirror borders, secondary mirror back and spider supports, external baffles with vanes as described in previous sections, a primary mirror internal baffle, Field and Lyot stop, a 13x13mm detector. Some notes:

- The baffle vanes walls have a 0.5 mm thickness centred on the reference positions of the geometrical scheme. The border of the edges are modelled as 40 micron flat surfaces, connected to the walls by 30° sloped section (see figure 4).
- EPB, ESB and IB are modelled as 3 tubes; the vanes are modelled singularly as diaphragms.
- The Field and Lyot stop are realized as diaphragms with round borders and a thickness of 0.5 mm.
- The BEO is realized as a tube, hosting the two doublets, the Field Stop and the Lyot stop, M3 and the detector.
- An internal primary baffle has been introduced, dimensioned as big as possible so not to vignette.

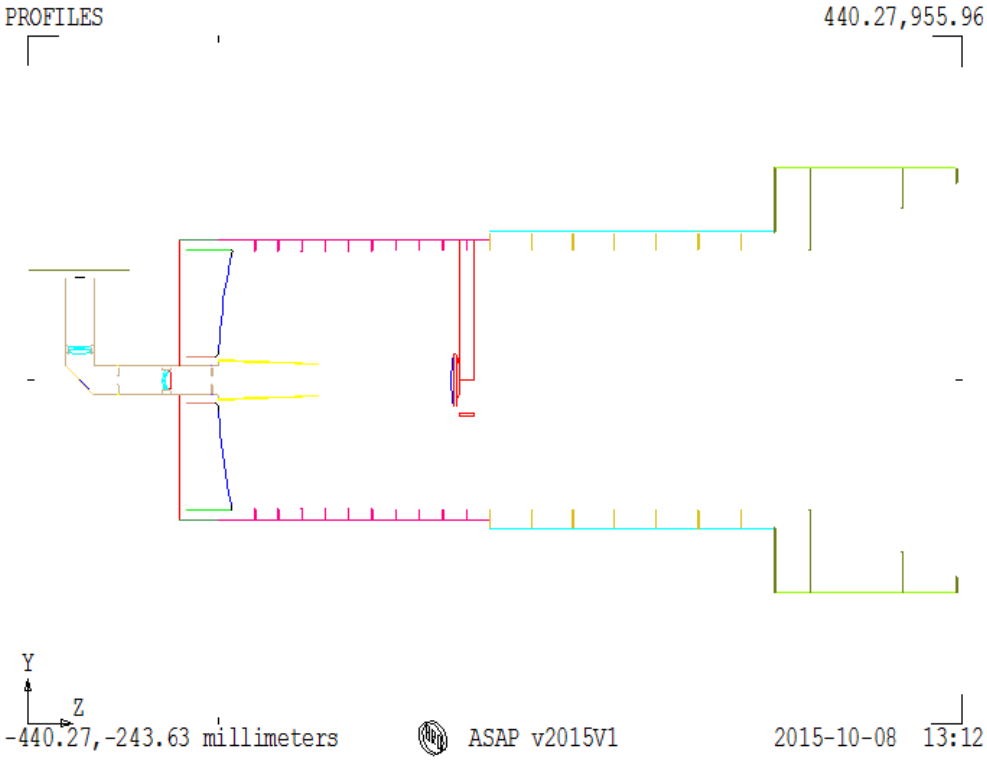


*Figure 3 ASAP model cut*


*Figure 4 Vane edge shape*

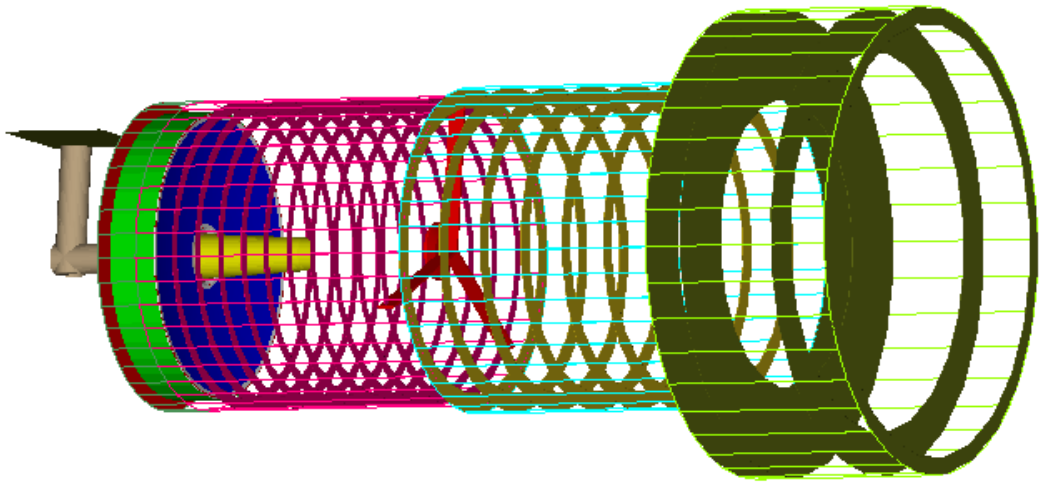

*Figure 5 ASAP model 3d view (external walls are wireframed to permit visualization of internal elements)*

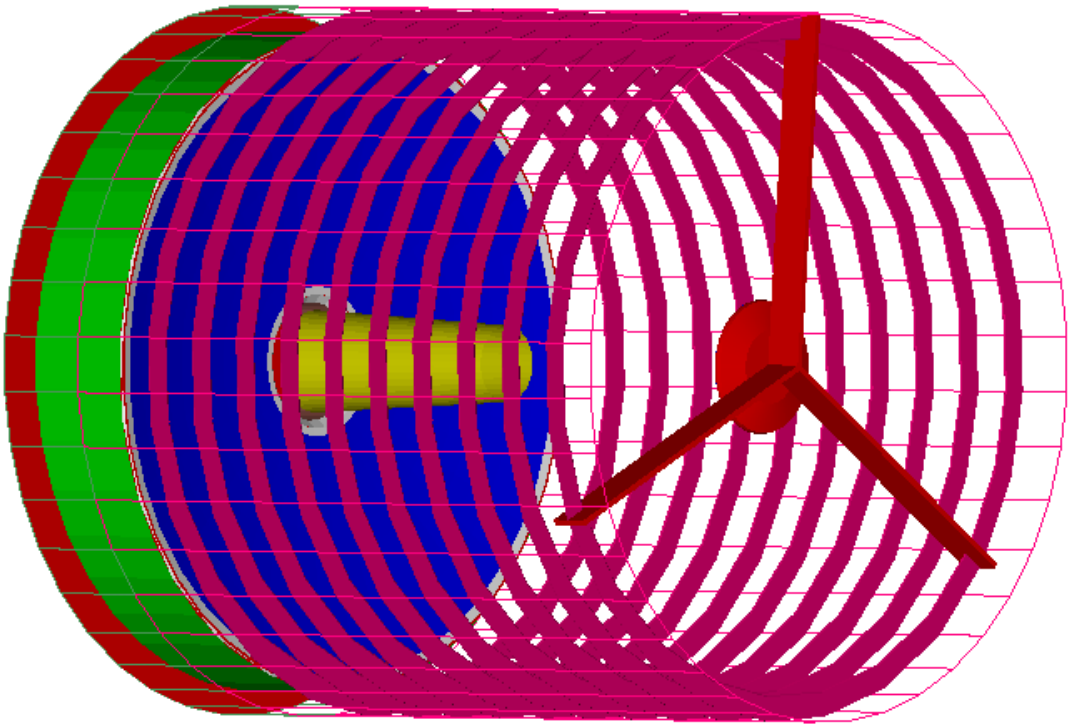

*Figure 6 primary mirror, primary internal baffle, secondary mirror with spider support*

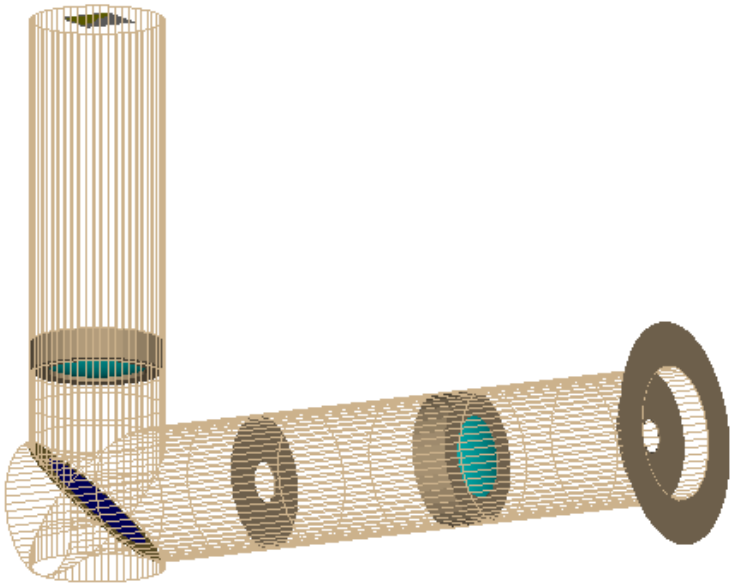

*Figure 7 BEO 3D view*

### 5.1.1 Correspondence with Zemax Model

To control the correctness of the ASAP model Vs the ZEMAX model, the on axis spot diagram for 400nm has been obtained for both models and compared. The diagrams are reported in table and both spots have about 400micron diameter.

*Table 2: On-Axis Spot Diagram of Zemax(left) and ASAP (right) @400nm*

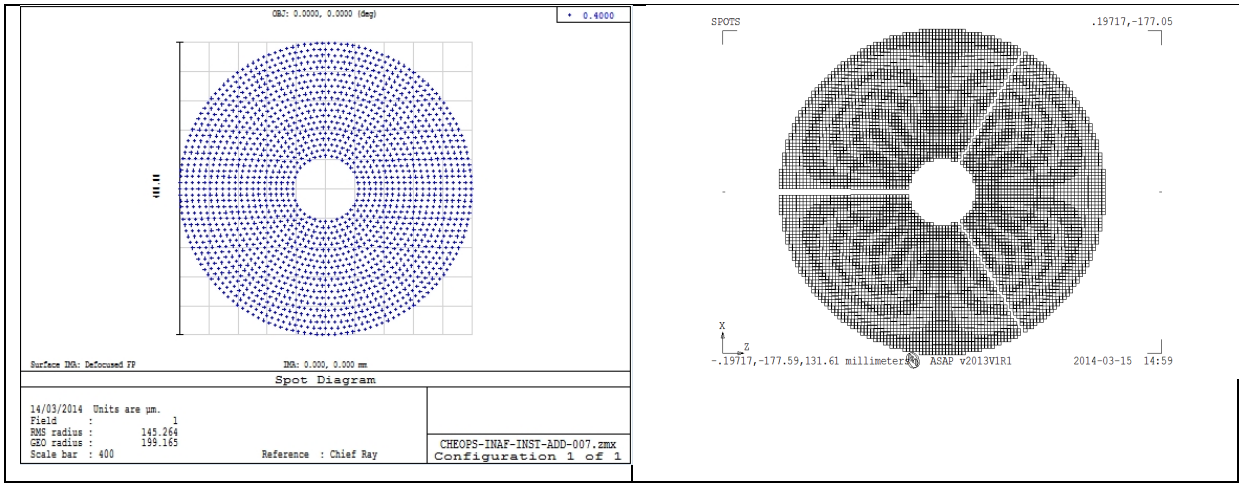

## 5.2 Materials

Given the “non-trivial” requirements for the CHEOPS instrument in terms of straylight, the choice of materials for the ‘black surfaces’ and the requirements for mirrors and lenses roughness is of main importance both to reach the required performances and to design a system that can be realized.

### 5.2.1 Non Optical surfaces

In previous Issues of this report several assumptions had been made about BRDFs of black coatings: at first a 2% lambertian coating model was used, after that models of some materials have been adopted. In particular two has been used as ‘base’ material:

- Aeroglaze 306, modelled via a standard polynomial model (see [RD10]) from ASAP examples (in the script ‘POLYNOMIAL_FIT02.INR’).Its TIS and BRDF are reported in Figure 8, and model is in the scripts files.
- Acktar Magic Black (RD3); a binomial model (see [RD10]) for Fractal Black has been developed by Photon Engineering (assuming an isotropic behaviour). BRDF of such model is reported in Figure 9; data of the model is in the scripts zip file.

After CDR, BRDF and TIS measurements of several coatings/paintings on different samples has been performed by both CSL and UBE. Results of these measurements can be read in (RD17). Even if useful to compare models with actual data, measures where not numerous enough to permit to derive completely new models for materials. It has been decided:

- For Internal Baffle (UBE) the base candidate painting is MAP painting, that will be simulated using the Aeroglaze model , that appears to be a pessimistic estimate of BRDF
- BRDF Models of Aeroglaze and Acktar coating are multiplied by a factor 1.3 and 1.5, respectively. Resulting models plots may be seen in Figure 10 and in Figure 11

More information about comparison of models and measures may be retrieved inRD17

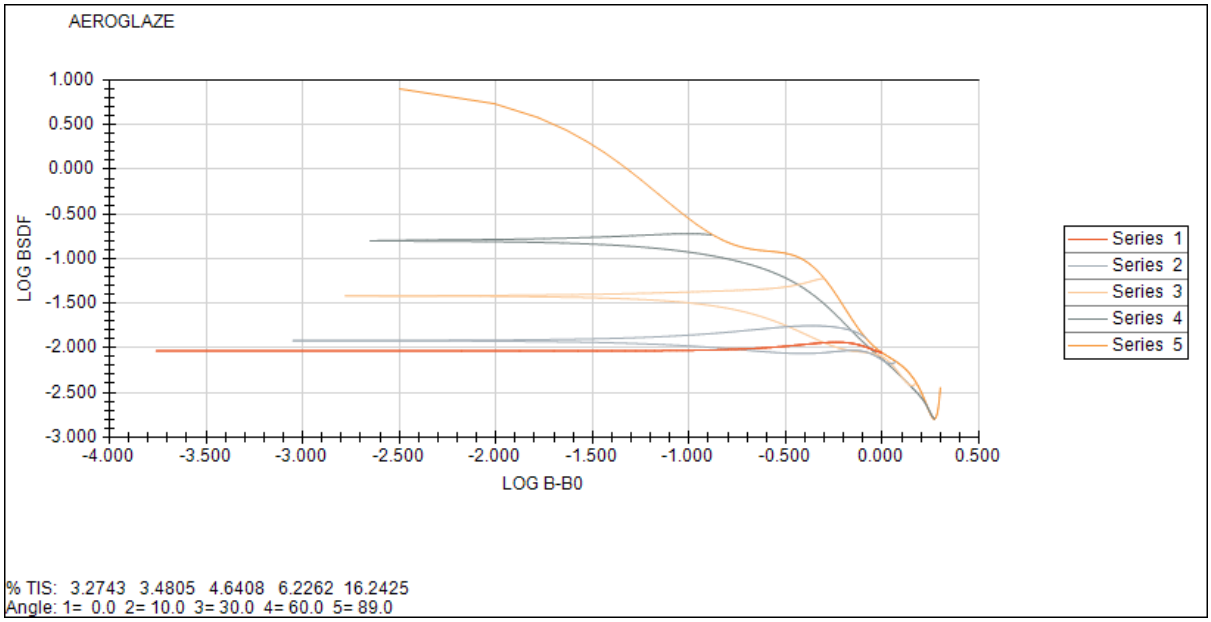


*Figure 8: ASAP Aeroglaze 306 model BRDF*

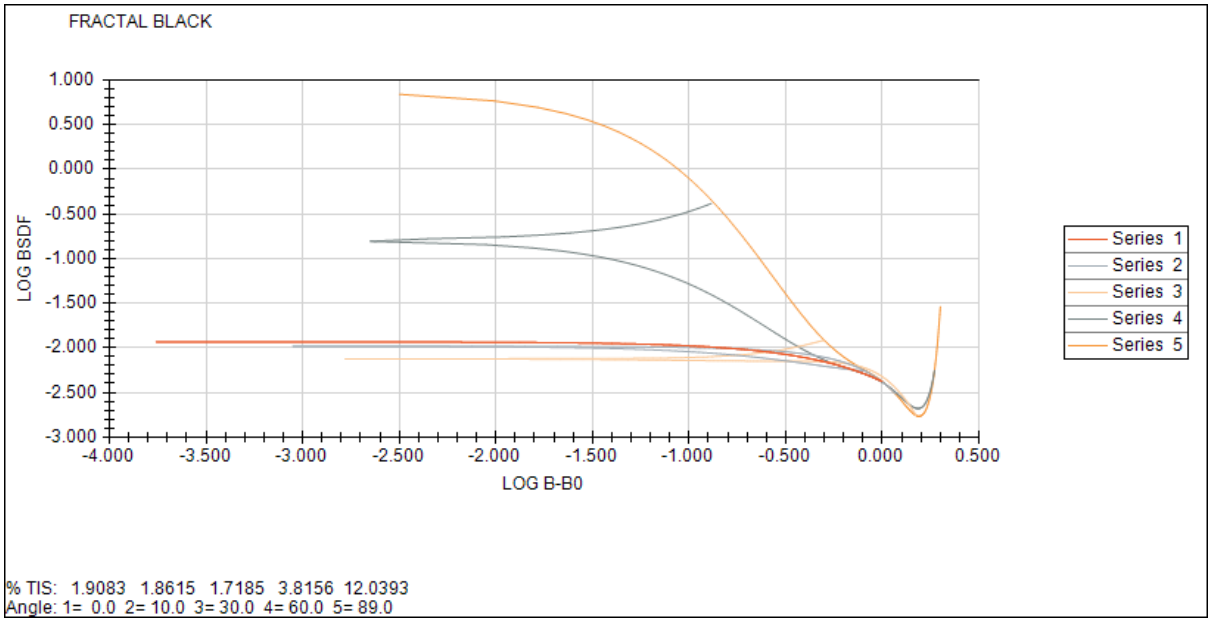


*Figure 9: Fractal Black BRDF, binomial model.*

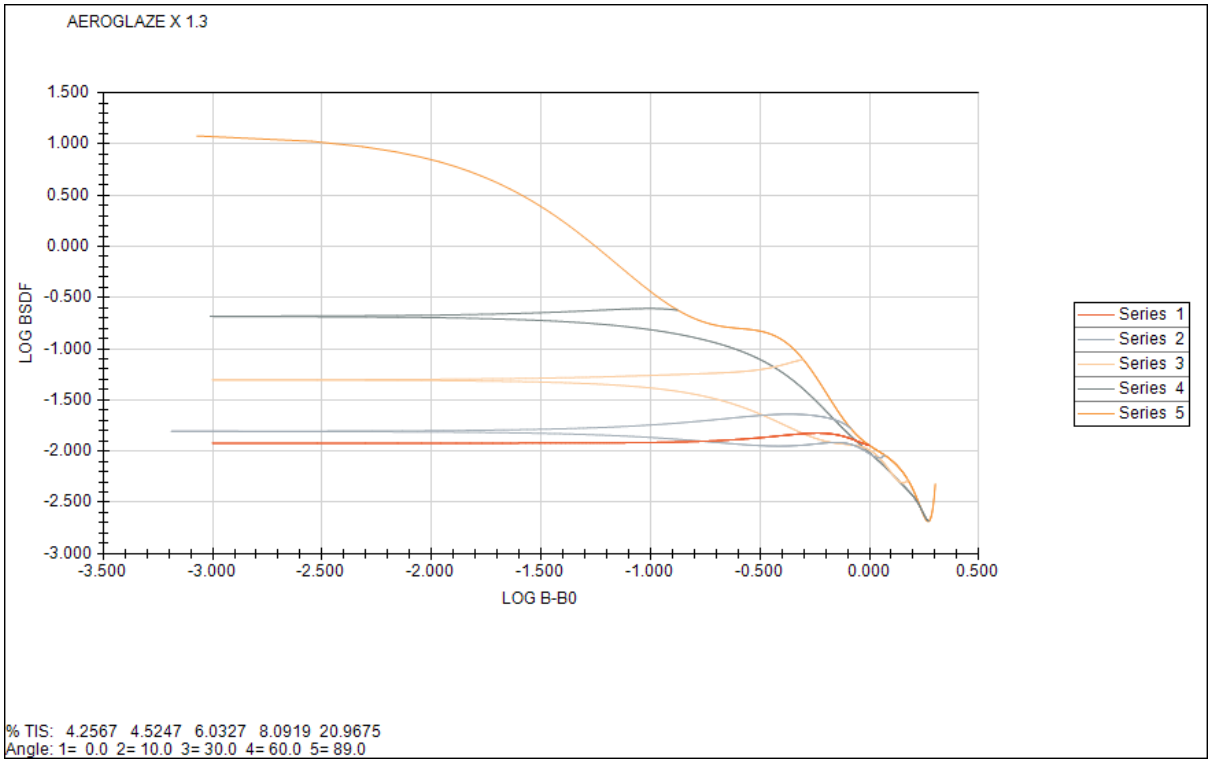


*Figure 10: ASAP Aeroglaze 306 model BRDF, 1.3 Factor*

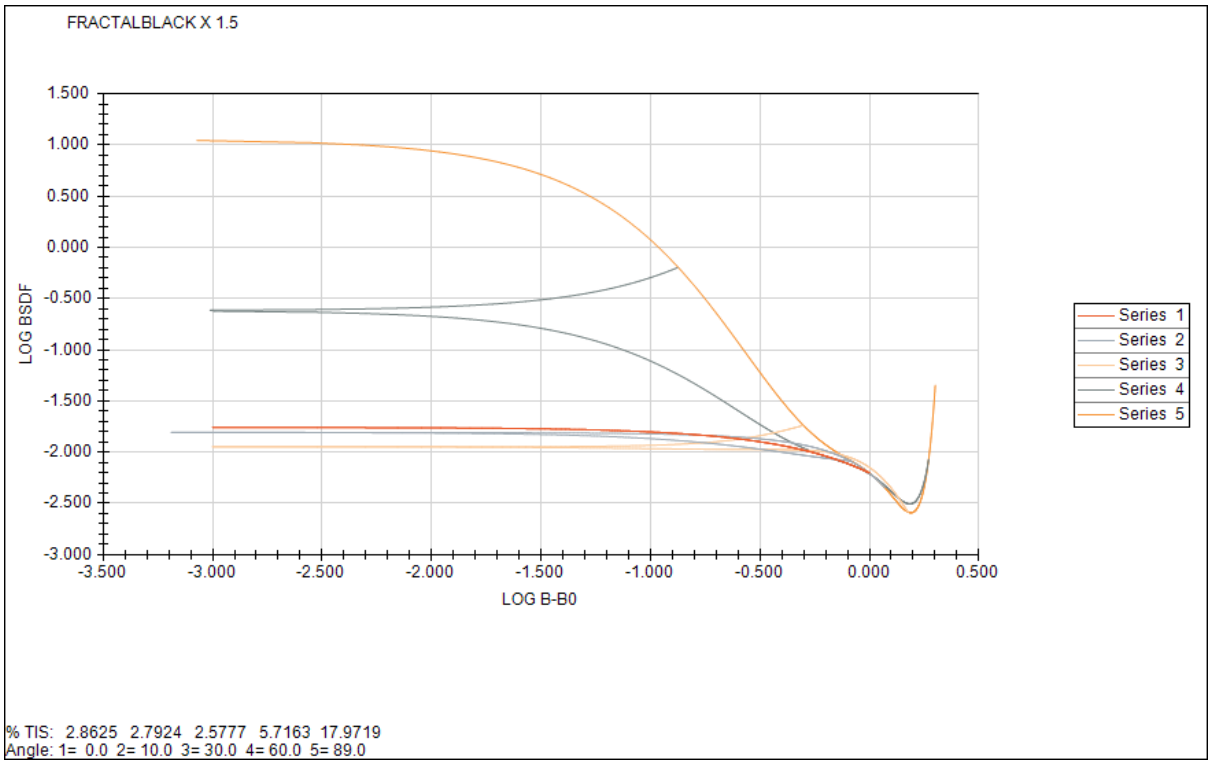


*Figure 11: Fractal Black BRDF, binomial model, 1.5 factor.*

### 5.2.2 Mirrors and lenses

The mirrors are supposed to have an rms micro-roughness (s) of 10A (M1) and 5A (M2 and M3); the lenses are supposed to have 5A micro-roughness. These values seem to be possible for optics given the small dimensions of the mirrors (see RD1 and several commercial vendors, e.g. RD5 and RD6).

To build the model for the analysis, the mirrors BRDF have been fitted with an ABg model (see [RD10]). The data and the plots of the BRDFs are shown in Table 3.

The vales of the 3 parameters A, B and g have been calculated using the method described in RD9:

- a typical slope of g=1.8 has been assumed
- assuming a roll-off angle of RA=0.01 and using the relation B^(1/g)=RA, the B parameter has been fixed in 2.5e-4.
- The A parameter has been obtained equating the TIS calculated from the ABg model with the TIS calculated from the rms of the surface, giving the relation A=2.05*(s*dn/wl)^2, where wl is the analysis wavelength (e.g. 400nm) and dn is the variation of the index of refraction of the surface (2 for the mirrors, while for the lenses 0.7 has been adopted for all the lenses)

*Table 3 Mirrors and lenses ABg scatter model plots and TIS @ 400nm*

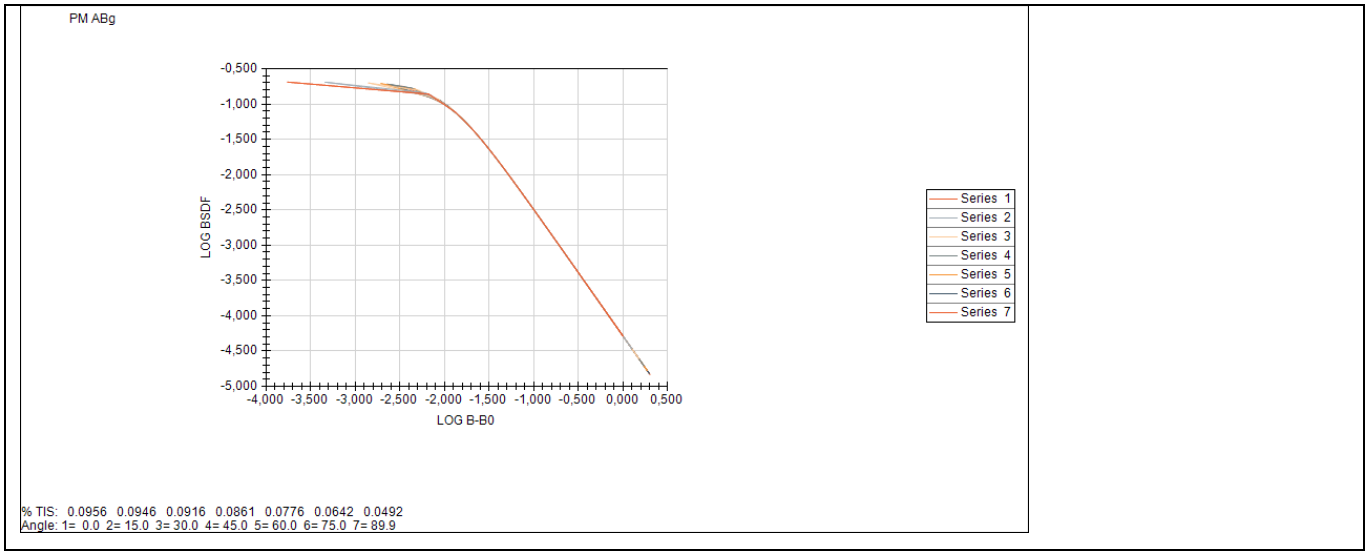

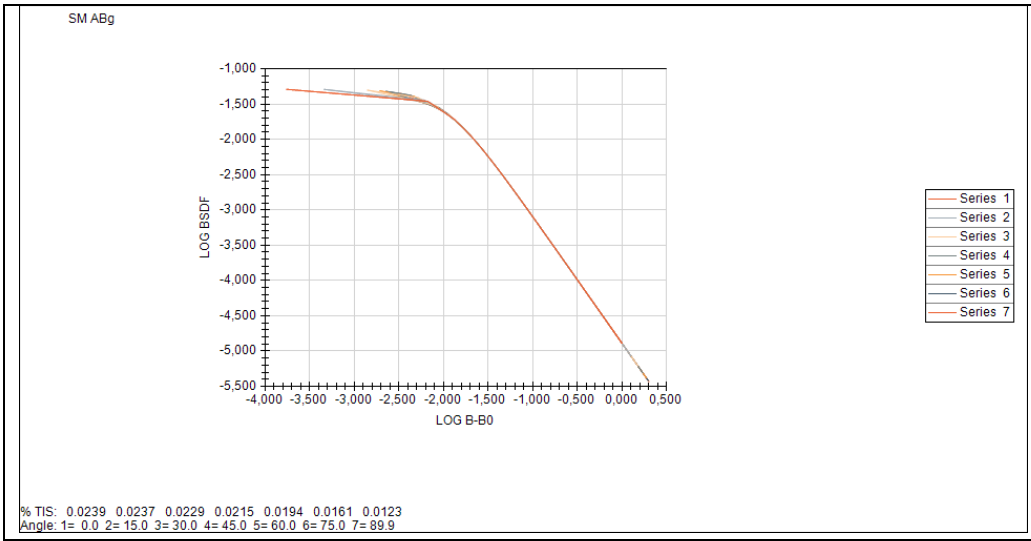


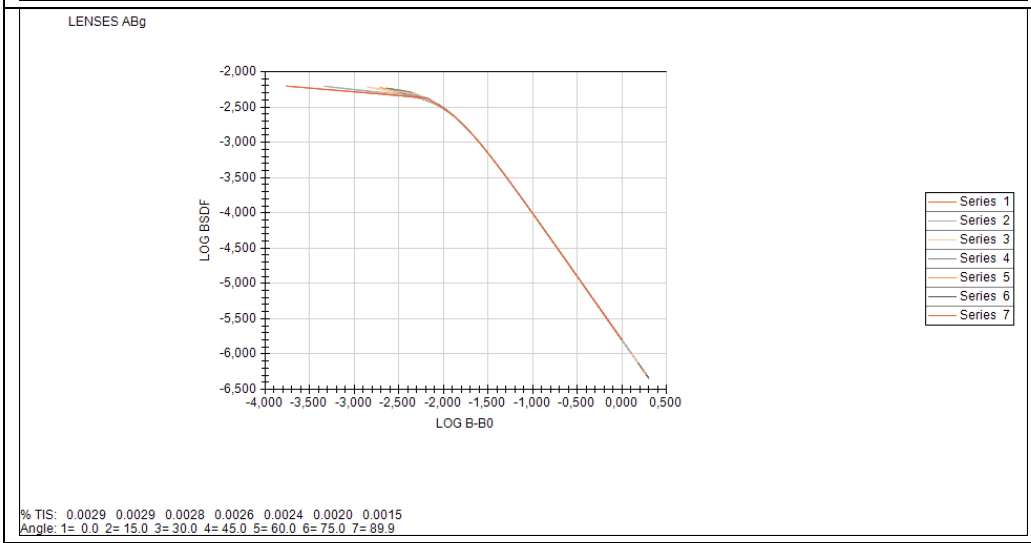


### 5.2.3 Dust contamination

To estimate the effect of dust contamination, the 'PARTICLES MIE' model of ASAP could have been adopted, in conjunction with the dust distribution described by the MIL1246 standard. Even if this scatter model could be used directly during the ray tracing, it would be extremely numerically intensive. To overcome this problematic, fitting function for the BRDF has been used, based on a simpler model: the sum of two 3-parameters Harvey functions.

The parameters of the fitting functions are summarized in the following table, coming from fits performed by Gary Peterson of the Breault Corporation and presented in the Stray Light analysis with ASAP advanced course of Breault Corporation
These parameters assumes a particle distribution as that described in MIL-1246C, with a PAC (particle Area Coverage) of 253ppm; different levels of contamination in ppm may be modelled simply rescaling $b_0$ by ppm/253

*Table 4: parameters for Dust Contamination scatter modelling (for 253 ppm, single lens surface)*

| WL (nm) | $b_0$ 1 | l 1 | s 1 | $b_0$ 2 | s 2 | g 2 | TIS (%) |
|---|---|---|---|---|---|---|---|
| **400** | 3.8 | 0.0025 | -2.4 | 2e-5 | 0.3 | -0.6 | 0.038 |
| **633** | 1.78 | 0.002 | -1.8 | - | - | - | 0.055 |
| **1150** | 0.562 | 0.0035 | -1.75 | - | - | - | 0.054 |

### 5.2.4 Coatings

The coatings are ideal ones: totally transmissive for lenses, totally reflective for the mirrors. This is (for scattering) a pessimistic assumption (being straylight not reduced traversing the optical elements of the system).

# 6 Simulations

## 6.1 Introduction

After PDR some modifications to the design of mirrors and baffles have been introduced, mainly for manufacturability / logistic issues:

- To reduce problems of alignment, the pupil mask, aimed to shield stray light coming from spider, has been definitely dropped
- For similar reasons diaphragms in intermediate focal plane and in Pupil plane have been oversized with respect to nominal measures (1 mm on radius for the focal plane, 0.5mm on radius for the pupil plane)
- As introduced in the 'black coatings' section, MAP painting has been proposed by manufacturer of IB as baseline for IB.
- EB totally coated in Acktar black has been judged impossible due to dimensions of the tube and logistic. The only parts that may be coated in Acktar Black are the diaphragms of the ESB.
- Primary mirror M1, for manufacturability reasons, has to have an external and an internal borders that will not respect nominal figures in terms of coating uniformity and figure. To keep performances stables in terms of photometric flux, it has been decided to black-coat this borders, so to have entrance pupil on the primary mirror and keep the flux constants as much as possible.

Due to these changes, the ASAP model has been changed and some simulations repeated so to evaluate the effects and the new PST.
Anyway, not all the analysis done for the CDR has been updated, some because not interesting anymore, some because are considered only marginally affected by modifications. These analyses may be retrieved in the previous issue of this report; some of them are anyway reported at the end of this section (6.5 ).

## 6.2 Methodology

The simulations have considered all the CIS as a whole: the entrance pupil of the system has been illuminated by a unitary irradiance plane source, simulating a point source at infinite distance; on D, the detector of the system, the flux has been recorded; once divided by the size of the detector (13x13mm) the PST of the system has been obtained.

The plane source has been moved at different angular positions from the CIS optical axis to study the PST vs Angle.

In the simulations, the borders of the vanes may be a problem, given their small axial size (40 micron), compared to the dimension of the entrance pupil: to adequately sample this borders via ray-tracing via an homogenous 'ray-dense' source, the number of necessary rays would make the simulation time too long.

For similar reasons (difficulties to illuminate) spiders supporting M2 effects may be difficult to estimate.

To overcome this problems, this analysis has been performed in two steps;

- In the first one, the borders and the spiders are absorbing and the system is fed with an elliptical source of ~7e3 rays

- In the second step, each vane border has been illuminated by an annular source, placed outside the baffle and dimensioned as to obtain ~3e4rays hitting the 40 micron border. The annular source was illuminating not only the vane border, but only the rays hitting the baffle vanes borders are allowed to being scattered and traced further.
    - Actually, not all the vanes border have been illuminated in such a way: one each three in the IB, one each two in the ESB and each one in the EPB. The not-illuminated one have been considered has having the same effect of the nearest one towards the entrance of the baffle.
- In the third step, spiders have been considered, splitting again analysis in three steps:
    - Direct illumination of spiders (for radiation angle of incidence smaller than 35°)
    - Spiders illuminated after 1 scattering on the baffle, and scattering again toward M1
    - Spiders illuminated after two scatters on the baffle

In all steps, different levels of scattering are allowed per object:

- 2 levels for the baffle
- 1 levels for the baffle vanes border (when non absorbing)
- 3 levels for the mirrors
- 1,2 or 3 levels for spiders scattering
- 5 levels for the BEO elements

Remaining objects have a scattering level of 5. Configurations

A ‘Baseline’ configuration has been first analysed, to serve as benchmark for possible variations. This standard configuration is characterized by

- EB painted with Aeroglaze306. Aeroglaze is simulated using the ‘multiplied’ version of the model (as described in 5.2.1 ). EBS diaphragms are coated with Acktar Fractal Black Coating.
- IB painted with MAP, whose BRDF is simulated using ‘standard’ model of Aeroglaze306
- All optical elements affected by dust contamination of 300ppm of Obscuration Factor
- M1 having 10A rms micro-roughness, all the remaining elements 5A rms.
- M1 borders black coated, with Acktar Fractal Black (simulated with the standard model, not multiplied)

After that, several other has been considered, each characterized by:

- the coating of the structure
- variations of the microroughness of mirrors
- coatings on M1 border

For all the configurations the wavelength of the illuminating radiation is 400nm.

## 6.3 Baseline Configuration

### 6.3.1 PST Values

PST values for the Baseline configuration are reported in Figure 12 and in Table 5

From the plot and the data appears that:

- Up to 20° scatter on structure (M1 and M2) is dominating
- From 20° to 30° scatter on the spiders is the main effect
- For angles larger than 30° scattering on the baffles is the dominating phenomenon.

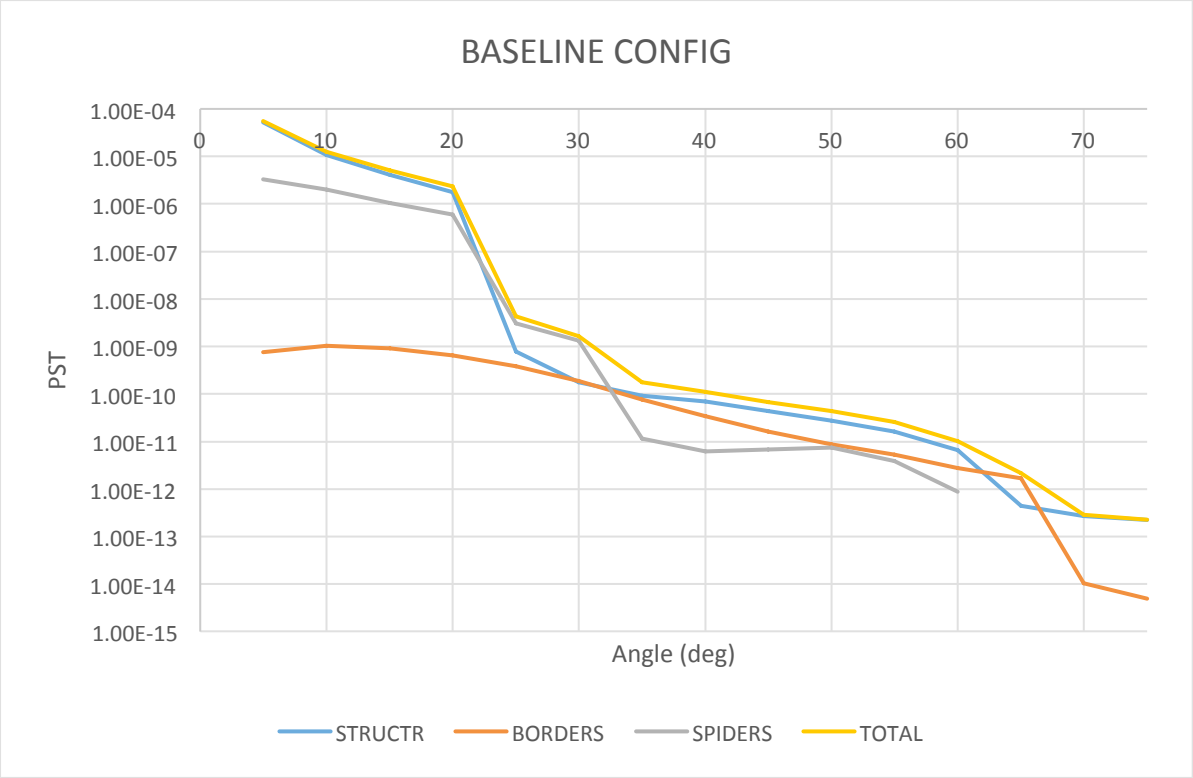


*Figure 12 PST of Baseline Configuration*

*Table 5: PST of Baseline Configuration, considering contribution from overall structure, borders of baffle and spiders*

| ANGLE | STRUCTR | BORDERS | SPIDERS | TOTAL |
|---|---|---|---|---|
| 5 | 5.19E-05 | 7.61E-10 | 3.33E-06 | 5.53E-05 |
| 10 | 1.06E-05 | 1.03E-09 | 1.98E-06 | 1.26E-05 |
| 15 | 4.10E-06 | 9.06E-10 | 1.04E-06 | 5.14E-06 |
| 20 | 1.76E-06 | 6.46E-10 | 6.05E-07 | 2.36E-06 |
| **25** | 7.82E-10 | 3.85E-10 | 3.11E-09 | 4.28E-09 |
| **30** | 1.75E-10 | 1.90E-10 | 1.31E-09 | 1.67E-09 |
| **35** | 9.22E-11 | 7.56E-11 | 1.14E-11 | 1.79E-10 |

| | | | | |
|---|---|---|---|---|
| **40** | 6.95E-11 | 3.46E-11 | 6.27E-12 | 1.10E-10 |
| **45** | 4.37E-11 | 1.64E-11 | 6.78E-12 | 6.69E-11 |
| **50** | 2.72E-11 | 8.62E-12 | 7.52E-12 | 4.33E-11 |
| **55** | 1.64E-11 | 5.35E-12 | 3.86E-12 | 2.56E-11 |
| **60** | 6.61E-12 | 2.73E-12 | 8.77E-13 | 1.02E-11 |
| **65** | 4.38E-13 | 1.70E-12 | | 2.14E-12 |
| **70** | 2.73E-13 | 1.05E-14 | | 2.84E-13 |
| **75** | 2.21E-13 | 4.85E-15 | | 2.26E-13 |

### 6.3.2 Straylight paths

In the following tables, the most energetic paths for angle of incidence of 5°, 25° 35° and 55° are reported. Data reported are the 'type' of paths (coming from analysis step involving all the structure, ST, only the borders, BD, or only the spiders SP); the number of rays collected, the energy of the path (in W, assuming a unitary irradiance source), and the objects involved in the path; meaning of the objects names can be read in Table 11Table 6.

They reflect what already highlighted in previous section§:

- At 5°, scattering is dominated by single scatter on M1 and M2 (including M1 borders)
- At 25°,paths involving spiders are the most energetic ones
- At 35° and 55°, scatter on the baffle (on the entire structure and on the borders) causes large part of straylight

Considering these results, appears that structural elements of BEO plays not an important role in straylight generation. This is the reason for which no vanes in BEO are foreseen.

*Table 6: meaning of elements names*

| OBJECT NAME | MEANING |
|---|---|
| **M1.MIRR, M2.MIRR** | M1 and M2 |
| **1……., 2……,3……** | Elements of IB , ESB, EPB respectively |
| **1.T,2.T,3.T** | Tubes of baffles (IB, ESB and EPB) |
| **m.V.n.W.F**<br>**m.V.n.W.B**<br>**mVnE.T** | Front face (toward EPB entrance),<br>back face<br>edge<br>of n-th vanes 'wall' in the m-th baffle. Vanes walls are numerated from entrance of the baffle toward M1. |
| **M2.sp…** | Spiders elements |

*Table 7: Most energetic paths @5°*

| TYPE | RAYS | FLUX /(W) | OBJECTS | | |
|---|---|---|---|---|---|
| **ST** | 182567 | 6.69E-03 | M1.MIRR | - | - |
| **ST** | 61547 | 1.11E-03 | M2.MIRR | - | - |

| | | | | | |
|---|---|---|---|---|---|
| **ST** | 8510 | 5.25E-04 | M1.BEXT.1 | - | - |
| **SP** | 122 | 4.00E-04 | M2.SP2.2 | - | - |
| **SP** | 52 | 1.60E-04 | M2.SP2.2 | - | - |
| **ST** | 72475 | 1.55E-04 | M1.MIRR | - | - |
| **ST** | 1591 | 1.32E-04 | M1.BINT.1 | - | - |
| **ST** | 2495 | 1.10E-04 | M1.BEXT.2 | - | - |
| **ST** | 1228 | 1.85E-05 | M1.BINT.2 | - | - |
| **ST** | 1426 | 7.33E-06 | M1.BEXT.3 | - | - |

*Table 8: Most energetic paths @25°*

| TYPE | RAYS | FLUX (W) | OBJECTS | | |
|---|---|---|---|---|---|
| **SP** | 21015 | 1.05E-07 | M2.SP1.1 | 1.V.2.W.F | - |
| **SP** | 16430 | 7.69E-08 | M2.SP1.1 | 1.V.4.W.F | - |
| **SP** | 14534 | 7.43E-08 | M2.SP1.1 | 1.V.3.W.F | - |
| **SP** | 12815 | 4.99E-08 | M2.SP1.1 | 1.V.5.W.F | - |
| **SP** | 13193 | 4.31E-08 | M2.SP1.1 | 1.V.6.W.F | - |
| **SP** | 17684 | 3.97E-08 | M2.SP1.1 | 1.V.1.W.F | - |
| **ST** | 41 | 2.06E-08 | M2.MIRR | 1.V.8.W.F | - |
| **SP** | 6986 | 1.87E-08 | M2.SP1.1 | 1.V.7.W.F | - |
| **ST** | 124 | 1.64E-08 | M2.MIRR | 1.V.6.W.F | - |
| **SP** | 7084 | 1.52E-08 | M2.SP1.1 | 1.V.8.W.F | - |
| **ST** | 39 | 9.95E-09 | M2.MIRR | 1.V.9.W.F | - |
| **ST** | 43 | 7.88E-09 | M2.MIRR | 1.V.7.W.F | - |
| **ST** | 107 | 7.04E-09 | M2.MIRR | 1.V.4.W.F | - |
| **ST** | 66 | 6.92E-09 | M2.MIRR | 1.V.5.W.F | - |
| **SP** | 16492 | 6.50E-09 | M2.SP3.1 | 1.V.6.W.F | - |
| **SP** | 16401 | 6.45E-09 | M2.SP2.1 | 1.V.6.W.F | - |
| **SP** | 11038 | 5.84E-09 | M2.SP2.1 | 1.V.8.W.F | - |
| **SP** | 10905 | 5.77E-09 | M2.SP3.1 | 1.V.8.W.F | - |
| **SP** | 2170 | 5.48E-09 | M2.SP1.1 | 1.T | - |
| **SP** | 9463 | 4.46E-09 | M2.SP2.1 | 1.V.7.W.F | - |
| **SP** | 14161 | 4.39E-09 | M2.SP3.1 | 1.V.5.W.F | - |
| **SP** | 14296 | 4.38E-09 | M2.SP2.1 | 1.V.5.W.F | - |
| **SP** | 9328 | 4.29E-09 | M2.SP3.1 | 1.V.7.W.F | - |
| **ST** | 62 | 4.26E-09 | M2.MIRR | 1.V.3.W.F | - |
| **SP** | 2375 | 3.96E-09 | M2.SP1.1 | 1.V.9.W.F | - |
| **SP** | 17195 | 3.76E-09 | M2.SP3.1 | 1.V.4.W.F | - |
| **SP** | 17341 | 3.73E-09 | M2.SP2.1 | 1.V.4.W.F | - |
| **SP** | 2012 | 3.52E-09 | M2.SP2.1 | 1.V.6.W.F | - |
| **SP** | 1692 | 3.11E-09 | M2.SP3.1 | 1.V.8.W.F | - |
| **SP** | 1849 | 3.09E-09 | M2.SP3.1 | 1.V.6.W.F | - |

| | | | | | |
|---|---|---|---|---|---|
| **SP** | 1674 | 3.08E-09 | M2.SP2.1 | 1.V.8.W.F | - |
| **BD** | 95696 | 2.88E-09 | M1.MIRR | 2.V.6.E.T | - |
| **BD** | 104578 | 2.79E-09 | M1.MIRR | 2.V.4.E.T | - |
| **BD** | 971 | 2.73E-09 | M1.MIRR | 3.V.2.E.T | - |
| **BD** | 104782 | 2.42E-09 | M1.MIRR | 2.V.2.E.T | - |
| **BD** | 100425 | 2.11E-09 | M1.MIRR | 2.V.0.E.T | - |

*Table 9: Most energetic paths @35°*

| TYPE | RAYS | FLUX | OBJECTS | | |
|---|---|---|---|---|---|
| **BD** | 925 | 1.03E-09 | M1.MIRR | 3.V.2.E.T | - |
| **BD** | 99554 | 8.69E-10 | M1.MIRR | 2.V.2.E.T | - |
| **BD** | 78785 | 8.50E-10 | M1.MIRR | 2.V.4.E.T | - |
| **BD** | 99730 | 7.51E-10 | M1.MIRR | 2.V.0.E.T | - |
| **ST** | 4417 | 6.68E-10 | M1.MIRR | 3.V.2.W.B | 2.V.0.W.F |
| **BD** | 6505 | 6.16E-10 | M1.BEXT.1 | 2.V.4.E.T | - |
| **BD** | 7240 | 5.43E-10 | M1.BEXT.1 | 2.V.2.E.T | - |
| **ST** | 7556 | 4.81E-10 | M1.MIRR | 2.V.0.W.B | 2.V.1.W.F |
| **ST** | 34605 | 4.75E-10 | M1.MIRR | 2.V.0.W.B | 2.V.1.W.F |
| **ST** | 34744 | 4.71E-10 | M1.MIRR | 2.V.1.W.B | 2.V.2.W.F |
| **ST** | 405 | 4.41E-10 | M1.BEXT.1 | 3.V.2.W.B | 2.V.0.W.F |
| **ST** | 6016 | 4.32E-10 | M1.MIRR | 2.V.1.W.B | 2.V.2.W.F |
| **ST** | 32920 | 4.27E-10 | M1.MIRR | 2.V.2.W.B | 2.V.3.W.F |
| **BD** | 7828 | 4.14E-10 | M1.BEXT.1 | 2.V.0.E.T | - |
| **ST** | 4605 | 4.08E-10 | M1.MIRR | 2.V.2.W.B | 2.V.3.W.F |
| **ST** | 32018 | 3.94E-10 | M1.MIRR | 2.V.3.W.B | 2.V.4.W.F |
| **BD** | 74 | 3.92E-10 | M1.BEXT.1 | 3.V.2.E.T | - |
| **ST** | 245 | 3.68E-10 | M1.BEXT.1 | 2.T | 2.T |
| **ST** | 25960 | 3.57E-10 | M1.MIRR | 2.V.4.W.B | 2.V.5.W.F |
| **BD** | 1 | 3.51E-10 | BEO.DIA.PM | 2.V.0.E.T | - |
| **ST** | 148 | 3.35E-10 | M1.BEXT.1 | 2.V.4.W.B | 2.V.5.W.F |
| **ST** | 2869 | 3.29E-10 | M1.MIRR | 2.V.3.W.B | 2.V.4.W.F |
| **ST** | 1524 | 3.13E-10 | M1.MIRR | 2.V.4.W.B | 2.V.5.W.F |
| **ST** | 2390 | 3.08E-10 | M1.BEXT.1 | 2.V.3.W.B | 2.V.4.W.F |
| **ST** | 1929 | 2.70E-10 | M1.BEXT.1 | 2.V.4.W.B | 2.V.5.W.F |
| **ST** | 567 | 2.65E-10 | M1.BEXT.1 | 2.V.0.W.B | 2.V.1.W.F |
| **ST** | 2433 | 2.64E-10 | M1.BEXT.1 | 2.V.0.W.B | 2.V.1.W.F |
| **ST** | 411 | 2.62E-10 | M1.BEXT.1 | 2.V.1.W.B | 2.V.2.W.F |
| **BD** | 113 | 2.58E-10 | M2.MIRR | 3.V.2.E.T | - |
| **ST** | 2062 | 2.53E-10 | M1.BEXT.1 | 2.V.1.W.B | 2.V.2.W.F |
| **ST** | 1937 | 2.37E-10 | M1.BEXT.1 | 2.V.2.W.B | 2.V.3.W.F |
| **SP** | 478771 | 2.35E-10 | M2.SP3.1 | 1.T | 2.T |

*Table 10: Most energetic paths @55°*

| TYPE | RAYS | FLUX | OBJECTS | | |
|---|---|---|---|---|---|
| **ST** | 6601 | 5.43E-10 | M1.MIRR | 3.V.2.W.B | 3.V.3.W.F |
| **ST** | 491 | 5.06E-10 | M1.BEXT.1 | 3.V.2.W.B | 3.V.3.W.F |
| **BD** | 821 | 3.61E-10 | M1.MIRR | 3.V.2.E.T | - |
| **ST** | 3326 | 2.97E-10 | M1.MIRR | 3.V.2.W.B | 2.T |
| **BD** | 62 | 1.72E-10 | M1.BEXT.1 | 3.V.2.E.T | - |
| **ST** | 19 | 1.43E-10 | M1.BEXT.1 | 2.T | 2.T |
| **ST** | 1982 | 1.34E-10 | M1.MIRR | 3.V.2.W.B | 2.V.0.W.F |
| **ST** | 189 | 1.21E-10 | M1.BEXT.1 | 3.V.2.W.B | 2.T |
| **ST** | 88 | 1.02E-10 | M1.BINT.1 | 3.V.2.W.B | 3.V.3.W.F |
| **ST** | 127 | 7.51E-11 | M1.BEXT.1 | 3.V.2.W.B | 2.V.0.W.F |
| **ST** | 112 | 6.88E-11 | M1.BEXT.2 | 3.V.2.W.B | 3.V.3.W.F |
| **SP** | 55111 | 6.70E-11 | M2.SP3.1 | 1.V.2.W.F | 2.T |
| **SP** | 303 | 6.63E-11 | M2.SP2.1 | 3.V.2.W.B | 2.T |
| **BD** | 41386 | 6.23E-11 | M1.MIRR | 2.V.0.E.T | - |
| **ST** | 8464 | 5.97E-11 | M1.MIRR | 2.V.0.W.B | 2.T |
| **BD** | 93 | 5.71E-11 | M2.MIRR | 3.V.2.E.T | - |
| **ST** | 10 | 5.50E-11 | M1.BEXT.2 | 2.T | 2.T |
| **SP** | 120649 | 5.30E-11 | M2.SP2.1 | 1.T | 2.T |

## 6.4 Variations

As done in the previous revision of this report, we here present some variations of the Baseline Configuration, based on different black coatings for EB and for border of M1, and on modification of micro-roughness of M1 and M2.

### 6.4.1 Coating Configurations

As stated above, baseline configuration foresees a system with:

- A ‘mixed coating’ baffle assembly, partially coated with Acktar Fractal Black; due to possible problems with this coating (both from the point of view of manufacturing and logistic) is possible that a solution completely painted with Aeroglaze will be adopted.
- M1 Borders coated with Acktar Fractal black. Again this is not trivial from the point of view of manufacturing, cost and logistics. So options with different coatings on the border have to be considered. A different option may foresee a system with M1 reflective border; this possibility is at the moment not baseline not for straylight reasons, but for photometric stability issues.

Given that, 6 possible configurations (5+baseline) are reported in the following table, for the angular range [25°-65°]:

- 2 with a totally reflective M1, one with the mixed baffle coating (FB), one with the baffle uniformly painted in Aeroglaze (AG)
- 2 with an M1 border black coated with Acktar Fractal Black, again with the two possible coatings combinations (AG+S(FB) and FB+S(FB), this being the baseline configuration)
- 2 with M1 borders coated with Aeroglaze (AG+S(AG), FB+S(AG)

| ANGLE | FB | AG | AG+S(FB) | FB+S(FB) (B) | AG+S(AG) | FS+S(AG) |
|---|---|---|---|---|---|---|
| **25** | 4.41E-09 | 4.36E-09 | 4.37E-09 | 4.28E-09 | 4.81E-09 | 4.64E-09 |
| **30** | 1.79E-09 | 1.85E-09 | 1.79E-09 | 1.67E-09 | 1.92E-09 | 2.00E-09 |
| **35** | 1.10E-10 | 1.78E-10 | 2.94E-10 | 1.79E-10 | 3.41E-10 | 2.07E-10 |
| **40** | 6.67E-11 | 1.08E-10 | 1.76E-10 | 1.10E-10 | 2.13E-10 | 1.26E-10 |
| **45** | 4.10E-11 | 7.04E-11 | 1.07E-10 | 6.69E-11 | 1.34E-10 | 8.15E-11 |
| **50** | 2.82E-11 | 3.66E-11 | 6.74E-11 | 4.33E-11 | 6.69E-11 | 5.31E-11 |
| **55** | 1.75E-11 | 1.99E-11 | 4.04E-11 | 2.56E-11 | 4.36E-11 | 3.36E-11 |
| **60** | 5.96E-12 | 6.10E-12 | 1.16E-11 | 1.02E-11 | 1.16E-11 | 1.40E-11 |
| **65** | 8.50E-13 | 2.65E-12 | 1.93E-12 | 2.14E-12 | 2.10E-12 | 1.42E-12 |

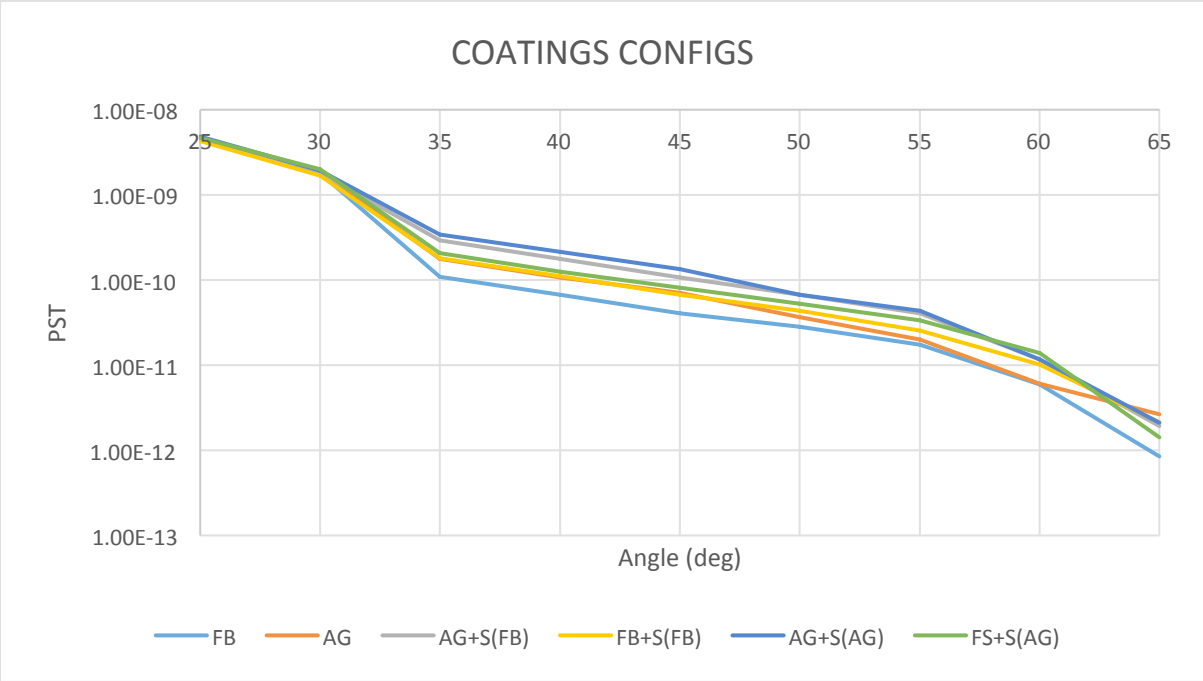


From data and plots appears that up to 30deg, where IB and spiders are dominating, few differences are present among the configurations, while at larger angles:

- Mixed coating configurations seems to be favourable
- A totally reflecting border for M1 is better form the point of view of SL (but, again, this solution has consequences from the point of view of photometric stability)
- Aeroglaze M1 borders may cause a worsening of PST of typically 20% order of magnitude

### 6.4.2 Mirrors Microroughness Configurations

Microroughness of 10A on M1 (and of 5A on M2) may be not trivial to obtain.

In this section we present PST values for 2 coating configurations, assuming a variation in Mirrors microroughness, so to evaluate what would be the impact in flight model.

First configuration is the Baseline one (ESB diaphragms coated with Acktar Fractal Balck, all the remaining elements coated with Aeroglaze, border of M1 reflective)

Second configuration is a worst case configuration, in which all elements are coated with Aeroglaze Z306.

Both configurations have a 300ppm Obscuration factor on the optics, and all the optics have the same microroughness values. Please note that even the 10A configuration gives higher PST values with respect to values presented in previous sections, due to the rise of microroughness of M2.

From the plots and the data it is clear that increasing the Microroughness may have a big impact even for a relatively small amount (from 10 to 13 A); it is then mandatory to keep microroughness as small as possible.

#### 6.4.2.1 Configuration 1

| Angle | 10 Angstrom | 13 Angstrom | 17 Angstrom | 20 Angstrom |
|---|---|---|---|---|
| **30** | 1.9E-09 | 2.1E-09 | 2.4E-09 | 2.7E-09 |
| **35** | 1.6E-10 | 2.0E-10 | 3.3E-10 | 4.6E-10 |
| **40** | 8.2E-11 | 1.3E-10 | 2.2E-10 | 2.8E-10 |
| **45** | 6.2E-11 | 8.1E-11 | 1.2E-10 | 1.6E-10 |
| **50** | 3.2E-11 | 6.4E-11 | 7.6E-11 | 9.4E-11 |
| **55** | 2.0E-11 | 2.8E-11 | 3.9E-11 | 6.8E-11 |
| **60** | 8.4E-12 | 1.5E-11 | 2.1E-11 | 2.4E-11 |
| **65** | 1.5E-12 | 2.6E-12 | 9.9E-12 | 9.1E-12 |
| **70** | 2.2E-13 | 3.2E-13 | 5.1E-13 | 6.7E-13 |
| **75** | 1.6E-13 | 2.3E-13 | 3.8E-13 | 5.1E-13 |

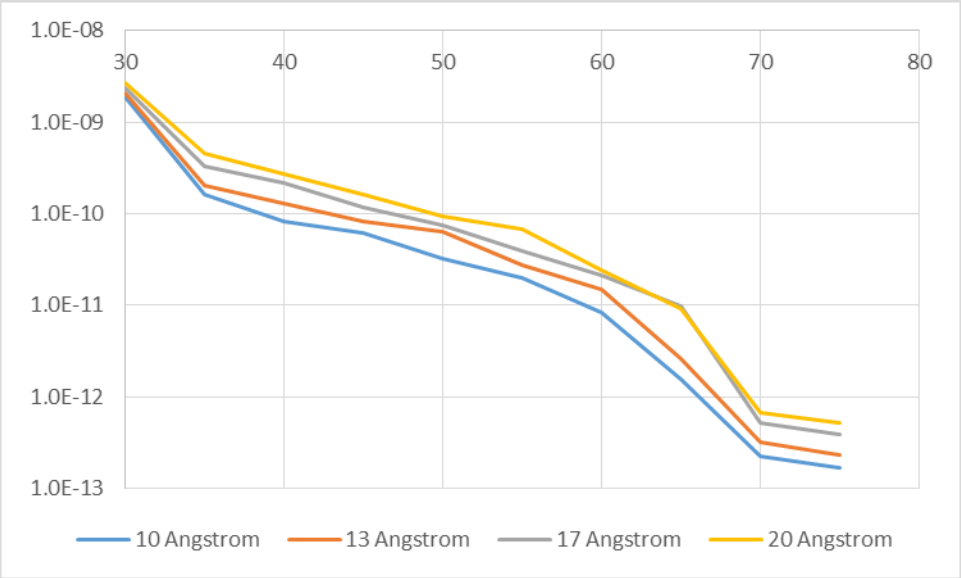


### 6.4.2.2 Configuration 2

| angle | 10 Angstrom | 13 angstrom | 17Angstrom | 20 Angstrom |
|---|---|---|---|---|
| **35** | 3.8E-10 | 4.9E-10 | 6.7E-10 | 8.6E-10 |
| **40** | 2.2E-10 | 2.8E-10 | 4.1E-10 | 5.1E-10 |
| **45** | 1.4E-10 | 1.7E-10 | 2.3E-10 | 2.9E-10 |
| **50** | 7.3E-11 | 1.1E-10 | 1.3E-10 | 1.9E-10 |
| **55** | 4.3E-11 | 4.9E-11 | 6.8E-11 | 8.1E-11 |
| **60** | 1.3E-11 | 1.5E-11 | 3.3E-11 | 3.8E-11 |
| **65** | 2.7E-12 | 2.7E-12 | 4.8E-12 | 4.9E-12 |
| **70** | 6.9E-13 | 7.8E-13 | 9.6E-13 | 1.5E-12 |
| **75** | 5.4E-13 | 5.7E-13 | 7.9E-13 | 1.1E-12 |

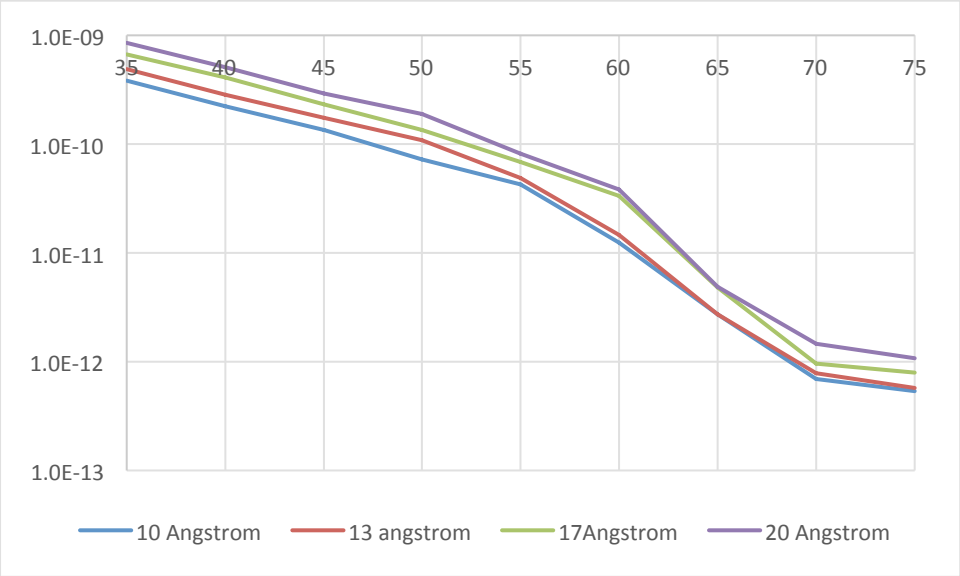


## 6.5 Previous revisions Configuration

In this section we report some of the analyses performed in previous versions of this report.

Some analyses has not been repeated since no more applicable (e.g. baffle completely coated with Acktar coating has been judged unfeasible; configurations with few vanes in the IB are disregarded since baffle has been realized with all vanes).

Some are reported as they were in previous version of the report, because variations introduced would not influence conclusion of the analysis (e.g. On Axis ghost scatter and ghost, or sensitivity to baffle vanes displacement.

All these analyses are relative to a 'old' baseline configuration characterized by:

- No M1 borders (entire M1 surface has nominal performances)
- No oversize of pupils
- All baffles (IB and EB) coated with Aeroglaze z306 (old BRDF model, not multiplied)
- 90% reflective coating on mirrors and 99% AR coating on lenses
- M1 Microroughness 10A, M2,M3 and lenses microroughness 5A
- All elements affected by 300ppm Obscuration factor
- Presence of Pupil Mask

### 6.5.1 Old Baseline Configuration PST values

The obtained values of PST for the Old Baseline Configuration are reported in Figure 13 and Table 11.

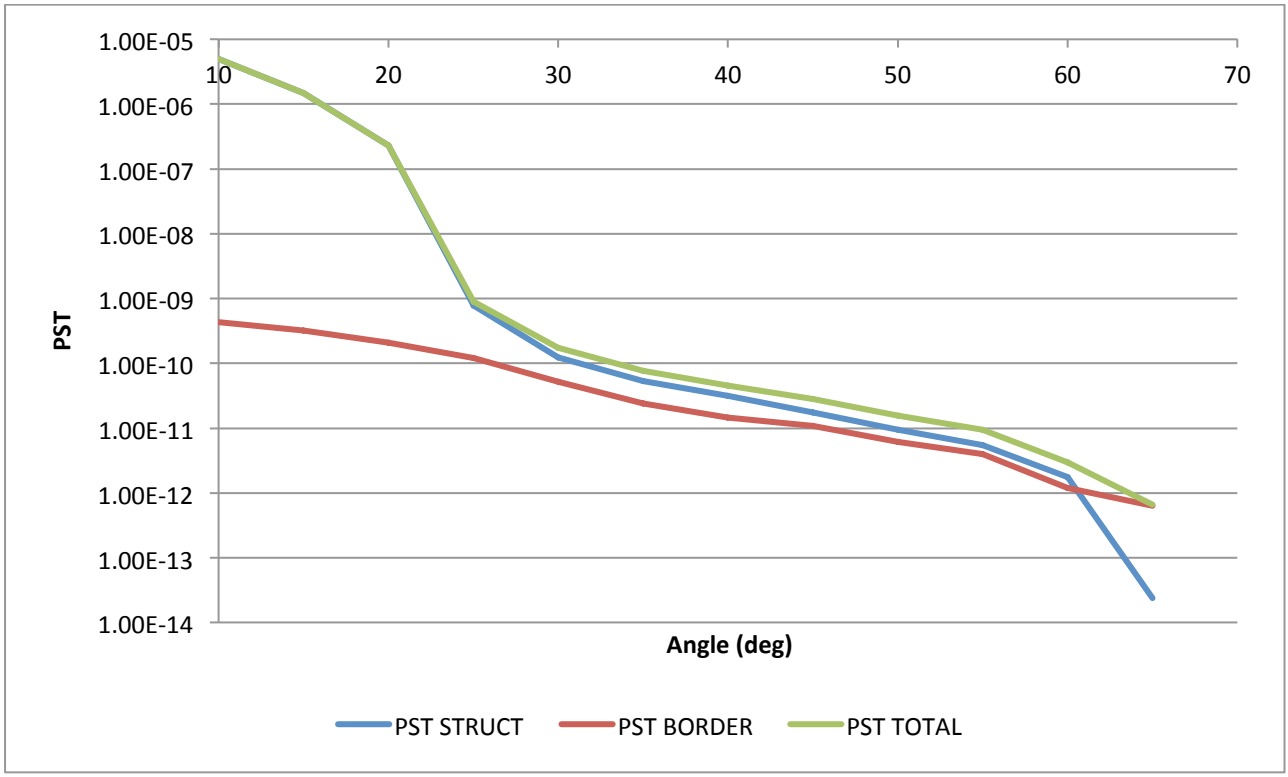


*Figure 13: PST of Standard Configuration*

*Table 11: PST of Standard Configuration, indicating contributions of all the structure and of only the borders of the baffle vanes.*

| ANGLE | PST STRUCT | PST BORDER | PST TOTAL |
|---|---|---|---|
| **10** | 4.91E-06 | 4.33E-10 | 4.91E-06 |
| **15** | 1.5E-06 | 3.24E-10 | 1.5E-06 |
| **20** | 2.28E-07 | 2.11E-10 | 2.28E-07 |
| **25** | 7.78E-10 | 1.21E-10 | 8.99E-10 |
| **30** | 1.23E-10 | 5.21E-11 | 1.75E-10 |
| **35** | 5.34E-11 | 2.39E-11 | 7.72E-11 |
| **40** | 3.14E-11 | 1.45E-11 | 4.59E-11 |
| **45** | 1.77E-11 | 1.09E-11 | 2.86E-11 |
| **50** | 9.42E-12 | 6.11E-12 | 1.55E-11 |
| **55** | 5.5E-12 | 3.97E-12 | 9.47E-12 |
| **60** | 1.77E-12 | 1.21E-12 | 2.99E-12 |
| **65** | 2.39E-14 | 6.38E-13 | 6.61E-13 |

### 6.5.2 Baffles and vanes displacements sensitivity

#### 6.5.2.1 EB displacements sensitivity

EB has been displaced (as in Figure 14) as a whole along XY and Z (Z is the optical axis) of +1mm, to simulate error in alignment of BCA and TEL.

PST resulting from simulations are reported in Figure 15 and in Table 12.

Results highlight no changes in PST (variations may be considered due to statistics); assuming that borders of vanes, even if displaced, will not behave differently than in the standard case, the total PST will be not changed by this kind of alignment errors.

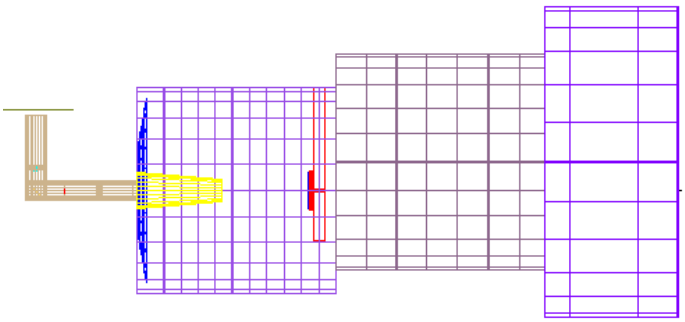

*Figure 14 Displaced EB (exaggerated)*

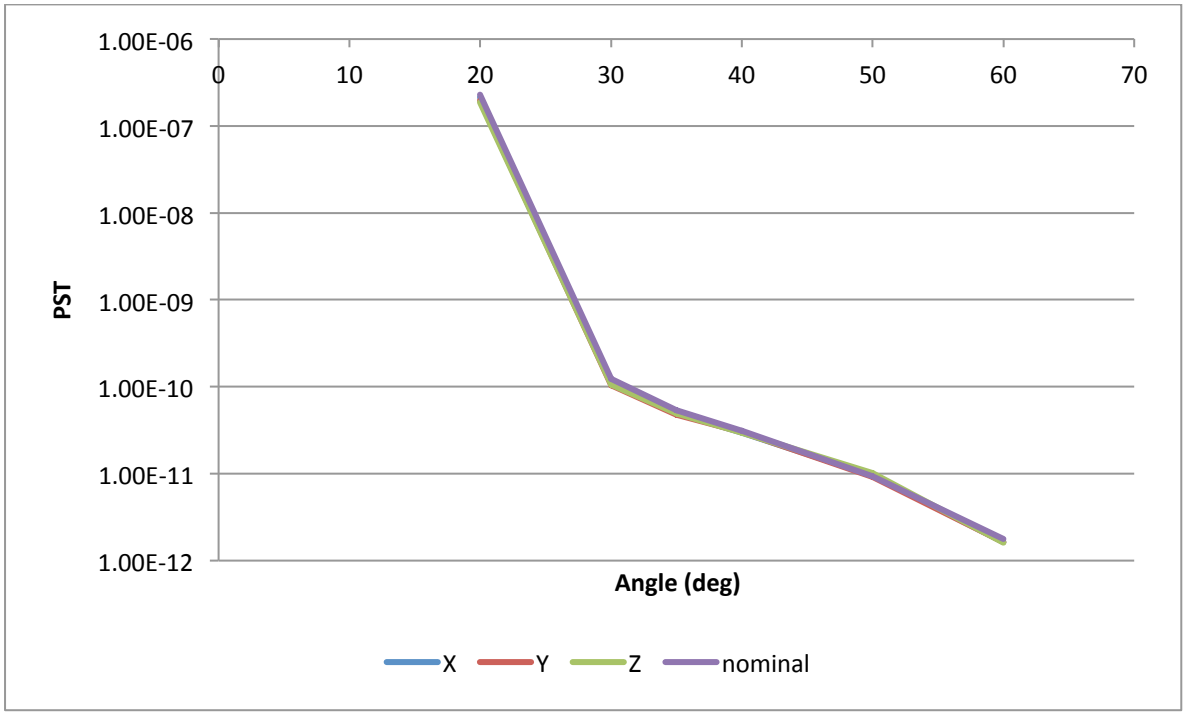


*Figure 15: PST (not considering vanes border) for EB translation along XYZ axis*

*Table 12: PST (not considering vanes border) for EB translation along XYZ axis*

| angle | X | Y | Z | nominal |
|---|---|---|---|---|

| | | | | |
|---|---|---|---|---|
| **20** | 2.14E-07 | 1.98E-07 | 1.88E-07 | 2.28E-07 |
| **30** | 1.09E-10 | 1.03E-10 | 1.06E-10 | 1.23E-10 |
| **35** | 5.00E-11 | 4.73E-11 | 4.96E-11 | 5.34E-11 |
| **40** | 2.97E-11 | 3.01E-11 | 2.96E-11 | 3.14E-11 |
| **50** | 9.44E-12 | 9.23E-12 | 1.02E-11 | 9.42E-12 |
| **60** | 1.64E-12 | 1.63E-12 | 1.61E-12 | 1.77E-12 |

#### 6.5.2.2 Random displacement of vanes +/-Z

While the external tubes of the baffles (IB & EB) are kept in the nominal positions, the vanes are placed with an error along optical axis; each vane has a random error extracted from a uniform distribution ranging from -0.5 to 0.5 mm, or from -1 to 1 mm, as depicted (exaggerated) in Figure 16.

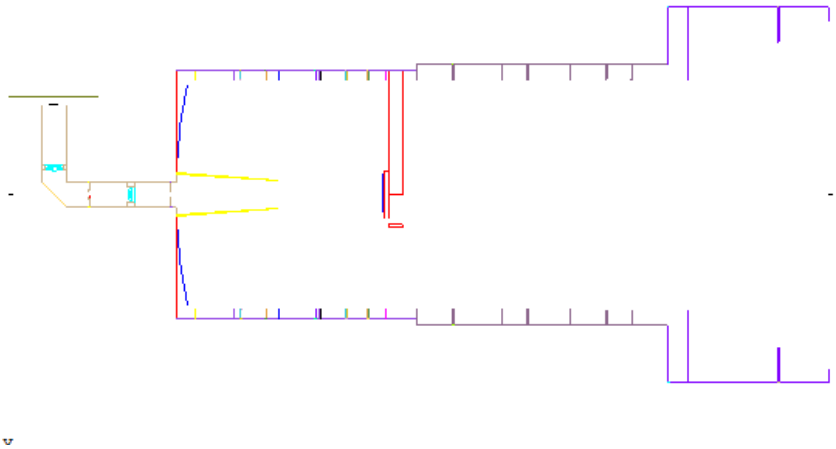

*Figure 16: Vanes placed with errors along the optical axis (exaggerated)*

Data in Figure 17 and Table 13 shows that no major degradation of PST for this kind of errors may be expected, even if the variation @25 suggests that a deeper analysis may be interesting. Has to be noted that the two configurations (0.5 and 1 mm max displacements) are based on the same displacements rescaled (the random numbers generator restarted at the same state), and so the fact that both shows the biggest increase @25 is in this sense explicable.

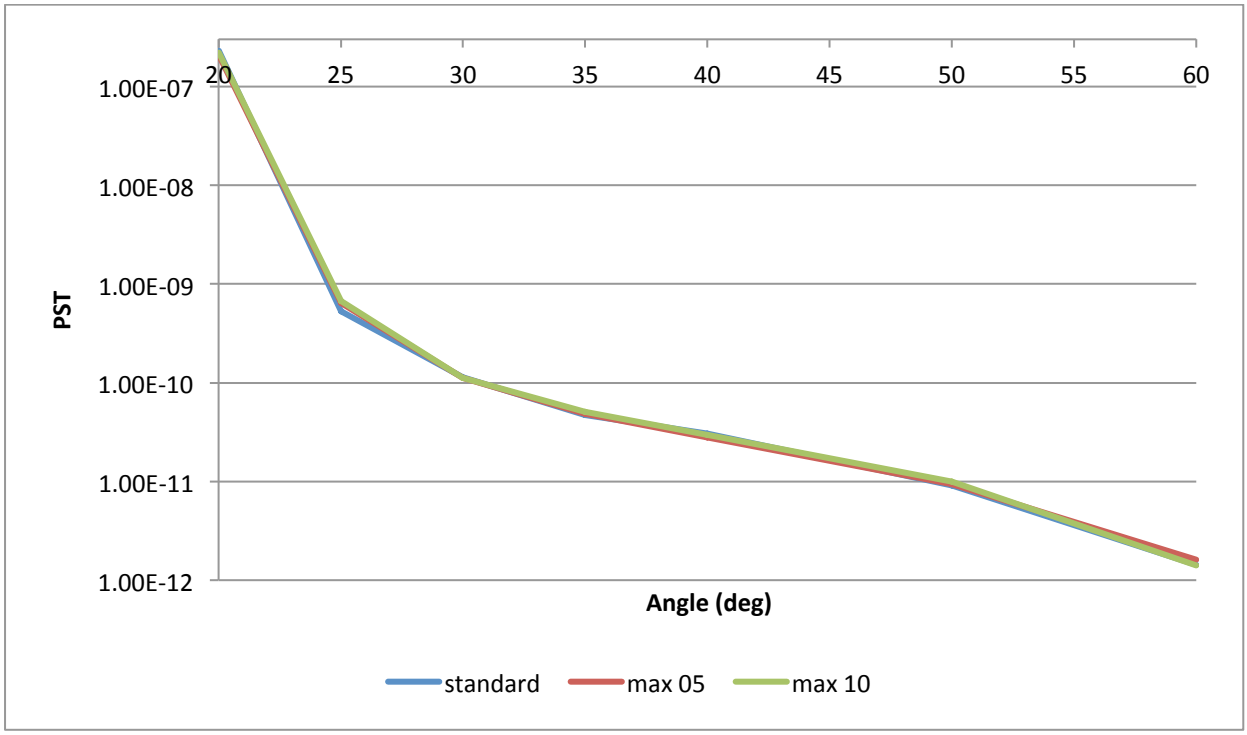


*Figure 17*

*Table 13*

| angle | standard | max 05 | max 10 | Ratio standard | max 05 | max 10 |
|---|---|---|---|---|---|---|
| **20** | 2.30E-07 | 2.07E-07 | 2.19E-07 | 1.00 | 0.90 | 0.95 |
| **25** | 5.29E-10 | 6.42E-10 | 6.72E-10 | 1.00 | 1.21 | 1.27 |
| **30** | 1.13E-10 | 1.12E-10 | 1.13E-10 | 1.00 | 0.99 | 1.00 |
| **35** | 4.72E-11 | 4.89E-11 | 5.10E-11 | 1.00 | 1.03 | 1.08 |
| **40** | 3.04E-11 | 2.80E-11 | 2.96E-11 | 1.00 | 0.92 | 0.97 |
| **50** | 9.06E-12 | 9.35E-12 | 9.90E-12 | 1.00 | 1.03 | 1.09 |
| **60** | 1.43E-12 | 1.60E-12 | 1.41E-12 | 1.00 | 1.12 | 0.99 |

At 25 deg we have repeated the simulations (for 0,0.5 and 1mm max displacement) for 100 times, considering absorbing borders and only one level of scattering on the baffle (path responsible for the vast majority of straylight)

Results are reported in Table 14and in Figure 18

*Table 14*

| | 0 mm | 0.5 mm | 1.0 mm |
|---|---|---|---|

| | | | |
|---|---|---|---|
| **Mean** | 5.16E-10 | 5.14E-10 | 5.15E-10 |
| **StDev** | 3.29E-11 | 3.08E-11 | 3.72E-11 |
| **StDev perc** | 6.4% | 6.0% | 7.2% |

From this data, we may assume for the calculated PST values an error of 3-5stdev, so approx. 20%-30%.

Given the mean values obtained it is clear that values @25deg are compatible, and vanes displacement doesn't introduce PST degradation.

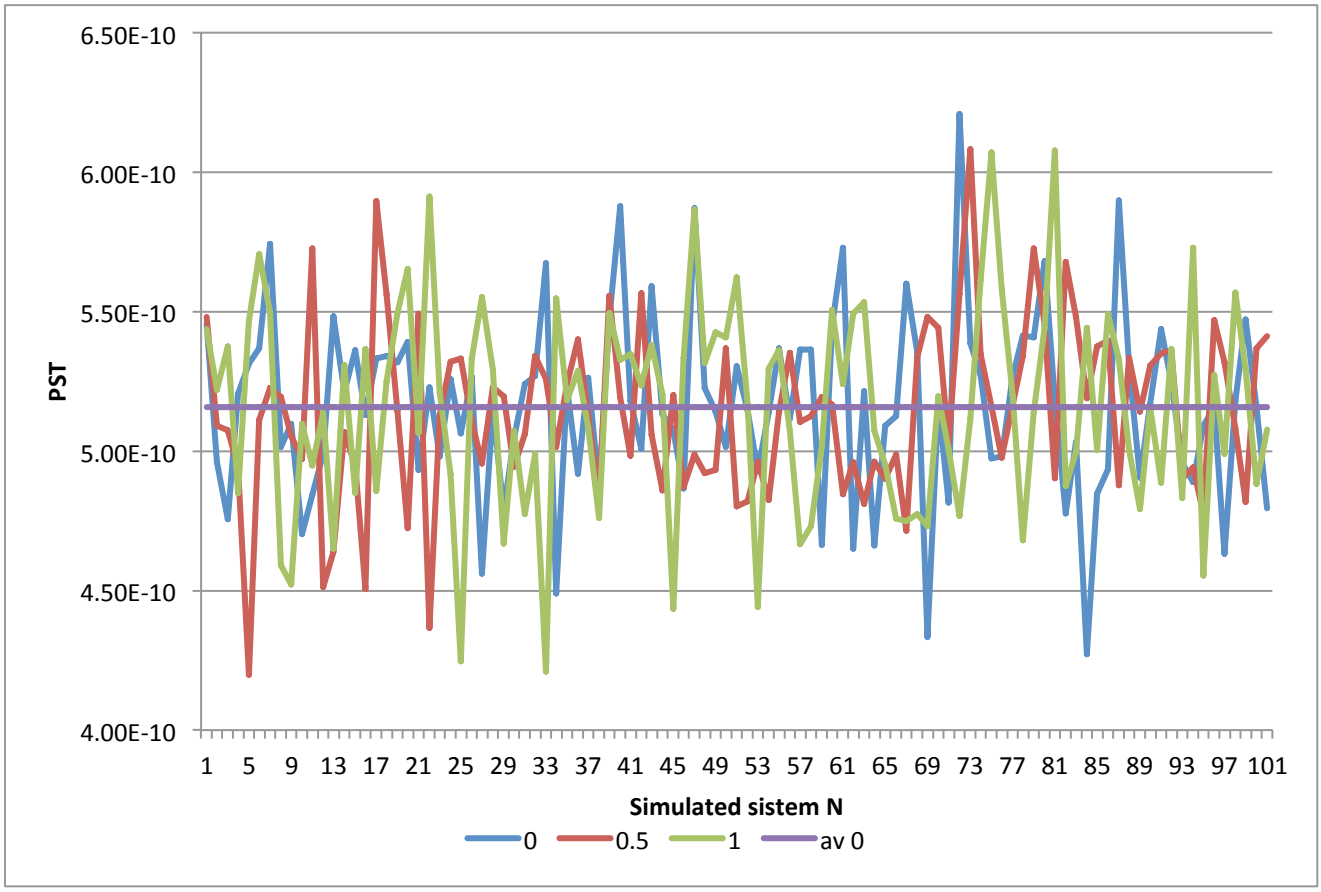


*Figure 18*

# 6.6 Variations

## 6.6.1 Dust Contamination

Dust contamination has been evaluated for three levels of Cleanliness level of Primary and Secondary mirrors of the telescope: 300, 504 and 1001ppm of dust coverage.
BEO optics are always at 300ppm.

All non-optical surfaces are coated with Aeroglaze, except a configuration with Fractal Black, reported as reference.

Results for a 'Clean' configuration are reported too as reference.

*Table 15: PST of configurations with different Cleanliness Levels*

| angle | NO DUST | 300PPM | 500PPM | 1000PPM | 300PPM(AKTAR) |
|---|---|---|---|---|---|
| **10** | 3.86E-06 | 4.72E-06 | 5.66E-06 | 8.21E-06 | 4.72E-06 |
| **15** | 9.9E-07 | 1.25E-06 | 1.4E-06 | 1.98E-06 | 1.19E-06 |
| **20** | 1.57E-07 | 2.35E-07 | 2.55E-07 | 3.91E-07 | 2.22E-07 |
| **25** | 3.99E-10 | 7.83E-10 | 9.79E-10 | 1.82E-09 | 5.00E-10 |
| **30** | 1.02E-10 | 1.64E-10 | 2.1E-10 | 3.52E-10 | 1.04E-10 |
| **35** | 5.01E-11 | 7.57E-11 | 8.26E-11 | 1.31E-10 | 3.73E-11 |
| **40** | 3.03E-11 | 4.57E-11 | 5.32E-11 | 8.09E-11 | 1.84E-11 |
| **45** | 1.87E-11 | 2.54E-11 | 3.06E-11 | 4.95E-11 | 9.79E-12 |
| **50** | 1E-11 | 1.45E-11 | 1.76E-11 | 2.88E-11 | 4.46E-12 |
| **55** | 5.25E-12 | 8.87E-12 | 9.64E-12 | 1.51E-11 | 2.08E-12 |
| **60** | 1.78E-12 | 3.11E-12 | 3.62E-12 | 5.55E-12 | 7.98E-13 |
| **65** | 2.94E-13 | 5.42E-13 | 6.07E-13 | 6.77E-13 | 1.42E-13 |

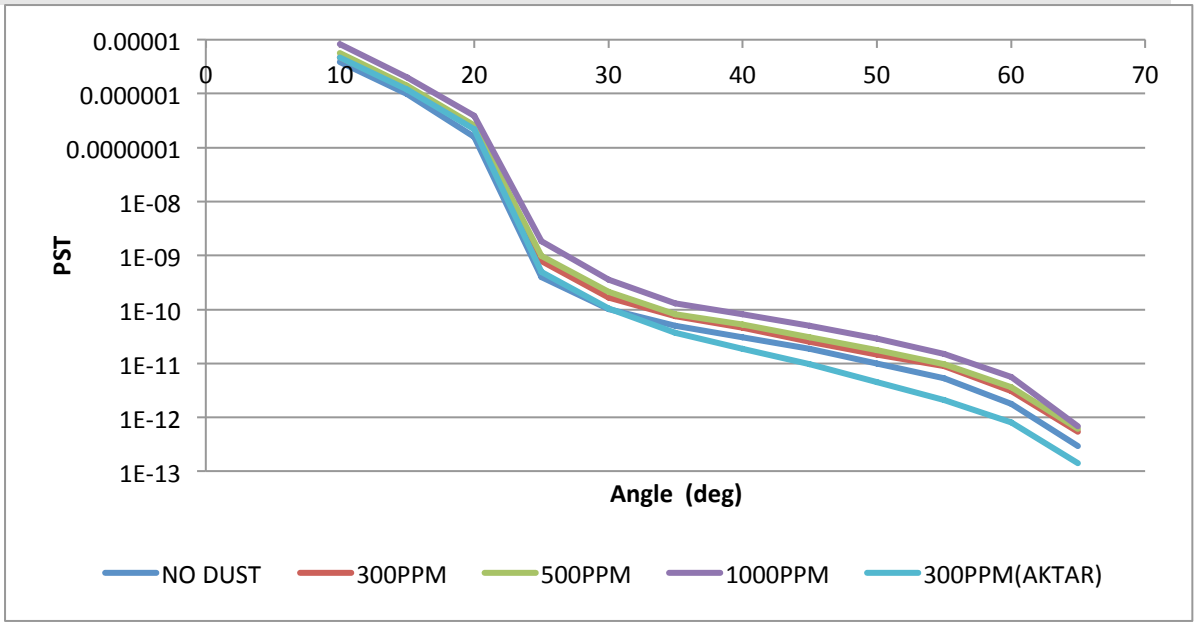


*Figure 19: PST of configurations with different Cleanliness Levels*

### 6.6.2 Geometry Configurations

#### 6.6.2.1 Vanes edges tip orientation

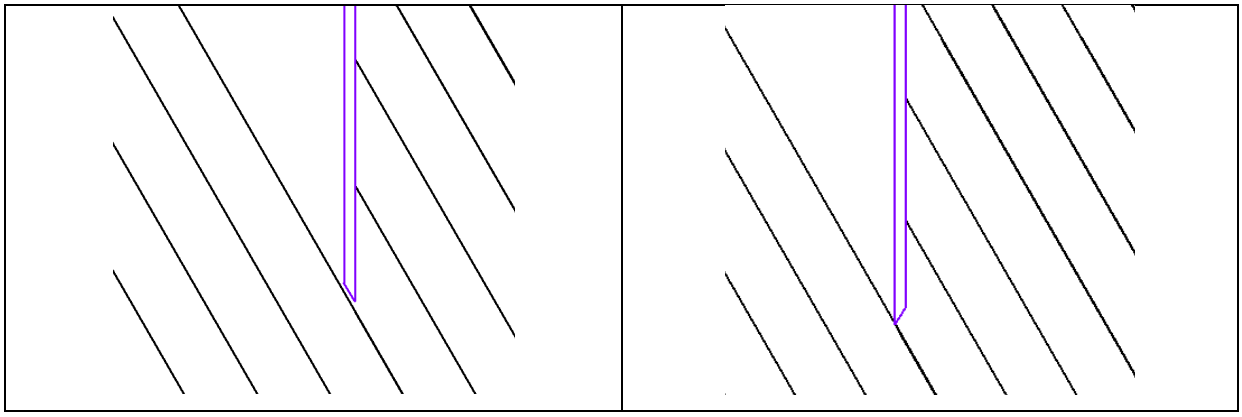

*Figure 20: Chamfer orientations*

In the standard configuration, all the edges of the vanes are oriented so that the 30° inclined section (the chamfer) is orientated toward the entrance of the baffle (the +X direction). From geometrical considerations (see e.g. RD13), may be favourable to orient the chamfers toward the primary mirror, for those vanes that may be reached only by radiation with an incident angle less than 60° (given that the inclination of Cheops Baffles Chamfers is 30°).

This corresponds in the CIS to the vanes edges of ESB and IB, as can be seen in Figure 21.

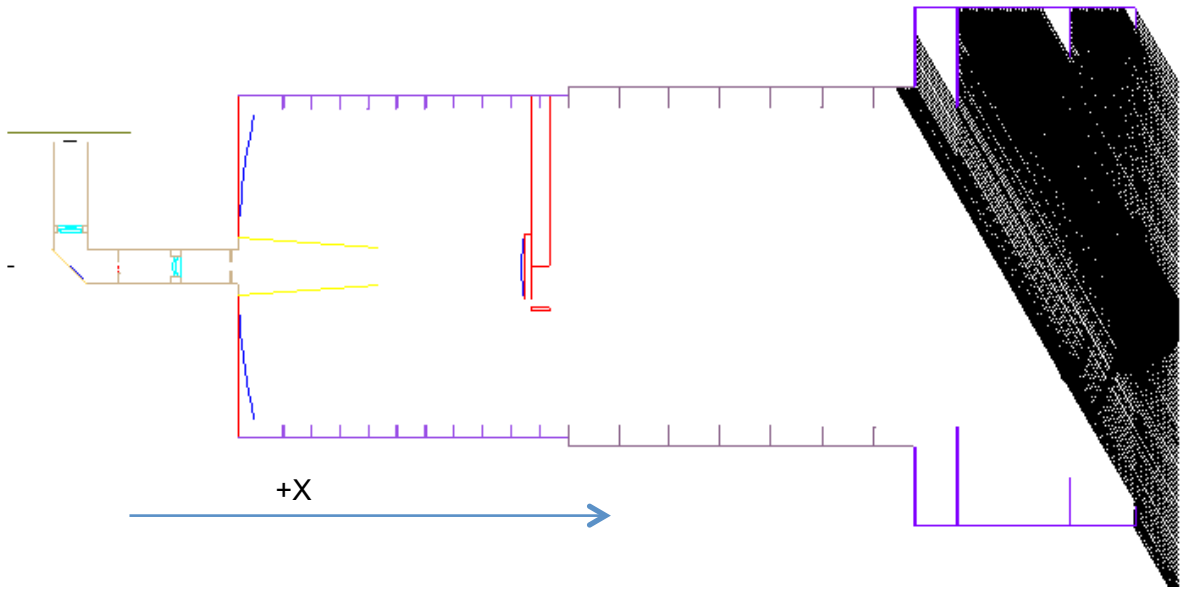


*Figure 21: Radiation impinging @60 deg*

To test this, simulations have been performed with only the chamfers (in the baffles) allowed to scatter light, once with all the chamfers oriented toward +X (Baffle entrance) direction and once toward –X (Primary Mirror). Figure *22* and Table 16 resume the results.

*Table 16: PST due to chamfers directed in +X (toward entrance of the baffle) and –X (toward M1), and PST of Standard Configuration as reference*

| ANGLE | +X | -X | STANDARD |
|---|---|---|---|
| 10 | 5.39812E-11 | 1.73179E-11 | 4.90709E-06 |
| 20 | 5.0247E-11 | 1.386E-11 | 2.28287E-07 |
| 30 | 7.37174E-12 | 2.265E-12 | 1.7548E-10 |
| 40 | 9.84993E-13 | 4.77451E-13 | 4.58934E-11 |
| 50 | 1.64887E-13 | 8.6264E-14 | 1.55313E-11 |
| 70 | 8.89594E-18 | 1.28998E-15 | - |

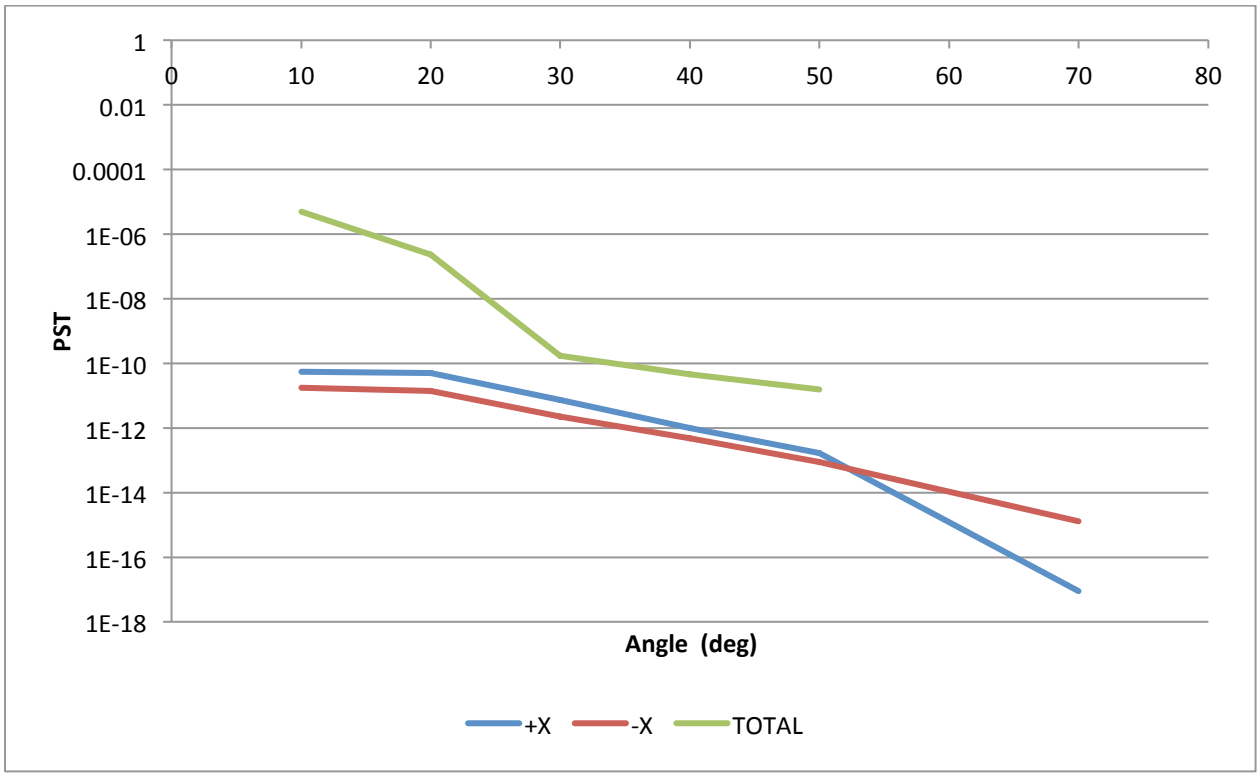


*Figure 22 PST due to chamfers with two different orientations*

From simulation results is clear that orienting toward the primary mirror the chamfers of IB and ESB may be favourable, even if the advantage is small wrt total PST.

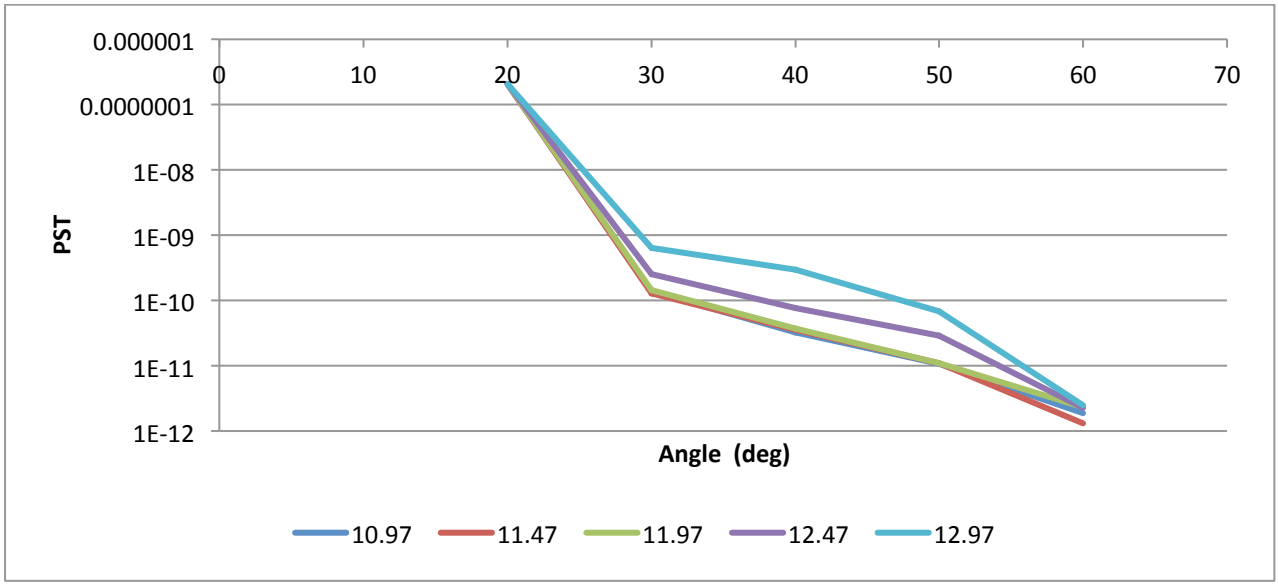


*Figure 23: PST Values for different values of LS diameter*

### 6.6.2.2 Pupil Mask

The Pupil Mask PM is located on the pupil plane and is essentially an opaque structure shaped as the spiders and M2 back shadow. Its purpose is to block straylight mainly from these structures without vignette the on axis field. In the reality, the Pupil Mask behaviour may be a little bit more complex:

- To correctly work, it has to be a little bit oversized wrt to the geometrical dimensions: The image of the spiders in the pupil plane is aberrated, and to totally shield the straylight coming from the spiders, the pupil mask 'spiders' has to be ~1.5 times larger than what calculated. This causes a vignetting.

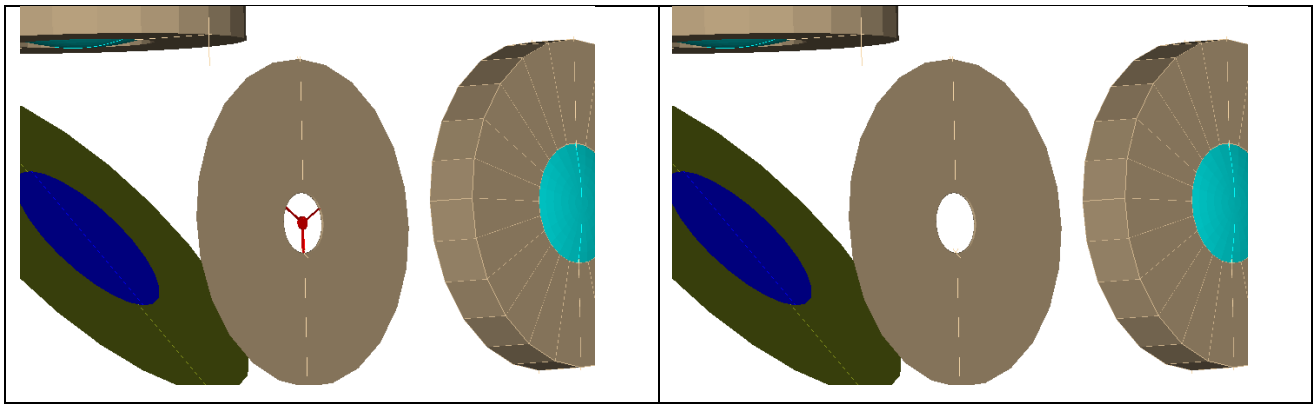

*Figure 24: Presence / absence of the Pupil mask (in red)*

- The dimensions of the PM are very small: the width of the 'spiders' is ~150micron. Align and keep aligned such a structure may be not trivial at all

It has been investigated then the possibility to drop this element and check what would be the effect on the PST.

First of all, the spiders (and the M2 back) are directly illuminated for radiation incident at angles <30°. A simple rectangular spider will then scatter toward primary mirror and directly be viewed by the Cheops detector. The result of a simulation aimed explicitly to highlight this is in Figure 25 (blue line; green line is the standard configuration, given as reference).

The simulations is realized using a source of 7e6 rays, but only those directly hitting the spiders are allowed to proceed, splitting in 1000 rays scattering toward M1.

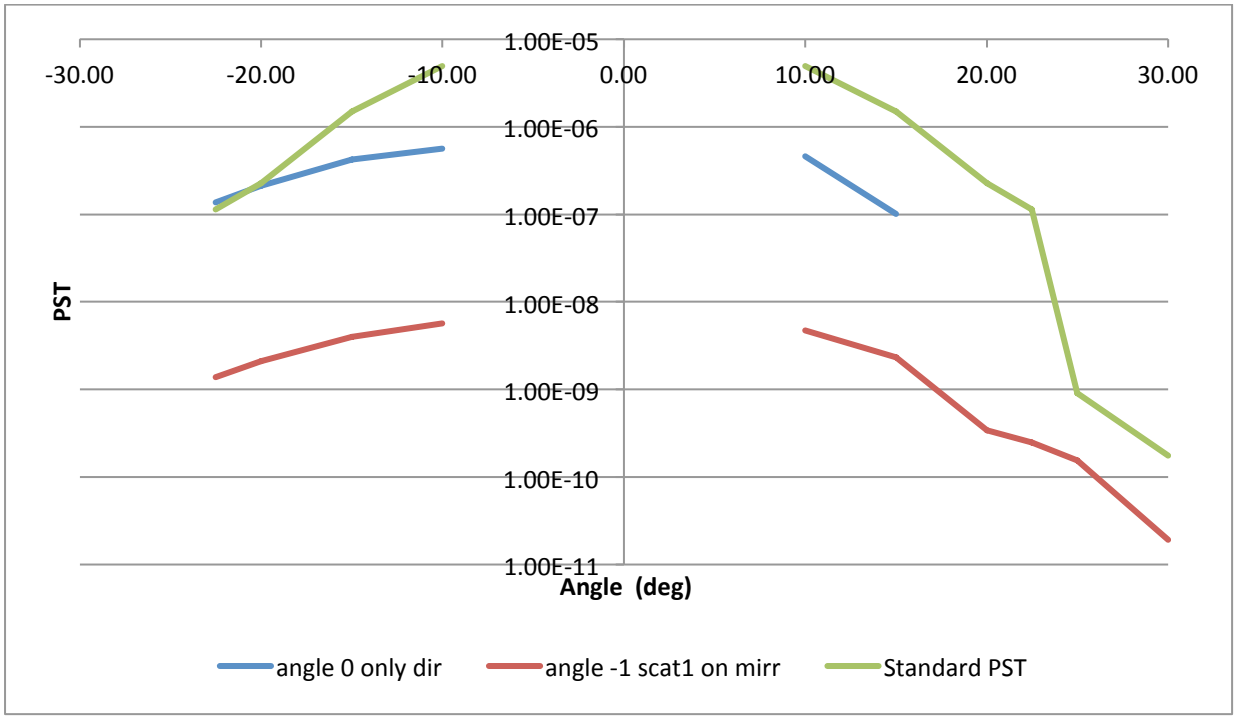


*Figure 25:Standard PST, PST of direct illumination and no scattering due to rectangular spider (blue line) and PST due to trapezoidal spiders(considering scatter of mirrors, red line)*

Plot is asymmetric due to the asymmetric disposition of the spiders.PST values due to spiders are one order of magnitude less than the standard PST for all the angles <=15°, where the scatter due to mirrors is dominating. For some angles (-20) the value of PST due to direct illumination of spiders is comparable with that of the Standard Configuration.

To overcome this a possible solution would be to change the profile of the spiders: in the standard design the spiders are essentially a parallelepiped having a rectangular section of 20x3 mm (3 mm is the width of the faces toward primary and baffle entrance). The sides of the spiders is so directly visible through the CIS by the detector. This may be avoided shaping the cross section of the spiders as a trapezoid, with the sizes inclined of an angle greater than the semi-FOV of the CIS and the largest base (the 'back') toward the mirrors. Doing so, sides of the spiders can no bee seen directly by the optical system (but only after a scattering on the mirrors). Red line in Figure 25 gives the PST due to this kind of spiders, considering a level of scattering on the mirrors.

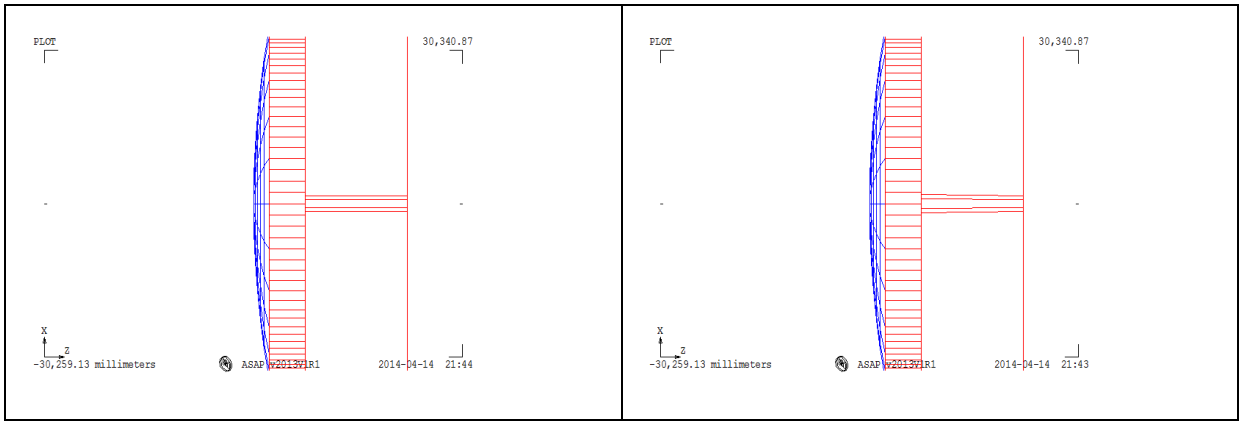


*Figure 26: Spiders profile*

Direct illumination of the spiders is not the only effect that has to be considered, anyway. A major effect that has to be checked is that due to the 'back' of the spiders, that even if not directly illuminated, once illuminated by other elements of the CIS (e.g. the baffle elements) may scatter directly in the CIS field.

To calculate the PST due to this effect two simulations have been run:

- One allowing baffle elements to scatter only toward the sides and the back of the spiders, for angles from 10° to 60°, allowing one scatter level on the baffle elements (IB, ESB and EPB), 2 on the spiders and three on the mirrors, using ~7e3 rays in entrance pupil and creating 10 rays in each scatter. This simulation highlights straylight caused by light hitting the baffle once, the spiders and then the mirrors
- Another one, for an angular range from 35° to 60°, to evaluate the straylight due to 2 scatters on the baffle, one on the spider and then the direct imaging of the spiders back by the optical system (no scatter on the mirrors), so elements of ESB and EPB scatter in a Pi angle, while elements of the IB scatter only towards spiders back. Rays number parameters:~3e4 rays in entrance pupil, 10 rays for each scatter (100 at the spiders).

Results are reported in Figure 27 and in Table 17. It is clear that for some angles (less than 35°) this process may become dominating and increase the PST.

*Table 17: PST values for the 'NO Pupil Mask' Configuration*

| ANGLE | STANDARD | 2 SCAT BAFF | 1 SCAT BAFF | NO PM | NO PM/STANDARD RATIO |
|---|---|---|---|---|---|
| **-60** | 2.98642E-12 | 3.80578E-13 | 0 | 3.367E-12 | 1.127436 |
| **-50** | 1.55313E-11 | 1.8864E-12 | 1.03531E-14 | 1.7428E-11 | 1.122125 |
| **-40** | 4.58934E-11 | 4.35766E-12 | 2.31608E-13 | 5.04827E-11 | 1.099998 |
| **-35** | 7.72315E-11 | 5.24801E-12 | 1.07825E-13 | 8.25873E-11 | 1.069348 |
| **-30** | 1.7548E-10 | | 1.62345E-10 | 3.37826E-10 | 1.925149 |
| **-20** | 2.28287E-07 | | 4.31999E-09 | 2.32607E-07 | 1.018924 |
| **-10** | 4.90709E-06 | | 8.391E-09 | 4.91548E-06 | 1.00171 |

| | | | | | |
|---|---|---|---|---|---|
| **10** | 4.90709E-06 | | 1.24873E-06 | 6.15583E-06 | 1.254475 |
| **20** | 2.28287E-07 | | 1.44833E-07 | 3.7312E-07 | 1.634434 |
| **30** | 1.7548E-10 | | 7.16407E-10 | 8.91887E-10 | 5.082548 |
| **35** | 7.72315E-11 | 6.40011E-12 | 1.52835E-13 | 8.37844E-11 | 1.084848 |
| **40** | 4.58934E-11 | 4.57014E-12 | 1.84886E-13 | 5.06484E-11 | 1.10361 |
| **50** | 1.55313E-11 | 2.30376E-12 | 1.45987E-13 | 1.7981E-11 | 1.15773 |
| **60** | 2.98642E-12 | 4.55489E-13 | 2.86171E-14 | 3.47053E-12 | 1.162103 |

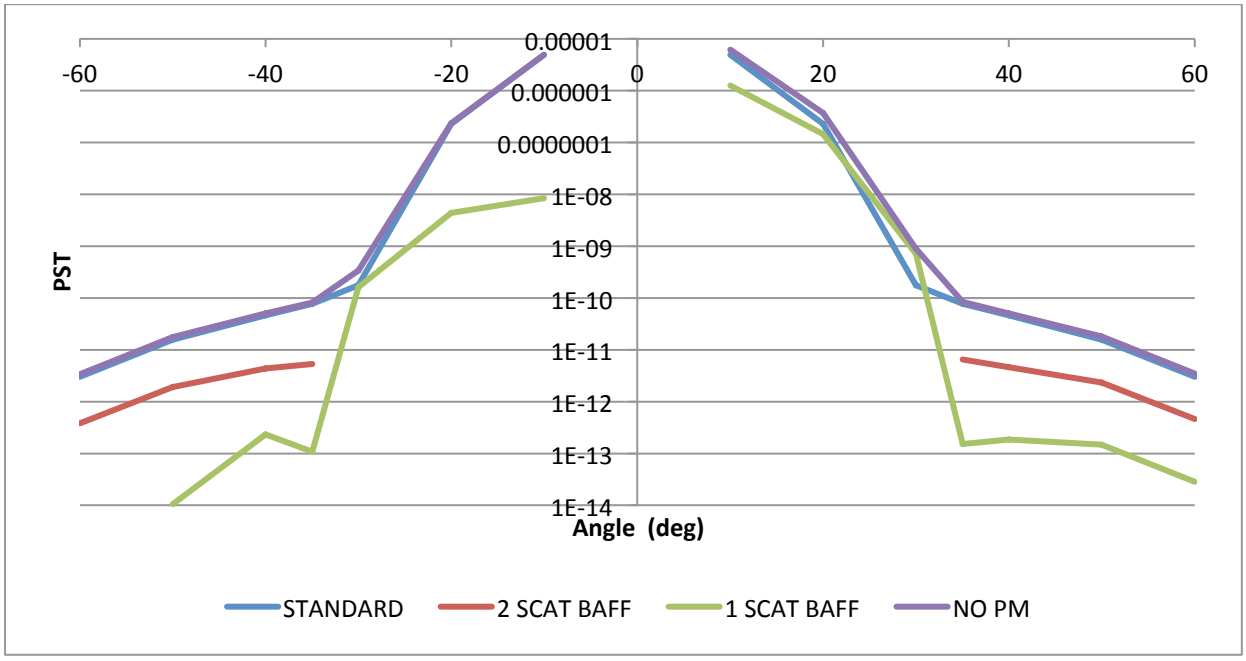


*Figure 27: PST values for the 'NO Pupil Mask' Configuration*

### 6.6.2.3 Round borders

The aim is to evaluate the effect of using not a flat vane edge with 40 micron width, but instead a round border of curvature radius the half of the vane wall edge (cfr Figure 28).

Values reported in Figure 29 and Figure 30 (and in Table 18 and Table 19) shows that adopting round borders for all vane edges would increase the PST values up to an order of magnitude, but adopting them only for the IB has not detectable effects, due even to the lower importance the borders have in the PST for angles <35 deg.

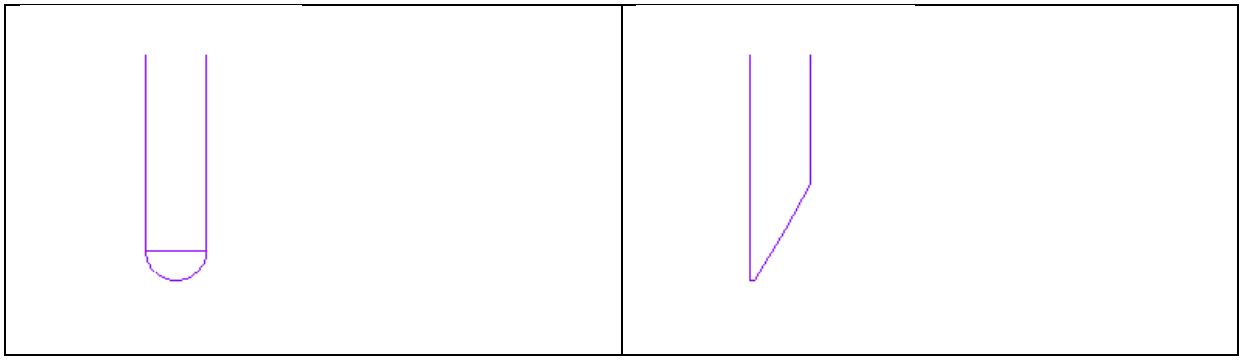

*Figure 28 Vane border shapes*

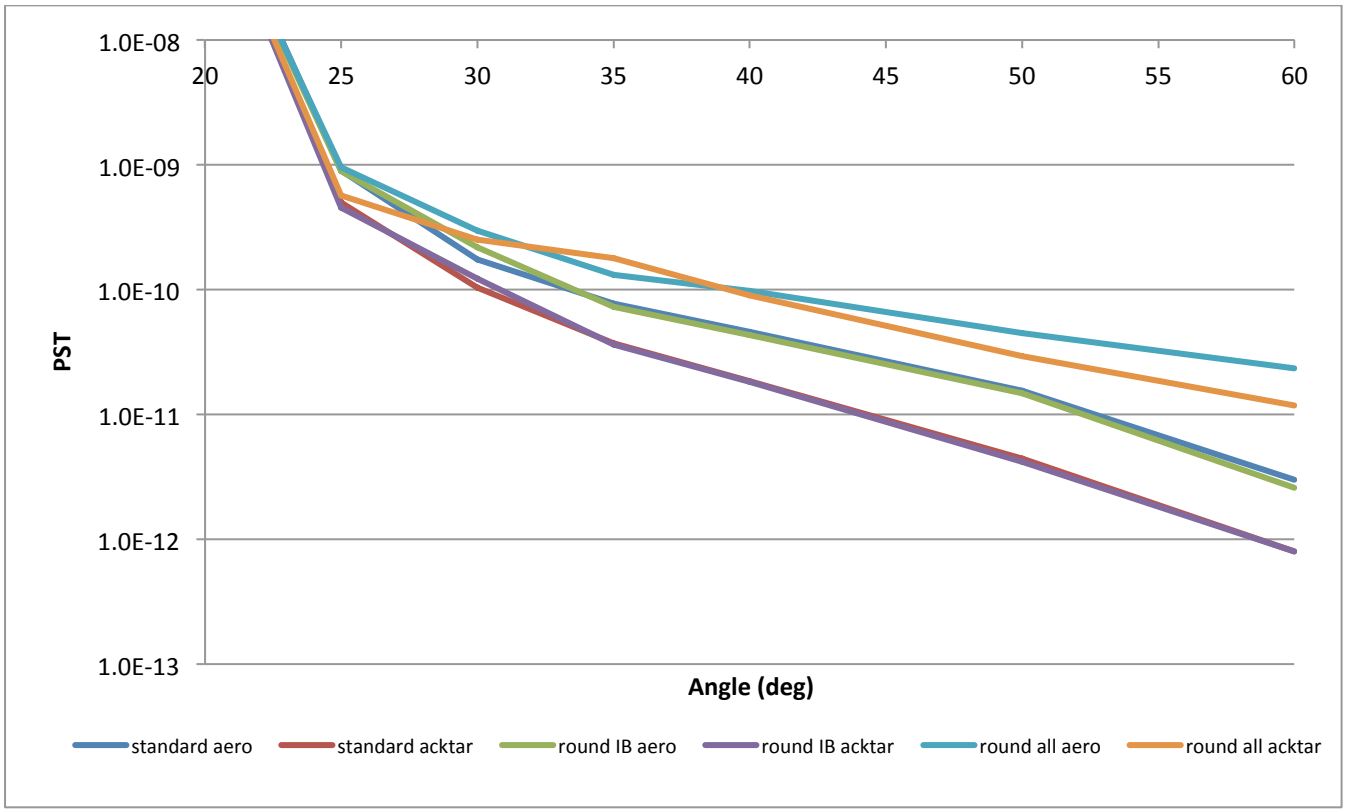


*Figure 29 Total PST using flat or round borders in different parts of the baffle, coated with Acktar or Aeroglaze*

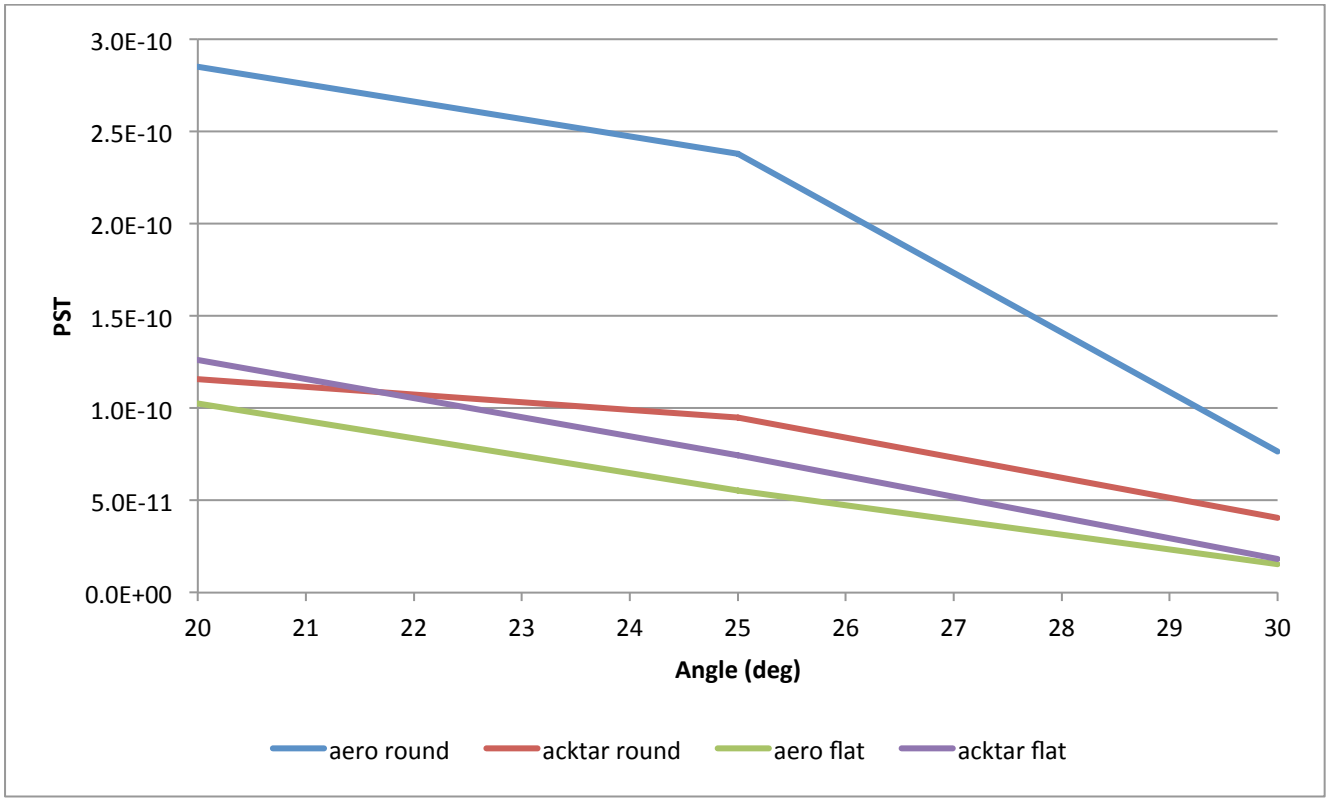


*Figure 30 PST contribution due IB borders with round and flat shape and coated with Aeroglaze or Acktar Fractlablack*

*Table 18 Total PST for different configuration of border shapes and coatings*

| Angle | standard aero | standard acktar | round IB aero | round IB acktar | round all aero | round all acktar |
|---|---|---|---|---|---|---|
| **20** | 2.3E-07 | 2.0E-07 | 2.0E-07 | 2.0E-07 | 2.0E-07 | 1.98E-07 |
| **25** | 9.0E-10 | 5.0E-10 | 8.9E-10 | 4.5E-10 | 9.6E-10 | 5.66E-10 |
| **30** | 1.8E-10 | 1.0E-10 | 2.2E-10 | 1.2E-10 | 3.0E-10 | 2.51E-10 |
| **35** | 7.7E-11 | 3.7E-11 | 7.3E-11 | 3.6E-11 | 1.3E-10 | 1.79E-10 |
| **40** | 4.6E-11 | 1.8E-11 | 4.3E-11 | 1.8E-11 | 9.8E-11 | 9.02E-11 |
| **50** | 1.6E-11 | 4.5E-12 | 1.5E-11 | 4.2E-12 | 4.5E-11 | 2.94E-11 |
| **60** | 3.0E-12 | 8.0E-13 | 2.6E-12 | 8.0E-13 | 2.3E-11 | 1.18E-11 |

*Table 19 PST contribution due to IB vanes edges with different shapes and coatings*

| angle | aero round | acktar round | aero flat | acktar flat |
|---|---|---|---|---|
| **20** | 2.9E-10 | 1.2E-10 | 1.0E-10 | 1.3E-10 |
| **25** | 2.4E-10 | 9.5E-11 | 5.5E-11 | 7.5E-11 |
| **30** | 7.6E-11 | 4.1E-11 | 1.5E-11 | 1.8E-11 |

### 6.6.2.4 Gap in vanes

An analysis has been performed to check what may be the effect of a void space between the vanes and the tube in the IB. This has been done foreseeing possible complications during AIVa and the necessity of have dismountable vanes in the IB.

So, leaving a gap between vanes and tube in IB causes an increasing of PST in the 20-35 deg of 2-4 times (not considering vanes edges, baffles coated with Aeroglaze).

*Table 20 PST and Ratio wrt standard configuration for different gap between IB tube and vanes (all Aeroglaze coated, vanes borders absorbing)*

| | 0 mm | 0.5 mm | 1 mm | 1.5 mm | 0 mm | 0.5 mm | 1 mm | 1.5 mm |
|---|---|---|---|---|---|---|---|---|
| **20** | 2.3E-07 | 1.78E-07 | 2.06E-07 | 2.48E-07 | 1 | 0.78 | 0.90 | 1.08 |
| **25** | 5.29E-10 | 6.73E-10 | 9.64E-10 | 1.19E-09 | 1 | 1.27 | 1.82 | 2.26 |
| **30** | 1.13E-10 | 2.31E-10 | 3.11E-10 | 5.22E-10 | 1 | 2.05 | 2.75 | 4.61 |
| **35** | 4.72E-11 | 4.88E-11 | 4.86E-11 | 5.12E-11 | 1 | 1.03 | 1.03 | 1.08 |
| **40** | 3.04E-11 | 2.96E-11 | 2.96E-11 | 3.03E-11 | 1 | 0.97 | 0.97 | 1.00 |

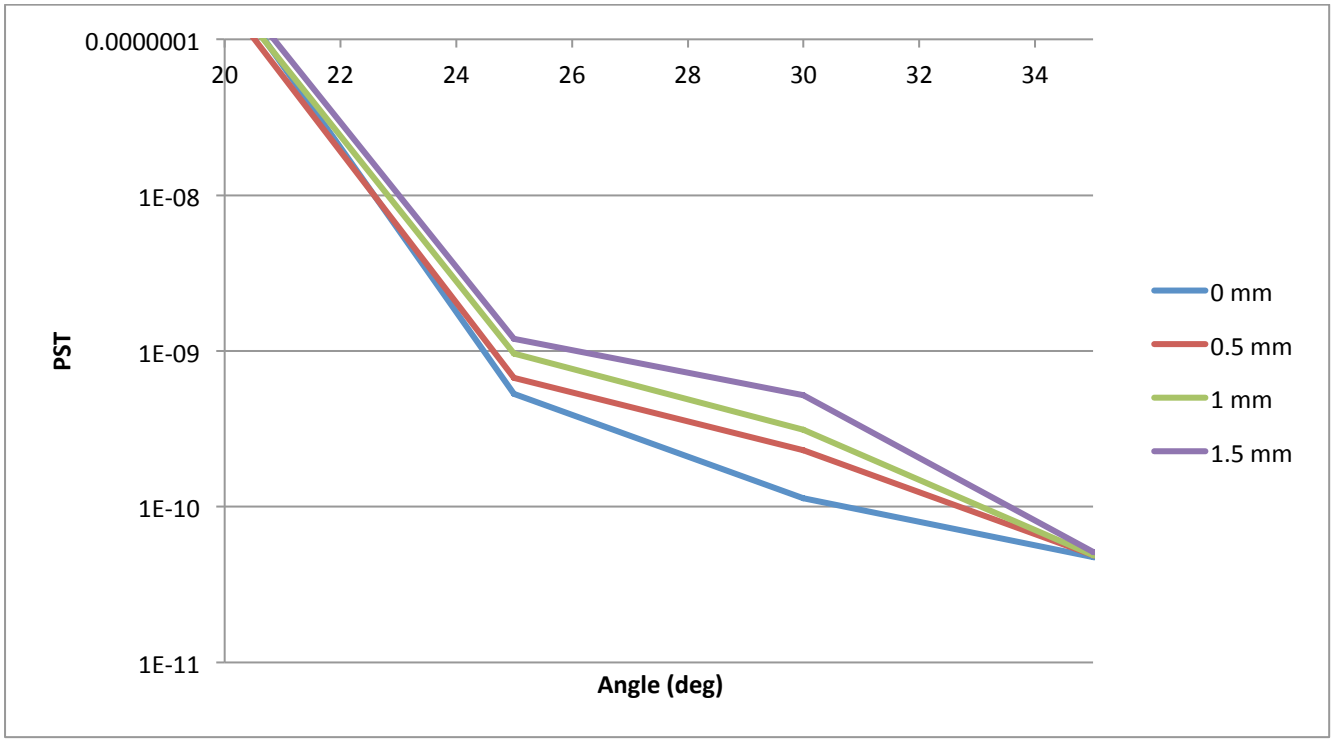


*Figure 31 for different gap between IB tube and vanes (all Aeroglaze coated, vanes borders absorbing)*

## 6.7 In Field Performances

### 6.7.1 Ghost analysis

#### 6.7.1.1 Coatings

Coatings values used in analysis have been updated, with respect to previous issues of this report:

- Anti-Reflection coatings of lenses taken in account are those described in §8.3 CHEOPS-SES-INST-DD-001 Rev. 1, that assure <0.8% in the CIS wavelength

- CCD Reflectivity: from private communication (email from Peter Verhoeve to Thomas Beck of Oct 2015) we got a plot of the Reflectivity of one of the CHEOPS CCD (Figure 32, green curve form measures)

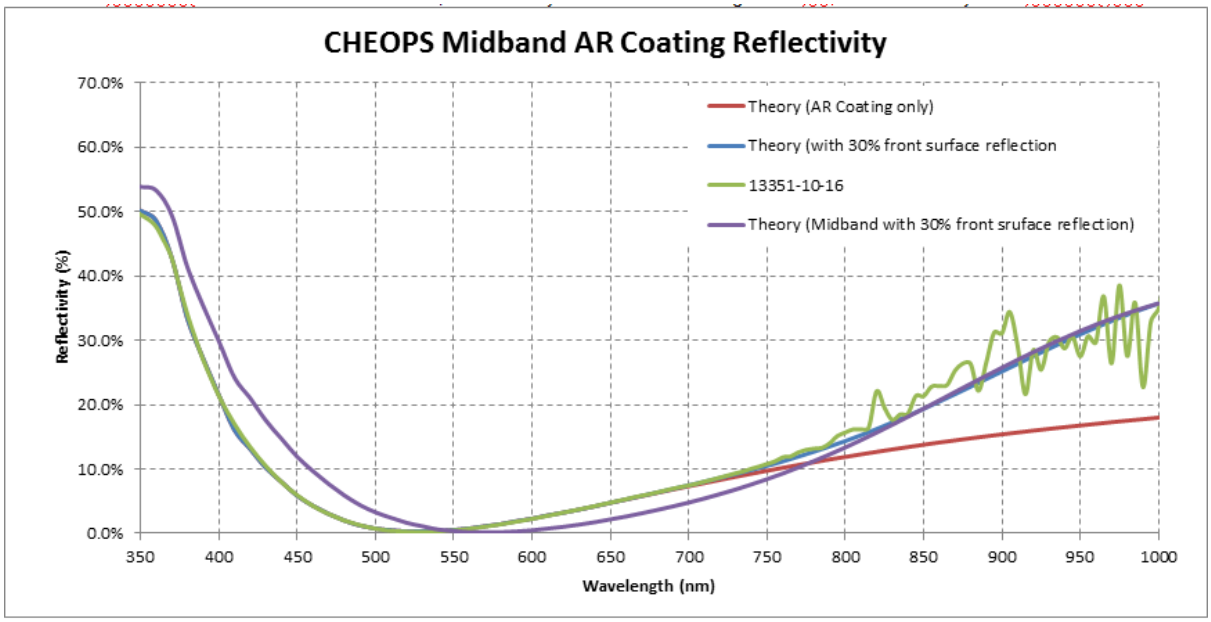


*Figure 32: CCD reflectivity, models and measures, from ESA.*

*Table 21: CCD R values extracted form plot*

| WL nm | R % | | WL nm | R % | | WL nm | R % | | WL nm | R % |
|---|---|---|---|---|---|---|---|---|---|---|
| 400 | 20 | | 550 | 0 | | 700 | 8 | | 850 | 20 |
| 450 | 6 | | 600 | 2 | | 750 | 11 | | 900 | 25 |
| 500 | 0 | | 650 | 5 | | 800 | 15 | | 950 | 30 |
| | | | | | | | | | 1000 | 35 |

From the plot approximate values are extracted (see Table 21), giving a mean R value of ~13.6%. We will use 15%.

### 6.7.1.2 Simulations and results

Simulations have been performed for positions on the field going from 0 to 0.2°,0.02° step, from the optical axis, along CCD side direction. Wavelength used is 750nm and coating values the average ones (0.8% and 15%). Ghost flux is hence an 'average' value for all the wavelength range.

In Table 22, data of the ghosts for an on axis source are reported: the path generating the ghost, the flux of the ghost expressed as the ratio with the flux of the nominal image. It can be noted that all the ghosts are extended: the size is about that of the detector. This can be appreciated in figures from Figure 33 to Figure 35 , showing to that irradiance of ghosts is approximatively 6 orders of magnitude lower than that of the image

*Table 22: On-Axis Ghosts data*

| PATH | FLUX RATIO | SIZE(mm) | RAYS |
|---|---|---|---|
| **DET->D2.L2.B** | 0.01586% | 12.938 | 34108 |
| **D2.L2.F->D2.L1.B** | 0.00639% | 12.032 | 257245 |
| **DET->D1.L2.B** | 0.00355% | 12.9975 | 8122 |
| **DET->D2.L1.F** | 0.00274% | 12.968 | 6162 |
| **D1.L2.F->D1.L1.B** | 0.00193% | 12.9995 | 77372 |
| **D2.L2.B->D2.L1.B** | 0.00067% | 12.8965 | 27598 |
| **D2.L2.B->D2.L2.F** | 0.00040% | 12.86 | 16116 |
| **DET->D1.L1.F** | 0.00030% | 12.7775 | 712 |
| **DET->D2.L1.B** | 0.00002% | 12.952 | 40 |
| **D2.L2.B->D2.L1.F** | 0.00002% | 12.9895 | 714 |
| **D1.L2.B->D1.L1.B** | 0.00002% | 12.838 | 694 |

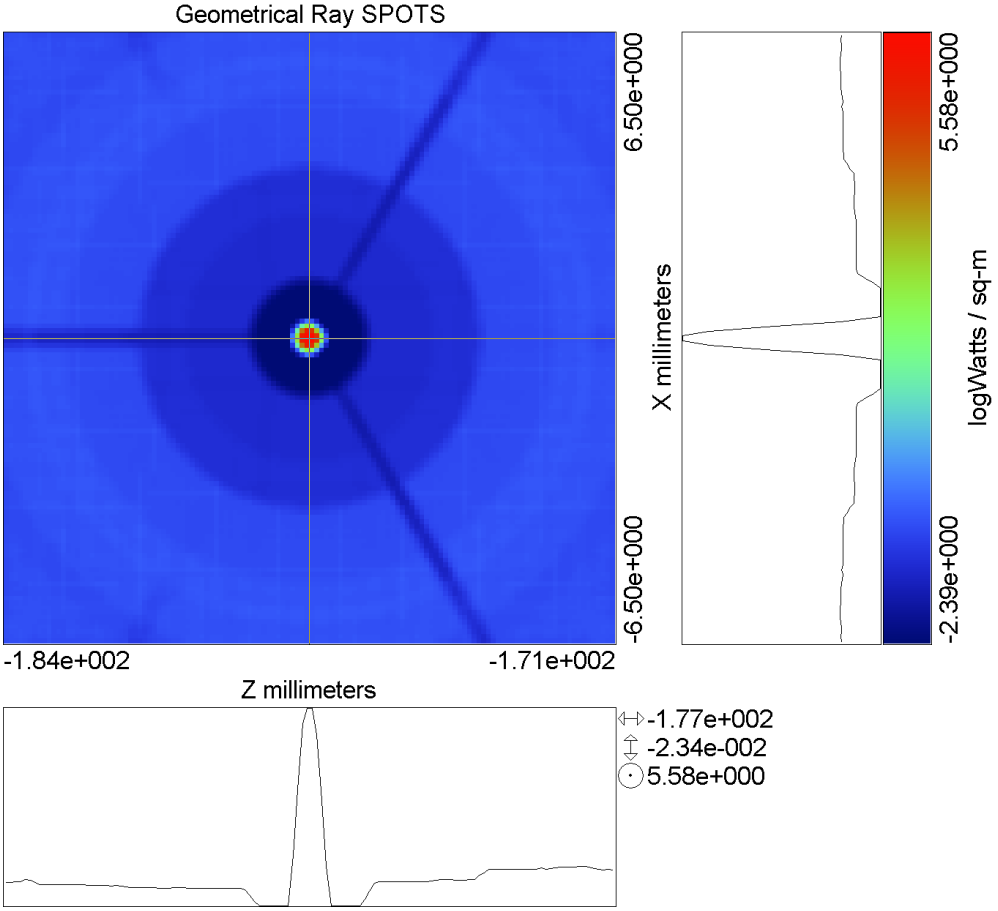


*Figure 33: On Axis Image and ghosts. Scale is logarithmic and values are relative to source of 1 W/mm$^2$*

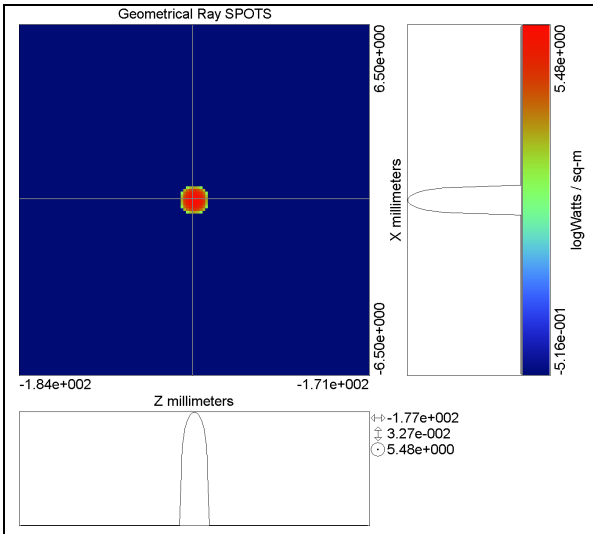


*Figure 34 Only nominal image*

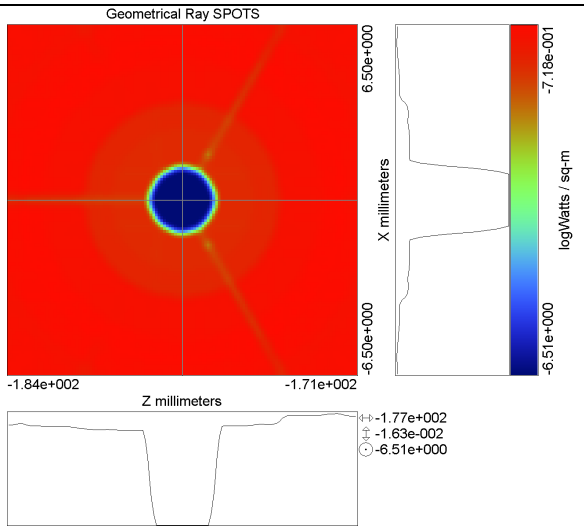


*Figure 35 Only ghosts*

Looking at the evolution of the ghosts flux with the position of the source (see Figure 36), it can be seen that ~0-8° total ghost flux has a maximum (about 2x on axis value), due to the shift of ghosts and the consequent exit of the shadow of M2 from the detector (see Figure 37)

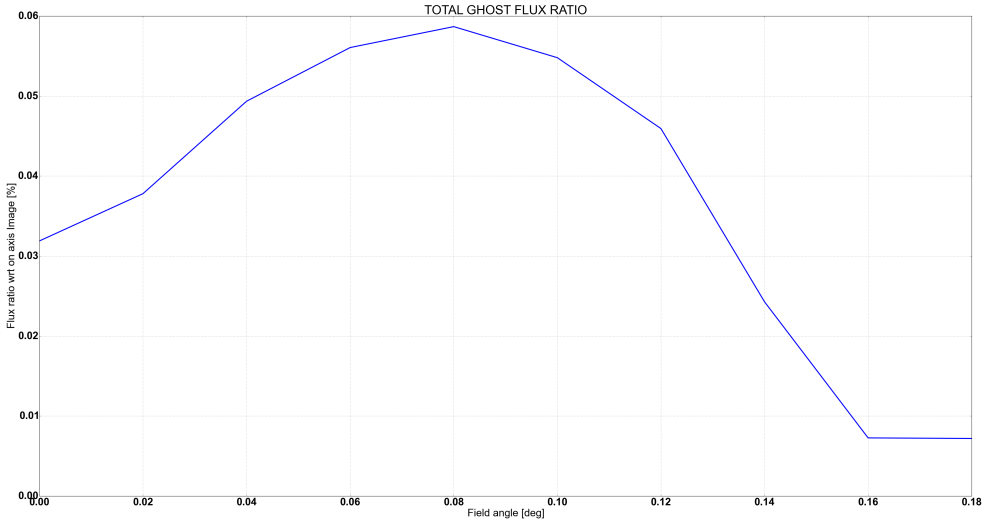


*Figure 36: Total Ghosts flux ratio (wrt on axis image) vs field*

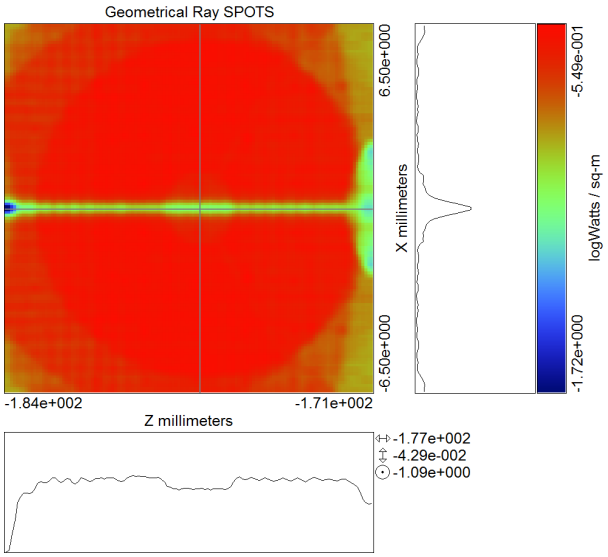


*Figure 37: Ghosts flux @0.08°*

At last , in Figure 38, the evolution of flux of most energetic ghosts with position of the source in the field is shown.

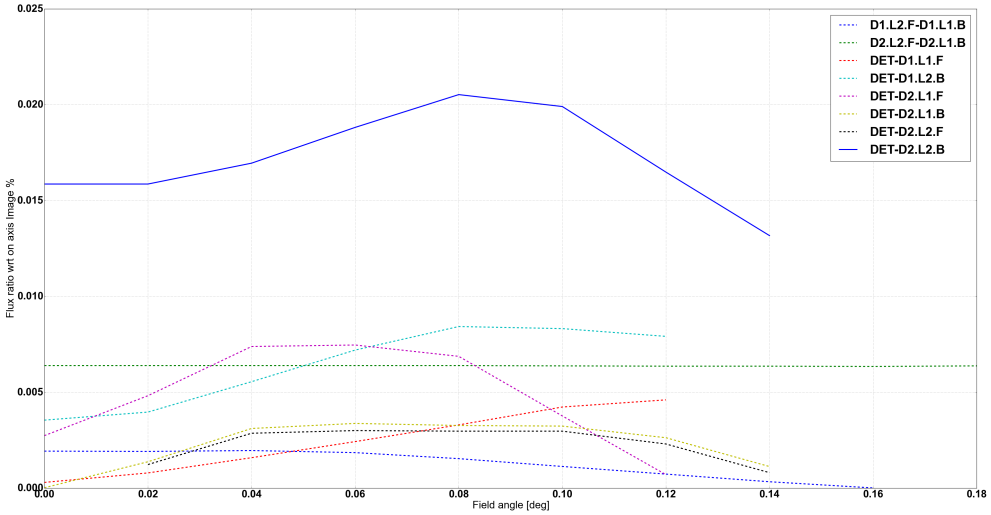


*Figure 38: most energetic ghosts flux (expressed as ratio wrt flux of on axis image).*

## 6.7.2 In-Field Scatter

The ASAP model has been used to evaluate scatter for an In-Field source; ASAP results has been compared to ZEMAX diffraction PSF and a Peterson model of the system [RD19], and a simplified model for irradiance on the detector plane is obtained.

### 6.7.2.1 ZEMAX PSF

Zemax PSF from [RD15] considers only diffraction effects.

In following plots, profile of Zemax PSF is presented. PSF is calculated at the centre of the field, for nominal configuration. PSF is polychromatic: sum of PSF calculated from 400 to 1100 nm each 50nm, summed up with no weighting (flat spectrum). PSF is calculated with a 4K x 4K sampling in pupil plane and 8K x 8K in image plane (1.3 micron sampling). In order to not consider effects of the FFT used to calculate PSF, only the central part (4K x 4K) of the image in considered. Data is then binned 10x in so to obtain a resolution of one Cheops pixel (13 micron).

X axis is CHEOPS pixels, Y axis is arbitrary (PSF normalized to its maximum.

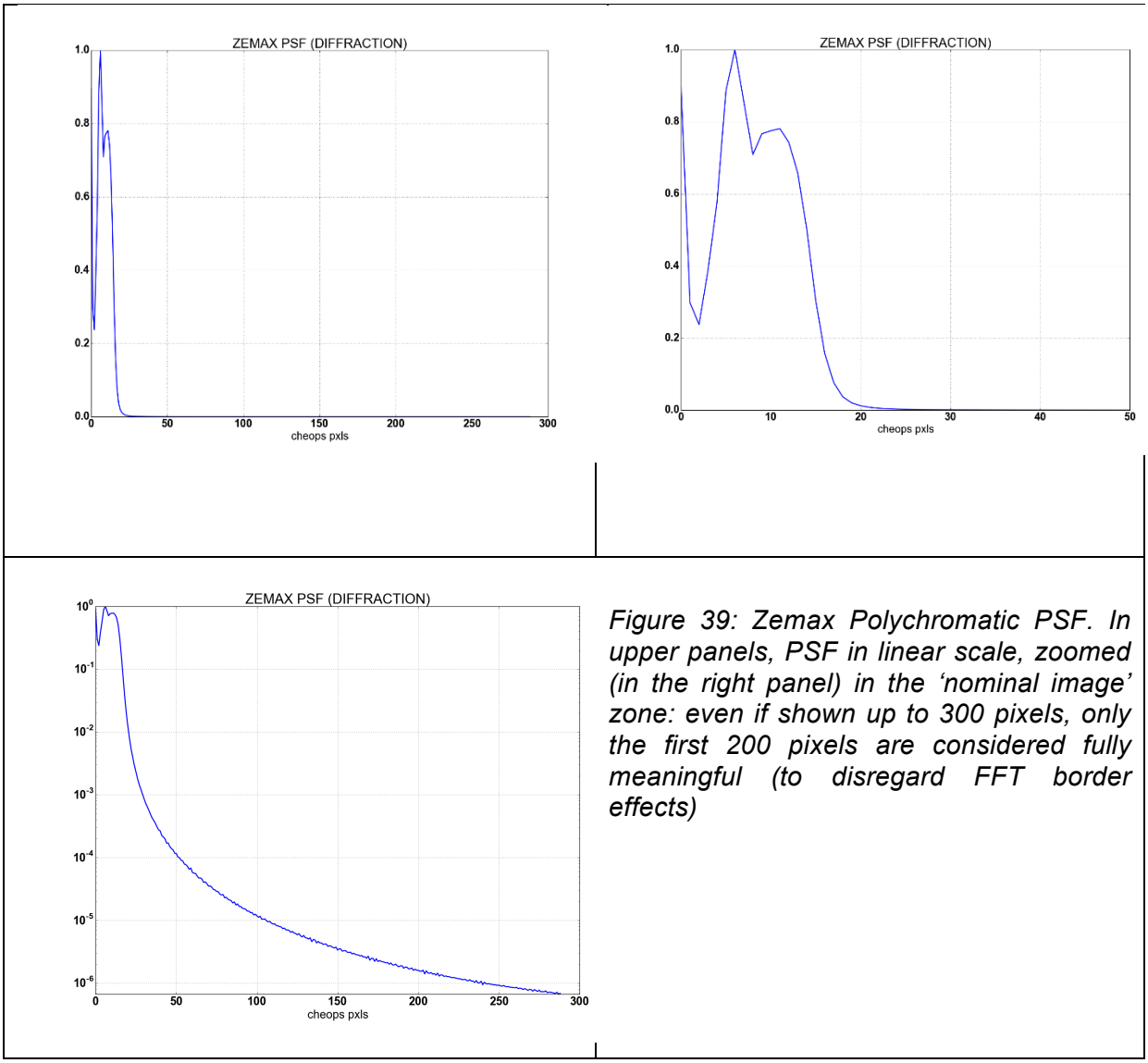


*Figure 39: Zemax Polychromatic PSF. In upper panels, PSF in linear scale, zoomed (in the right panel) in the 'nominal image' zone: even if shown up to 300 pixels, only the first 200 pixels are considered fully meaningful (to disregard FFT border effects)*

### 6.7.2.2 ASAP simulations

To evaluate effects of scattering (and ghosts, see previous section) ASAP simulations have been run, collecting data on a 1000 x 1000 pixels, 13x13 mm detector, using an on-axis source of about 3e6 rays. Pixels are of the same side of those of the Cheops Detector (13 micron). Detector efficiency is 85%; remaining 15% is reflected. Optics are modelled as in

previous sections:300ppm dust contaminated; mirrors are 100% reflective, lenses are 99.2% transmitting (0.8% reflective); one level of scattering is considered.

PSF given by ASAP simulations considers only reflection/refraction/scattering (no diffraction). The results are given in Irradiance (energy/area, W/mm^2). In the simulations, a source of unitary Irradiance (1W/mm^2) has been used to feed the system @400nm. Consequently obtained values are in W/mm^2 and may be used to obtain irradiance on the detector, for any source, once known the irradiance of the source at the entrance of the system.

Following images presents irradiance on the focal plane due to different phenomena.

*Table 23: irradiance on the detector due to different phenomena (ghost and scatter)*

| | |
|---|---|
| 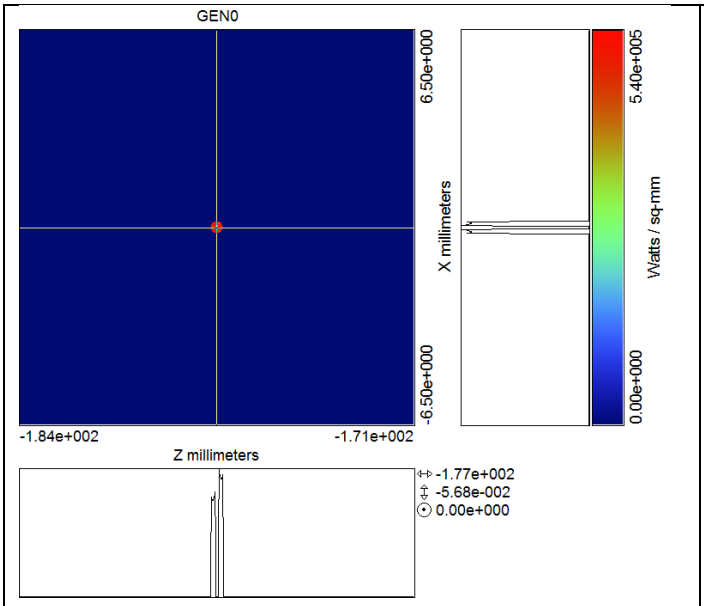 | In this image only **nominal image** is show: max irradiance reaches 5.4e5 W/mm^2, in good accordance with a simple calculation:<br>Entrance energy E=(160^2-31^2)*PI W<br>Trasmittance T=0.85 x (1-0.008)^8<br>Image Area<br>IA=(15 x 0.013)^2 PI mm<br>Image Irradiance II=5.7e5 Wmm^2<br>By the way , total power of the image in simulations is about 65e3 W |
| 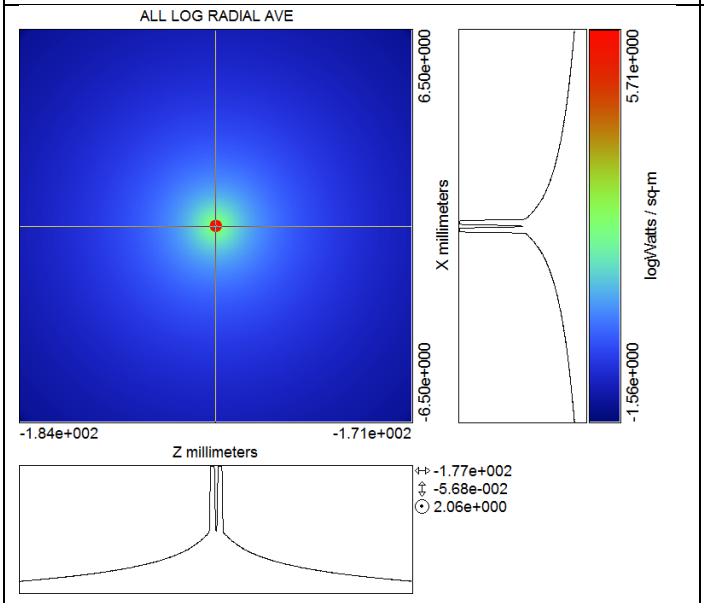 | In this image, effects of scatter due to microroughness and particulate contamination are present; the image (in log scale) shows that the scatter allows decrease from a value of irradiance of about 10^2 W/mm^2 (at the centre) down to 10^(-1.5) W/mm^2 at the borders of the detector.<br>Total power due to scatter recorder on the CCD is about 187W (1.1 W/mm^2 on average on the detector) |
| | |

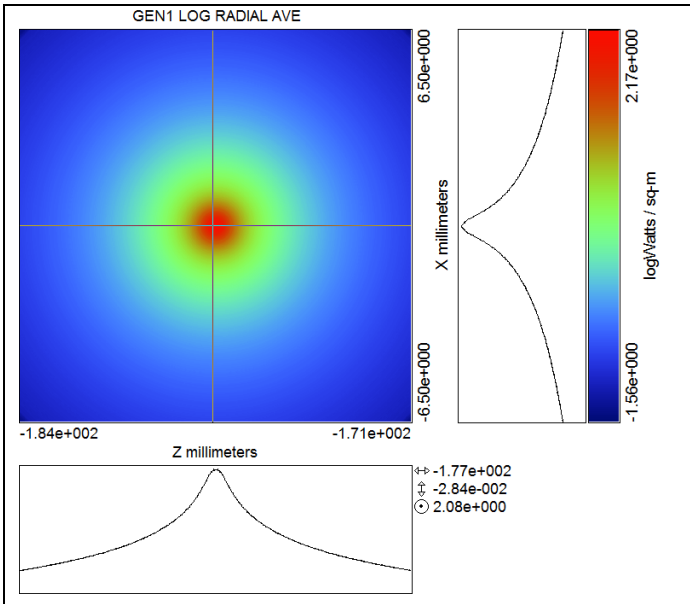


In this image, nominal image is filtered out so to better see effects of scatter

Some approximate values (n log scale) are

Dist from axis__Irr base 10 log [log W/mm2]

@0.0mm_____+2,10

@1.0mm_____+0,80

@2.0mm_____+0,19

@3.0mm_____-0,18

@4.0mm_____-0,42

@5.0mm_____-0,66

@6.0mm_____-0,84

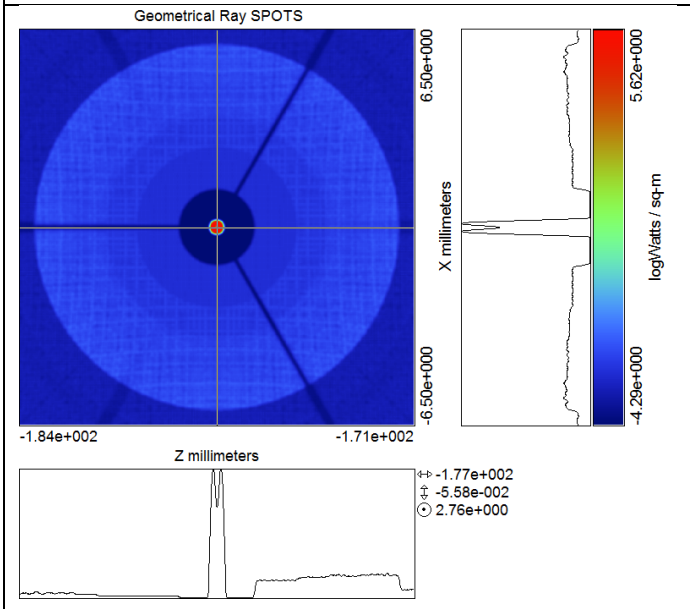


In this image, no scatter is present, but only Ghosts

Total Ghost power is 20.5W, distributed in a quite uniform way (at least wrt scatter)

Mean irradiance due to Ghost on the detector is 012W, so one order of magnitude less then scatter

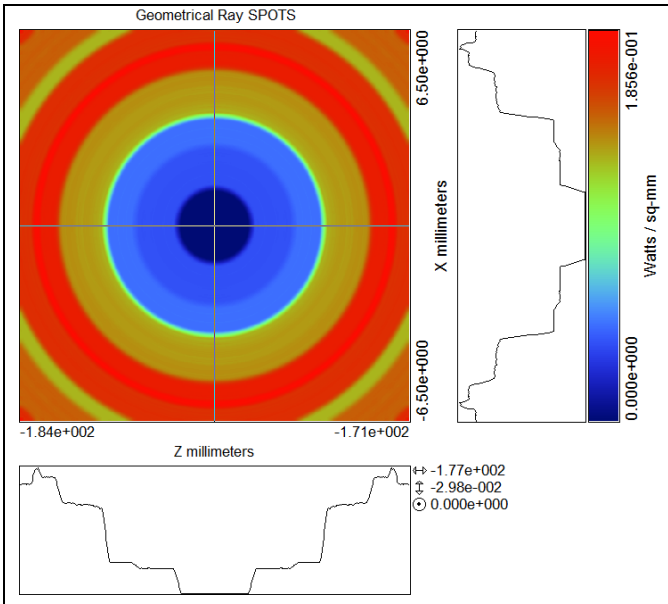


An image in linear scale (filtering out nominal image) shows better the structure of ghosts for on axis source

Irradiance (in W/mm^2) may be approximated by annular areas of constant irradiance:

From 0.00 to 1.25mm _ 0.00 W/mm^2

From 1.25 to 2.70mm _ 0.036 W/mm^2

From 2.70 to 3.60mm _ 0.045 W/mm^2

From 3.60 to 5.30mm _ 0.130 W/mm^2

From 5.30 to 7.70 mm_ 0.170 W/mm^2

From 7.70 to ____mm _ 0.140 W/mm^2

### 6.7.2.3 Peterson analytical model

An analytical geometrical formulation of the irradiance due to scatter may be found In Peterson 2004 [RD19].

This formulation is based on several properties of the system, and on the scattering properties of the optical surfaces described by 3 parameters Harvey models. BRDF models used in Cheops ASAP model are the sum of three Harvey model (one for the microroughness of the surfaces, two for fitting the dust contamination); the Peterson model is then applied to each of the Harvey model and the results summed up.

Used parameters of the optical system are reported in Table 24

*Table 24: system parameters used in Peterson Model*

| | | |
|---|---|---|
| T | 0.8 | Transmissivity (0.85 x (1-0.008)^8) |
| F | 8.37 | F number |
| NA | 0.0597 | Numerical aperture |
| A | 160 | Entrance pupil radius mm |
| E | 1 | Source Irradiance (w/mm2) |
| LAMBDA | 4.00E-04 | Wavelength used (in mm) |

Surfaces used parameters are reported in Table 25

*Table 25 surfaces parameters for Peterson model*

| Surface | footprint semidia [mm] | Microroughness [A] | Delta N | Harvey param s,l,b | Particulate cont PPM | Harvey param s,l,b | Harvey param s,l,b |
|---|---|---|---|---|---|---|---|
| M1 | 160 | 10 | 2 | -1.8,0.01,0.21 | 300 | -2.4,0.0025,4.56 | -0.6,0.3,2.4e-5 |
| M2 | 31.1 | 5 | 2 | -1.8,0.01,0.052 | 300 | -2.4,0.0025,4.57 | -0.6,0.3,2.4e-6 |
| D1L1F | 5.2 | 5 | 0.7 | -1.8,0.01,0.0064 | 300 | -2.4,0.0025,4.58 | -0.6,0.3,2.4e-7 |
| D1L1B | 5.4 | 5 | 0.7 | -1.8,0.01,0.0064 | 300 | -2.4,0.0025,4.59 | -0.6,0.3,2.4e-8 |

| | | | | | | | |
|---|---|---|---|---|---|---|---|
| D1L2F | 5.3 | 5 | 0.7 | -1.8,0.01,0.0064 | 300 | -2.4,0.0025,4.60 | -0.6,0.3,2.4e-9 |
| D1L2B | 5.4 | 5 | 0.7 | -1.8,0.01,0.0064 | 300 | -2.4,0.0025,4.61 | -0.6,0.3,2.4e-10 |
| M3 | 6.6 | 5 | 2 | -1.8,0.01,0.052 | 300 | -2.4,0.0025,4.62 | -0.6,0.3,2.4e-11 |
| D2L1F | 5.4 | 5 | 0.7 | -1.8,0.01,0.0064 | 300 | -2.4,0.0025,4.63 | -0.6,0.3,2.4e-12 |
| D2L1B | 5.3 | 5 | 0.7 | -1.8,0.01,0.0064 | 300 | -2.4,0.0025,4.64 | -0.6,0.3,2.4e-13 |
| D2L2F | 5.1 | 5 | 0.7 | -1.8,0.01,0.0064 | 300 | -2.4,0.0025,4.65 | -0.6,0.3,2.4e-14 |
| D2L2B | 5.1 | 5 | 0.7 | -1.8,0.01,0.0064 | 300 | -2.4,0.0025,4.66 | -0.6,0.3,2.4e-15 |

In plot of Figure 40, irradiance due to each surface is visible; total irradiance and diffraction (from Peterson model), are also reported. Plot highlights that:

- Main contributors are BEO elements ( in accordance with ASAP simulation results)
- Scatter becomes dominant over diffraction for distances > 1.5 mm

Plot in Figure 41 shows contributors to total due to the 3 BRDF models (one for Microroughness, 2 for particulate), showing that largely the main contributor is the scatter due to particulate.

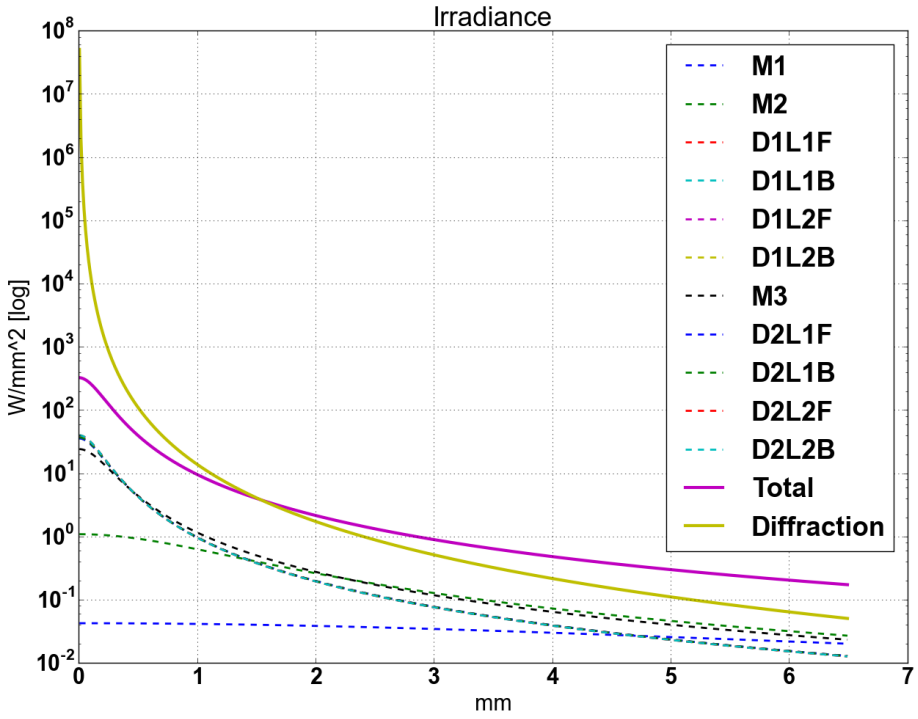


*Figure 40: Irradiance profile, per element / surface*

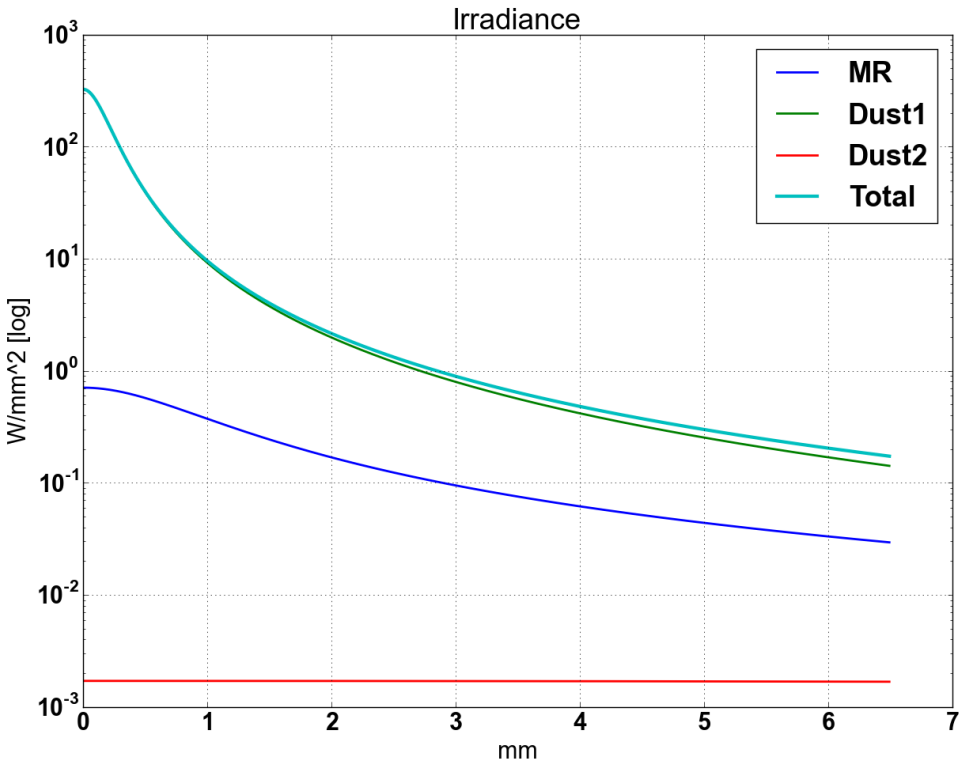


*Figure 41: Irradiance profile, per Harvey profile.*

Given that BEO elements are the biggest contributors, that their surfaces characteristics are all similar (BRDF profiles, footprints size) we can try to simplify the Peterson model, disregarding the effects due to M1 and M2 (and assuming for M3 the same scatter properties of lenses); moreover, we can use only one dust profile.

So, considering:

- 9 surfaces
- An average footprint radius of 5.5mm
- Harvey parameters s,l,b=-2.27,0.0025,4.57 ( 2.27 instead of 2.4 to better take into account contributes at large R due to disregarded elements, found by trial)
- T=0.8, na=0.06,Aent=160mm

and using formula 20 of Peterson:

$$E_{sj}(r) = \pi T (na)^2 \frac{a_{ent}^2}{a_j^2} b_o \left[ 1 + \left( \frac{(na) r}{l a_j} \right)^2 \right]^{s/2} E_{ent}. \qquad (20)$$

where Esj(r) is the irradiance at distance r from axis due to a single surface,

plugging in numbers, we get an easy expression for E(R), irradiance on the detector due to scatter at a radial distance R, due to a source on-axis having an irradiance of 1w/mm^2:

E(R)=315*[1+19R^2]^(-1.135)

In plots in Figure 42 and Figure 43 complete Peterson model and the simplified one and their ratio are displayed, showing  that the two models are in agreement in a +/-10% range.

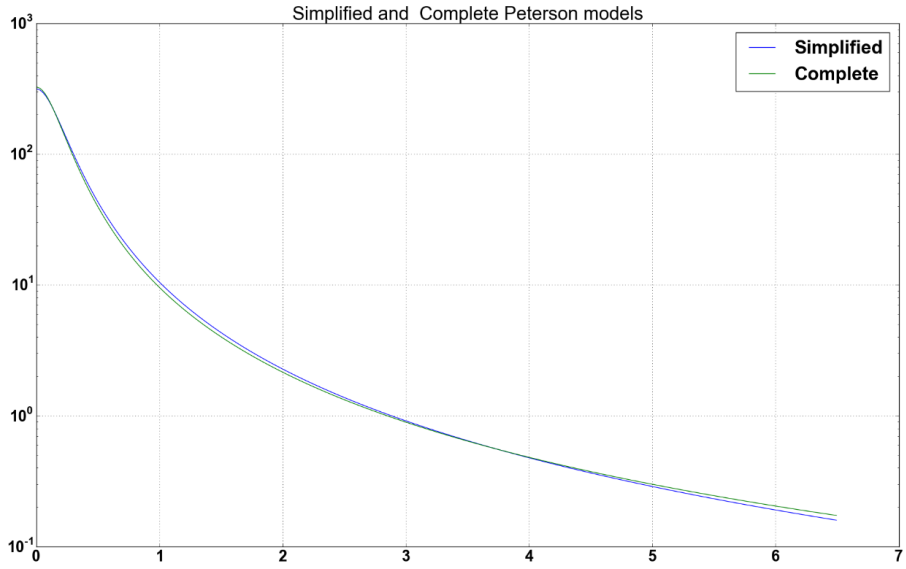


*Figure 42: Peterson complete and simplified Models*

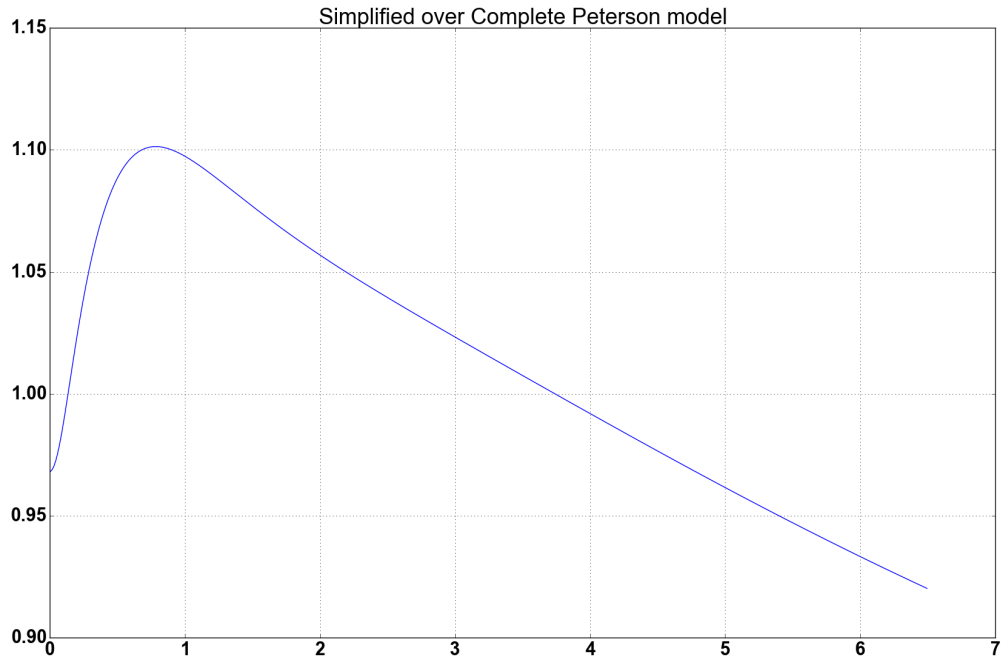


*Figure 43:Ratio of simplified and complete Peterson Models*

### 6.7.2.4 Models comparison

We want to compare the different PSF:

- Zemax
- ASAP
- Peterson (both complete and simplified)

Zemax PSF has been rescaled assuming integral of energies of Zemax PSF and ASAP PSF to be the same.

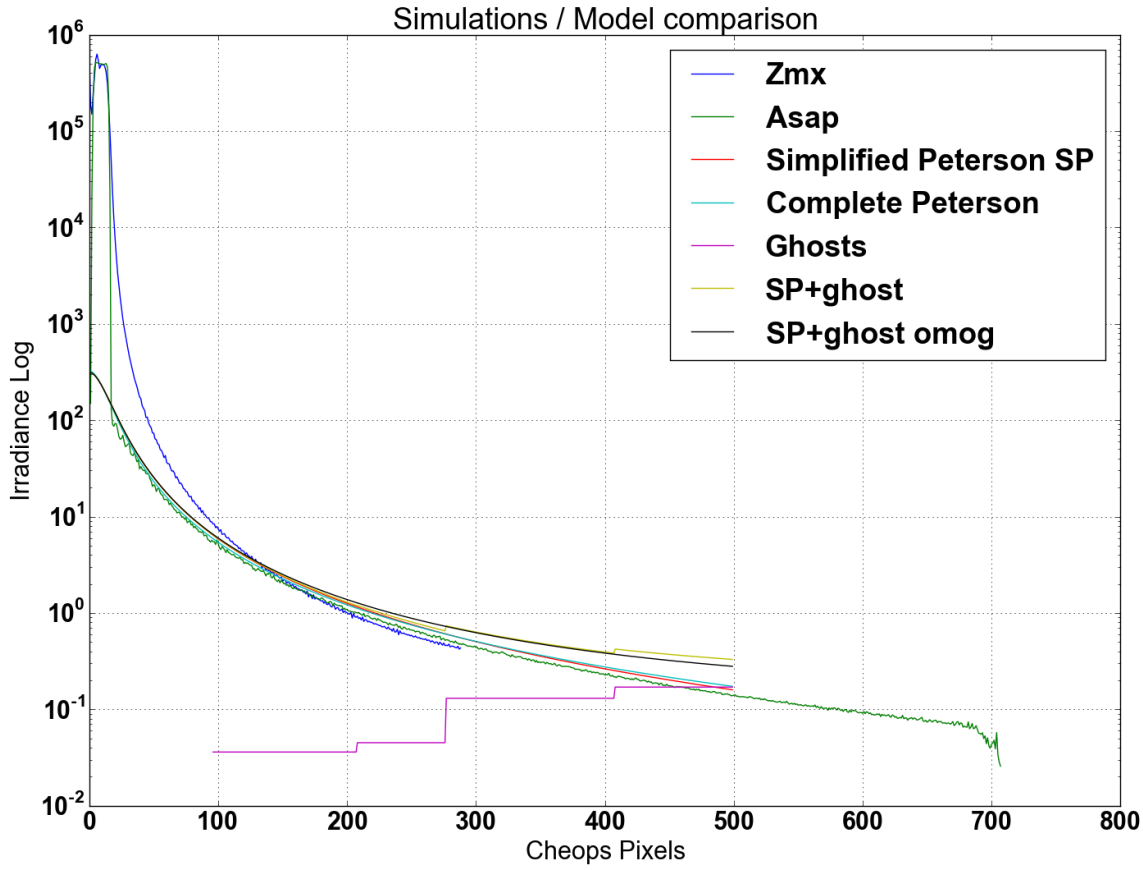


*Figure 44: models comparison in lin log scale*

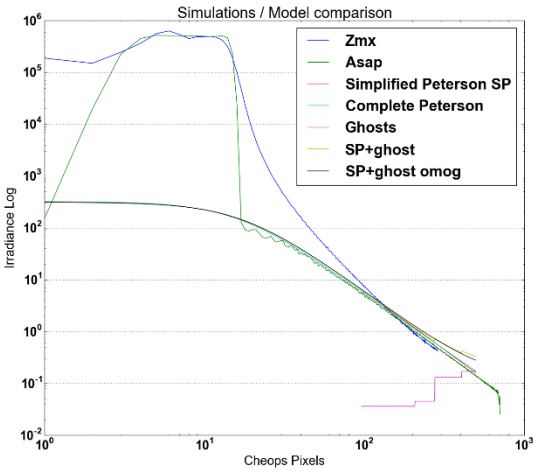


*Figure 45 Models comparisons in log log scale*

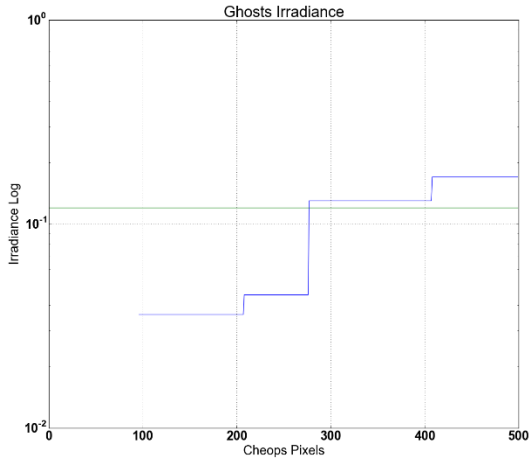


*Figure 46 Ghosts irradiance in lin log scale*

In the plots in Figure 44 and Figure 45, all the models /simulations are reported: Zemax and ASAP simulations, complete and simplified (SP) Peterson model, Ghost irradiance .The last is simulated both with a ladder function (blue line in lower right plot), and a with a constant irradiance(green line).

Some considerations can be sketched:

- Scatter models and simulations data (ASAP and PETERSON) are dominant over ZEMAX data from (Diffraction) starting from about 100-150 pixels from the centre of the nominal image (r=0). Obviously this is partially dependant by the way one normalize Zemax PSF, but is in accordance with the estimate due to Peterson model, foreseeing the ‘change of regime’ @ 1,5mm (about 120px)
- ASAP simulations and Peterson Models are quite in good agreement, as can be seen in next plot, where the ratio of Simplified model and ASAP data is shown (Figure 47). Peterson Model presents values 15-20% higher that simulations. Assuming the SP model for further analysis is so a non-optimistic choice wrt simulations.

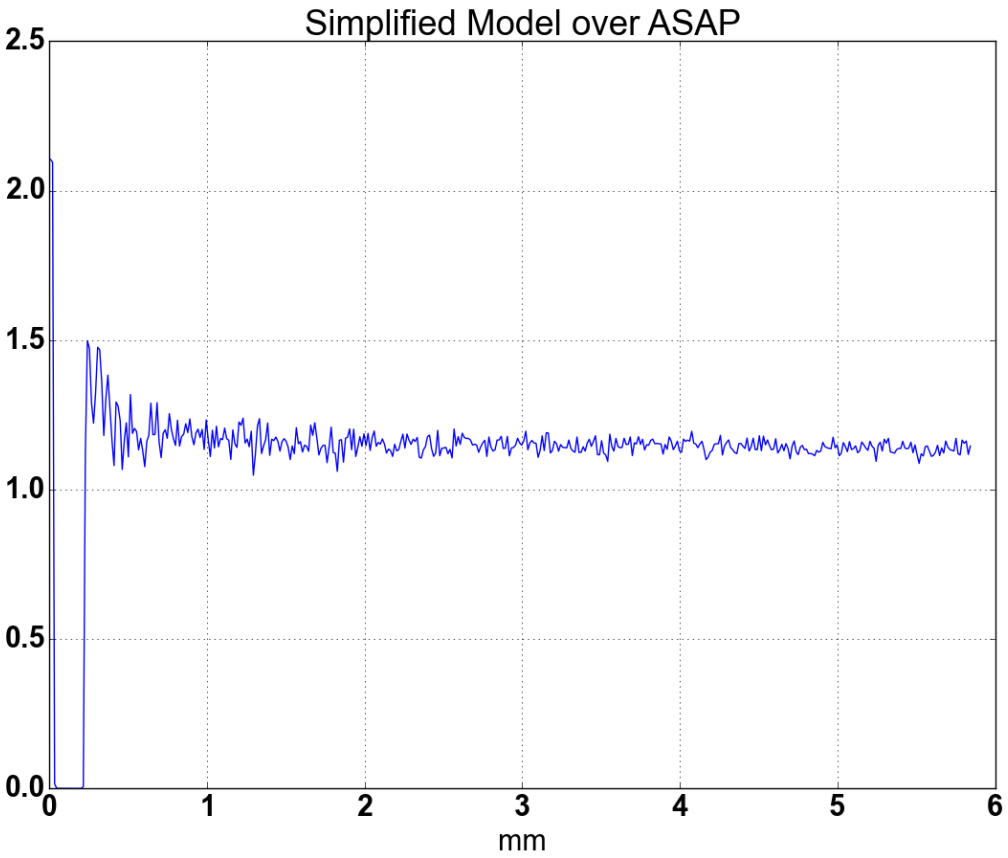


*Figure 47 ratio of irradiance given by simplified model and ASAP simulations*

- Ghost irradiance is not negligible wrt scatter irradiance, mainly at large distance from axis, both assuming ladder and homogeneous distribution. Moreover, used data are for a on Axis source, while for sources out of axis (but in-field) total flux (and irradiance) due to ghost may rise , e.g. at 0.8° is about 2 times larger); on the contrary, scatter Irradiance distribution remains more or less constant over the positions of the field (anyway centred in the nominal image)

# 7 Summary, comments and Conclusions

An ASAP model of the Cheops Instruments System has been developed and used to estimate stray light rejection performances. The analysis considered a ‘standard model’, characterized by:

- Structural elements painted / coated with several material: MAP Paint for the IB structure and vanes edges, Aeroglaze 306 for EB, with the exception of ESB diaphragms, coated with Acktar fractal Black. Has to be noted that for this materials, ‘updated’ BRDF models have been used, , having worst performances that those used up to last issue of this report.

- Optical elements, with microroughness 10 and 5 A rms, contaminated with 300ppm OF.
- Baffle vane tip chamfers  all directed toward the entrance of the baffle

Values of PST for this configuration have been derived.

According to analyses, the errors of +/- 1 mm on the positioning alignment of EB as a whole and of vanes as single elements have no impact on the PST.

Following this, several variations of the standard configurations have been considered, to evaluate possible advantages of possible changes. From that appears that:

- Having Acktar Fractal Black (even if limited to some diaphragms of the EB) is beneficial in terms of PST with respect to configurations fully 'Aeroglazed'
- Changing the baffle vanes edges chamfer have a very marginal but positive effect.
- Removing the pupil mask may have big effects that may be mitigated, at least for large angles of radiation incidence, shaping the spiders so that sides are not seen by the optical system.
- Leaving a Gap in the IB between tube and vanes as a 2-4 times effect in the 20-35 deg range (depending on the magnitude of the gap), and no effect for greater angles.
- Using round borders in the IB have no major effects on total PST.

In general, The PST curve clearly reflects the geometric properties of the baffle:

- For angle smaller than 35 deg, the possibility of scatter toward PM and SM causes a growth in the PST, even bigger for angle <=20 deg, when the PM is directly illuminated by radiation.
- For >60deg only the Primary external Baffle is directly illuminated, and no part of it can directly scatter toward the PM, causing a steep diminution of the PST.

Comparing results here presented with requirements present in [AD1] (L2-DSN-37a and b), shows that PST is not compliant; to mitigate that, should be taken into account that UBE sky coverage simulations using values of the Baseline configurations give results that are satisfactory from the scientific point of view.

Finally, we report here the plot result of the analysis conducted (on previous model) to study the variation of energy collected by the detector with the numbers of rays used to sample the system (vanes border excluded, @35°, contamination 300ppm). The following plot reports the results.

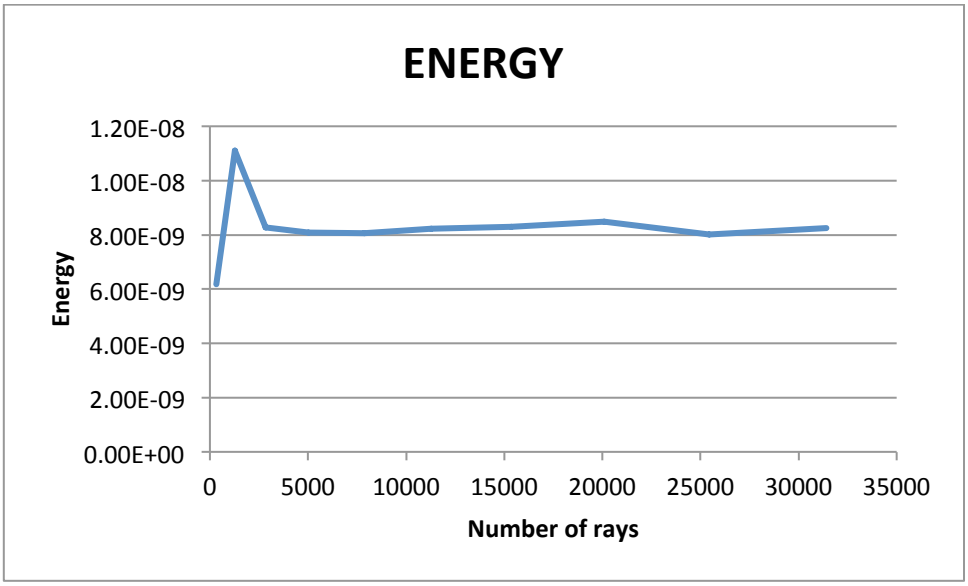


Stability of results that an error of ~20-30% may be associated with PST values presented in this document.

# 8 Appendix: PST values obtained with measured microroughness

During 2017, measures of several elements microroughness has become available. Since they where out of specifications, ASAP simulations have been repeated using updated values, that may be found in .Table 26.

| Surface | Roughness [Å] | 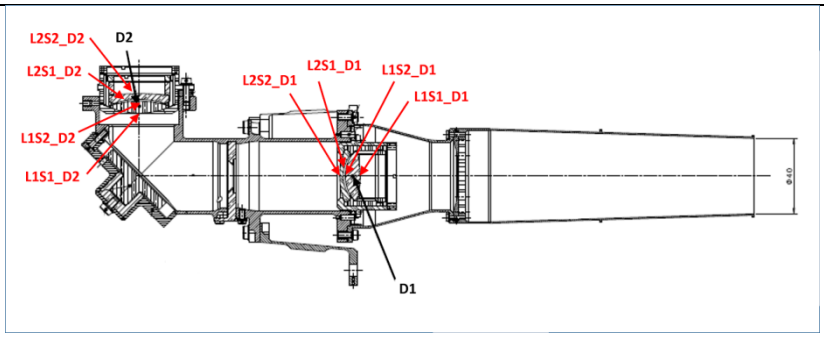 |
|---|---|---|
| L1S1_D1 | 9 | |
| L1S2_D1 | 10 | |
| L2S1_D1 | 29 | |
| L2S2_D1 | 15 | |
| L1S1_D2 | 9 | |
| L1S2_D2 | 8 | |
| L2S1_D2 | 22 | |
| L2S2_D2 | 22 | |
| M3 | 8 | |
| M2 | 7.6 | |



*Table 26: elements microroughensses*

## 8.1 PST Values

Configuration used for the simulation is:

- Source wavelength .400nm
- Microroughness of elements. M1=10A, other elements as in previous table
- Detector QE=1
- Mirrors reflectivity and lenses transmittance = 1
- Particle contamination;: 300ppm
- M1 and M2 borders coated with Aeroglaze
- Oversized pupil and focal plane diaphragm

Obtained values for PST are reported in the following table, for angles from the line of Sight from 2.5 to 87.5

| Angle [°] | PST | angle[°] | PST | angle[°] | PST |
|---|---|---|---|---|---|
| | | 30 | 1.96547E-09 | 60 | 1.37422E-11 |
| 2.5 | 0.000326 | 32.5 | 6.28365E-10 | 62.5 | 5.30568E-12 |
| 5 | 6.57E-05 | 35 | 2.06387E-10 | 65 | 2.36193E-12 |
| 7.5 | 3.6E-05 | 37.5 | 1.63309E-10 | 67.5 | 3.88922E-13 |
| 10 | 1.39E-05 | 40 | 1.24205E-10 | 70 | 3.729E-13 |
| 12.5 | 8.59E-06 | 42.5 | 1.05296E-10 | 72.5 | 5.49262E-13 |
| 15 | 5.64E-06 | 45 | 8.01668E-11 | 75 | 3.47687E-13 |
| 17.5 | 3.93E-06 | 47.5 | 6.286E-11 | 77.5 | 2.36421E-13 |
| 20 | 2.67E-06 | 50 | 5.56901E-11 | 80 | 1.20309E-13 |
| 22.5 | 1.25E-06 | 52.5 | 4.15949E-11 | 82.5 | 9.34931E-14 |
| 25 | 5.71E-09 | 55 | 2.90407E-11 | 85 | 8.60932E-14 |
| 27.5 | 3.48E-09 | 57.5 | 1.88612E-11 | 87.5 | 4.69983E-14 |

## 8.2 In field effects

The increased microroughness of BEO elements will have effects for the in-field scatter.

Peterson model presented in in 6.7.2.3 may be updated using a factor given by (MRm/MRr)^2,where MRm is the measured microroughness and MRr is the requirement microroughness, to rescale the Harvey 3 parameters model, in order to take in account the growth of TIS due to micro-roughness.

Effect of this rescaling may be appreciated in Figure 48, where the new irradiances curves due to MR (microroughness) and due the two models used to fit the particulate contamination (Dust1 and Dust2), and their sum (Total) is shown. Wrt the model with microroughness =5A for all the surfaces, in this model it is not possible anymore to disregard the effect of the microroughness on the irradiance.

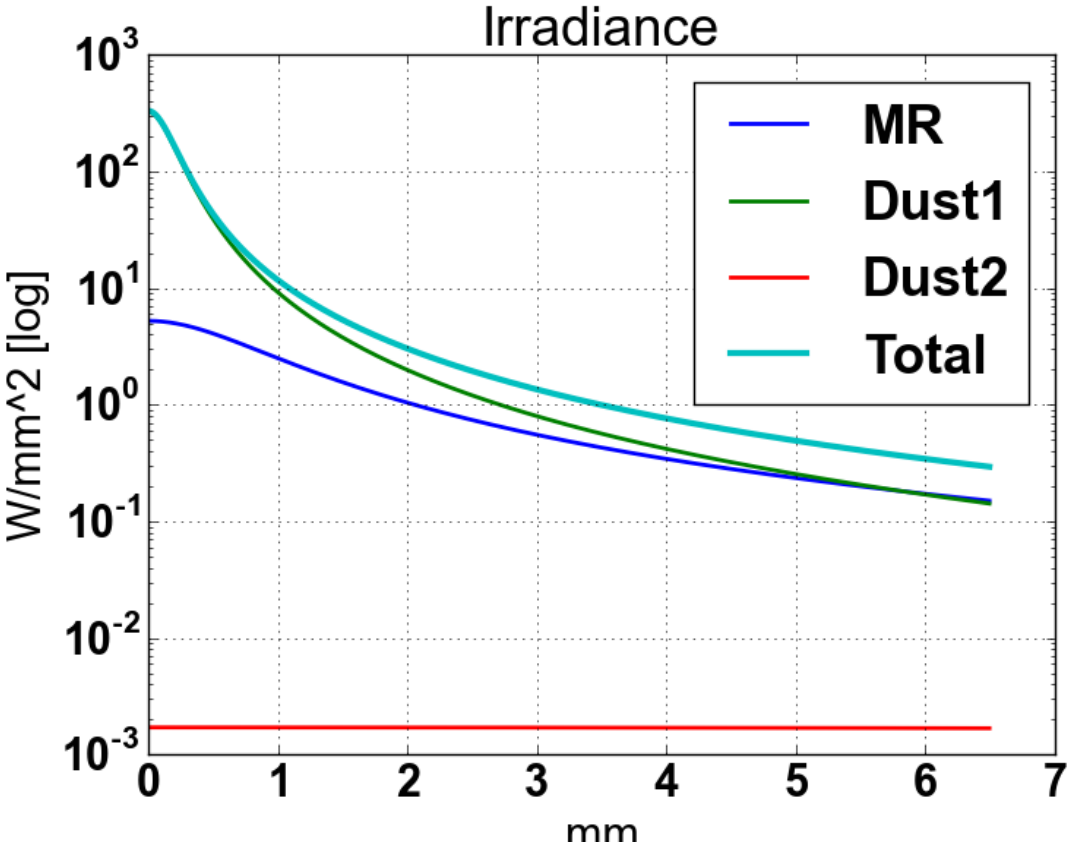


*Figure 48 Plots of irradiance on the focal plane of CIS, according to a Peterson model using the measured micro-roughness.*

The simplified Peterson model should be consequently updated from

E(R)=315*[1+19R^2]^(-1.135)

to

E(R)=315*(1+19 R^2) ^(-1.13) +0.441*(15/5.)^2(1+1.2R^2)^(-1.8/2),

where the second addendum is the Irradiance term due to the lenses micro-roughness, and the (15/5)^2 factor is to take in account the growth of the roughness, assuming an average roughness of 15A.

In Figure 49, the models (old an new) are put in comparison, showing the growth of the irradiance on the focal plane due to the measured micro-roughness.

The effect on photometry of the roughness increase has been confirmed through a dedicated simulation using CheopSIM (see [RD20]).

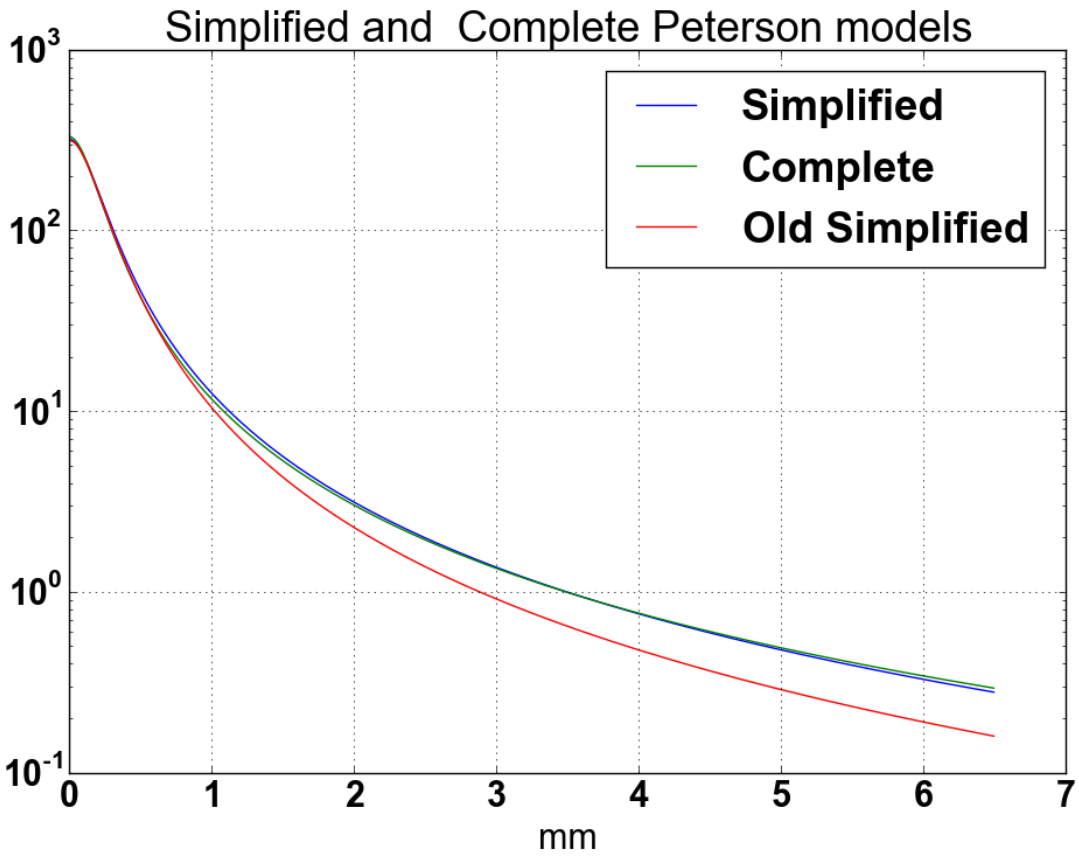


*Figure 49Simplified Peterson models in comparison*